

AUTOMATED BRAIN TISSUE SEGMENTATION OF MAGNETIC RESONANCE IMAGES IN MULTIPLE SCLEROSIS

Sergi Valverde Valverde

Per citar o enllaçar aquest document:
Para citar o enlazar este documento:
Use this url to cite or link to this publication:
<http://hdl.handle.net/10803/386468>



<http://creativecommons.org/licenses/by-nc-sa/4.0/deed.ca>

Aquesta obra està subjecta a una llicència Creative Commons Reconeixement-NoComercial-CompartirIgual

Esta obra está bajo una licencia Creative Commons Reconocimiento-NoComercial-CompartirIgual

This work is licensed under a Creative Commons Attribution-NonCommercial-ShareAlike licence



DOCTORAL THESIS

Automated brain tissue segmentation of
magnetic resonance images in multiple
sclerosis

Sergi Valverde

2016



DOCTORAL THESIS

**Automated brain tissue segmentation of
magnetic resonance images in multiple
sclerosis**

Sergi Valverde

2016

DOCTORAL PROGRAM in TECHNOLOGY

Supervised by:
Dr. Arnau Oliver
Dr. Xavier Lladó

Work submitted to the University of Girona in partial fulfillment of
the requirements for the degree of Doctor of Philosophy

A mis padres, cuyo sacrificio ha alimentado siempre mis sueños
To my parents, whose sacrifice has always nourished my dreams

Acknowledgments

This doctoral thesis is the result of my research efforts over the last three years. However, this work would not be possible without the collaboration and support of a wide number of colleagues, friends and institutions. First of all, I am infinitely grateful to my supervisors, Dr. Arnau Oliver and Dr. Xavier Lladó, for giving me the opportunity to work in this project. I really appreciate their enthusiasm, insight, unconditional support and friendship specially when difficulties arose. I owe them a lot for continuously encourage me not to stop forward. Without Arnau and Xavi, this doctoral thesis would simply not be possible.

Several institutions and medical centers have been involved also. I want to express my gratitude to the Generalitat de Catalunya for awarding me with the research grant FI-DGR2013, which has been used to fund this doctoral thesis. Most of the images used in this work have been gently facilitated by different research hospital centers in Catalunya. Furthermore, I want to thank to Dr. Lluís Ramió-Torrentà, Dr. Hector Perkal, René Robles and Dr. Brigitte Beltrán from the Hospital Dr. Josep Trueta of Girona, Dr. Joan Carles Vilanova from the Hospital Santa Caterina of Girona, Dr. Deborah Pareto and Àlex Rovira from the Vall d'Hebrón research hospital of Barcelona and Dr. Jaume Sastre-Garriga from the Multiple Sclerosis Center of Catalunya for their support, continuous reviewing processes and patience answering our medical questions. Moreover, I am sincerely grateful to all the reviewers that have been involved in the non-profit effort of reviewing not only this final manuscript but also each one of the research papers that compose it.

I am indebted with so many colleagues and friends for inspiring me with their work. I would like to thank all the permanent staff, post-doctoral researchers, PhD students and administrative staff of the VICOROB team for their help during these years. I am specially indebted with Aina, for her continuous efforts and patience helping me with my master's grant stuff and documentation. I want to express my appreciation to Dr. Jordi Freixenet and Dr. Joan Martí for their expert advices and the discussions about the medical image analysis field. I also want to thank the rest of my office colleagues Josep, Konstantin, Ricard P., Ricard C., Mojdeh, Eloi G., Ferran, Habib, Marc, Albert P., and Christian for their revealed patience and friendship. Likewise, I would like to express my gratitude as well for Guillaume, Sik,

Robert, Xevi and Yago for their technical discussions thorough the time we were running across the university's nearby forests. And very especially, I am very grateful to my colleagues Sandra, Mostafa, Onur, Mariano, and Eloy of the NeuroImaging Computing group for the inspiring discussions, for sharing their knowledge and helping me so much during these last few years.

Not without a high probability to forget anyone, I want to express also my gratitude to my old friends Albert, Eloi, Miquel, Presser, Aida, Mònica, Clara, Sergio, Dani MC, etc... for being so close during these years. Not to mention my old friends at FUNIAL: Moisès, Alfred, Antonio, Moi, Antonio C., Francesc, Dani, Edu, Mena, etc... for helping me to grow as a person. Besides that, I will be forever indebted to Alicia, for her constant support, joy, and love during most of these years.

However, this thesis would also not be possible without the unconditional love of my parents and my brother. Eight years ago, barely nobody but them were crazy enough to understand and support my decision of quitting my job position to start my degree in computer engineering. During these years, I have forgotten the number of times that their love and faith in me have been my light in the darkness. This doctoral thesis is entirely dedicated to them, whose sacrifice has always nourished my dreams.

Last but not least, I wish to thank to Mireia for her advice, support, daily infinite love, patience during the last months of intense work and for this smile that reminds me that this world is a very nice place to stay, when shared with her: like Marina and Núria, our coming daughter Helena will be very proud of you.

Publications

The presented thesis is a compendium of the following research articles:

- **Sergi Valverde**, Arnau Oliver, Eloy Roura, Sandra González, Deborah Pareto, Joan Carles Vilanova, Lluís Ramió-Torrentà, Àlex Rovira and Xavier Lladó. Automated brain tissue segmentation of MR images in the presence of white matter lesions. *Submitted to Medical Image analysis*. 2016. Elsevier. Quality index: [JCR CSAI IF 3.654, Q1 (10/121)].
- **Sergi Valverde**, Arnau Oliver, Eloy Roura, Deborah Pareto, Joan Carles Vilanova, Lluís Ramió-Torrentà, Jaume Sastre-Garriga, Xavier Montalban, Àlex Rovira and Xavier Lladó. Quantifying brain tissue volume in multiple sclerosis with automated lesion segmentation and filling. *NeuroImage: Clinical*. Vol. 9, pp 640-647. 2015. Elsevier. Quality index: [JCR N IF 2.526, Q2(6/14)].
- **Sergi Valverde**, Arnau Oliver, Yago Díez, Mariano Cabezas, Joan Carles Vilanova, Lluís Ramió-Torrentà, Àlex Rovira, and Xavier Lladó. Evaluating the effects of white matter multiple sclerosis lesions on the volume estimation of six brain tissue segmentation methods. *American Journal of Neuroradiology*. Vol. 36(6), pp. 1109-1115. 2015. American Society of Neuroradiology. Quality index: [JCR RNMMI IF 3.589, Q1(19/125)].
- **Sergi Valverde**, Arnau Oliver, Mariano Cabezas, Eloy Roura and Xavier Lladó. Comparison of ten brain tissue segmentation methods using revisited IBSR annotations. *Journal of Magnetic Resonance Imaging*. Vol. 41, Issue 1, pp. 93-101. January 2015. Wiley. Quality index: [JCR RNMMI IF: 3.210 Q1(23/125)].
- **Sergi Valverde**, Arnau Oliver, and Xavier Lladó. A white matter lesion-filling approach to improve brain tissue volume measurements. *NeuroImage: Clinical*. Vol. 6, pp 86-92. 2014. Elsevier. Quality index: [JCR N IF 2.526, Q2(6/14)].

The rest of publications and conferences related with this PhD thesis are the following:

Journals

- Eloy Roura, Nicolae Sarbu, Arnau Oliver, **Sergi Valverde**, Sandra González, Ricard Cervera, Nuria Bargalló and Xavier Lladó. Automated detection of Lupus white matter lesions in MRI images. *Submitted to Frontiers in Human Neuroscience*. 2016. Frontiers. Quality index: [JCR PS IF 3.626, Q1(13/76)].
- Eloy Roura, Arnau Oliver, Mariano Cabezas, **Sergi Valverde**, Deborah Pareto, Joan Carles Vilanova, Lluís Ramió-Torrentà, Àlex Rovira and Xavier Lladó. A toolbox for multiple sclerosis lesion segmentation. *Neuroradiology*. Vol. 57(10), pp. 1031-1043. 2015. Springer. Quality index: [JCR RNMMI IF 2.485, Q2(41/125)].
- Mariano Cabezas, Arnau Oliver, **Sergi Valverde**, Brigitte Beltrán, Joan Carles Vilanova, Lluís Ramió-Torrentà, Àlex Rovira and Xavier Lladó. BOOST: a supervised approach for multiple sclerosis lesion segmentation. *Journal of Neuroscience Methods*. Vol. 237, pp 108-117. 2014. Elsevier. Quality index: [JCR N IF 2.025, Q3(174/252)].
- Yago Díez, Arnau Oliver, Mariano Cabezas, **Sergi Valverde**, Robert Martí, Joan Carles Vilanova, Lluís Ramió-Torrentà, Àlex Rovira and Xavier Lladó. Intensity based methods for brain MRI longitudinal registration. A study on multiple sclerosis patients. *Neuroinformatics*. Vol 12(3), pp 365-379. 2014. Springer. Quality index: [JCR CSTM IF 2.825, Q1(13/102)]

Conferences

- Eloy Roura, Arnau Oliver, Mariano Cabezas, **Sergi Valverde**, Deborah Pareto, Joan Carles Vilanova, Lluís Ramió-Torrentà, Àlex Rovira and Xavier Lladó. An SPM12 extension for multiple sclerosis lesion segmentation. *SPIE Medical Imaging 2016*. February 2016, San Diego, USA.
- **Sergi Valverde**, Arnau Oliver, Eloy Roura, Deborah Pareto, Joan Carles Vilanova, Lluís Ramió-Torrentà, Jaume Sastre-Garriga, Xavier Montalban, Àlex Rovira and Xavier Lladó. Evaluation of two automated lesion segmentation and filling pipelines for brain tissue segmentation of multiple sclerosis patients. *ECTRIMS 2015. Multiple Sclerosis*. October 2015, Barcelona, Spain. Quality index: [JCR CN IF:4.472 Q1(25/191)].
- Eloy Roura, Arnau Oliver, Mariano Cabezas, **Sergi Valverde**, Deborah Pareto, Joan Carles Vilanova, Lluís Ramió-Torrentà, Àlex Rovira and Xavier Lladó.

A toolbox for segmenting multiple sclerosis lesions using T1w and FLAIR images. *ECTRIMS 2015. Multiple Sclerosis*. October 2015, Barcelona, Spain. Quality index: [JCR CN IF:4.472 Q1(25/191)].

- **Sergi Valverde**, Arnau Oliver, Deborah Pareto, Joan Carles Vilanova, Àlex Rovira, Lluís Ramió-Torrentà and Xavier Lladó. SLF: a MS white matter lesion filling toolbox for the SPM software. *ECTRIMS 2014. Multiple Sclerosis*. September 2014, Boston, USA. Quality index: [JCR CN IF:4.822 Q1(22/192)].
- Ester Quintana, Brigitte Beltrán, **Sergi Valverde**, René Robles-Cedeno, Hector Perkal, Xavier Lladó, José Manuel Fernández-Real and Lluís Ramió-Torrentà. Expression of miRNAs in multiple sclerosis cerebrospinal fluid and their relation to MR activity. *ECTRIMS 2014. Multiple Sclerosis*. September 2014, Boston, USA. Quality index: [JCR CN IF:4.822 Q1(22/192)].
- Ester Quintana, Brigitte Beltrán, **Sergi Valverde**, René Robles-Cedeno, Hector Perkal, Xavier Lladó, José Manuel Fernández-Real and Lluís Ramió-Torrentà. Relación entre la expresión de mirnas en LCR y variables de RM. *Neurología*, vol 29, pp 66-67. 2014. Quality index: [JCR CN IF:1.322 Q3(142/191)].
- **Sergi Valverde**, Arnau Oliver, Mariano Cabezas, Yago Díez, Jordi Freixenet, Xavier Lladó, Joan Carles Vilanova, Àlex Rovira and Lluís Ramió-Torrentà. A quantitative study of the effects of White Matter MS lesions on tissue segmentation methods. *ECTRIMS 2013. Multiple Sclerosis*. October 2013, Copenhagen, Denmark. Quality index: [JCR CN IF:4.472 Q1(25/191)].

Acronyms

ANN Artificial Neural Network
BET Brain Extraction Tool
BSE Brain Surface Extractor
CSF Cerebrospinal Fluid
CIS Clinically Isolated Syndrome
EDSS Extended Disability Status Scale
FANTASM Fuzzy and Noise Tolerant Adaptive Segmentation Method
FAST FMRIB's Automated Segmentation Tool
FCM Fuzzy-C Means
FLAIR Fluid Attenuated Inversion Recovery
FMRIB Oxford Centre for Functional MRI of the Brain
FSL FMRIB Software Library
GAMIXTURE Image segmentation toolbox based on genetic algorithm and mixture model optimization
GM Gray Matter
IBSR Internet Brain Segmentation Repository
LST Lesion Segmentation Toolbox
MARGA Multispectral Adaptive Region Growing Algorithm
MRI Magnetic Resonance Image
MRBrainS13 Magnetic Resonance Brain Segmentation Challenge 2013
MS Multiple Sclerosis
KNN K-Nearest Neighbor
PD Proton Density
PVC Partial Volume Classifier
SLF SALEM Lesion Filling
SLS SALEM Lesion Segmentation
SVPASEG Image segmentation toolbox based on local Markov random fields
SPM Statistical Parametric Mapping
T1-w T1-weighted
T2-w T2-weighted
WM White Matter

List of Figures

1.1	MRI image modalities	3
1.2	MRI pre-processing steps	4
1.3	Lesion filling example on a T1-w sequence	6
1.4	Organization of the document	11

Contents

Abstract	xiii
Resum	xvii
Resumen	xxi
1 Introduction	1
1.1 Research context	1
1.1.1 Multiple Sclerosis	1
1.1.2 Magnetic Resonance Imaging in MS	2
1.1.3 Image analysis in MS	3
1.2 Research background	7
1.3 Objectives	8
1.4 Document structure	10
2 Comparison of 10 brain tissue segmentation methods using revisited IBSR annotations	13
3 Evaluating the effects of white matter multiple sclerosis lesions on the volume estimation of 6 brain tissue segmentation methods	23
4 A white matter lesion-filling approach to improve brain tissue volume measurements	31
5 Quantifying brain tissue volume in multiple sclerosis with automated lesion segmentation and filling	39

6	Automated tissue segmentation of MR brain images in the presence of white matter lesions	49
7	Main results and discussion	69
7.1	Effect of WM lesions on tissue segmentation	69
7.2	Effect of lesion filling in tissue segmentation	71
7.3	Effect of automating lesion segmentation and filling on tissue segmentation	72
7.4	Fully automated tissue segmentation of images containing WM lesions	74
8	Conclusions	77
8.1	Future work	79

Abstract

Multiple Sclerosis (MS) is the most common chronic immune-mediated disabling neurological disease affecting the central nervous system, in which the insulating covers of the nerve cells in the spinal chord and brain are damaged. MS is characterized by the presence of lesions in the brain, predominantly in the white matter (WM) tissue of the brain. Due to the sensitivity of structural Magnetic Resonance Imaging (MRI) disseminating WM lesions in time and space, it has become an essential tool in the diagnosis and evaluation of MS. Furthermore, MRI measurements of atrophied tissue in the brain have shown to correlate with the disability status, demonstrating that tissue loss is an important component of the disease's progression.

This correlation between the amount of atrophied tissue in the brain and MS disability status has increased the necessity of developing robust, automated brain tissue segmentation methods capable of measuring the brain's tissue volume accurately. However, automated segmentation of brain tissue is still a challenging problem due to the complexity of the images, lack of contrast between tissues, noise, intensity inhomogeneities and the absence of anatomy models that fully capture the possible deformations in each structure. Moreover, it has been shown that WM lesions reduce the accuracy of automated tissue segmentation methods, which highlights the necessity of handling these lesions before tissue segmentation, a process known as lesion filling. However, lesion filling requires manually annotating lesions before tissue segmentation, which is time-consuming, prone to variability among expert radiologists, or not always readily available. This fact along with the need of analyzing focal MS lesions quantitatively in individual and temporal studies has led to the development of a large number of automated lesion segmentation methods of MS lesions.

The main goal of this thesis is to develop a novel, fully automated brain tissue segmentation method capable of computing accurate measurements of tissue volume from images of MS patients with lesions. In order to fulfill this goal, we have focused on each of the concatenated processes necessary to develop a fully automated tissue segmentation method. Firstly, we have analyzed and evaluated the state-of-the-art of tissue segmentation methods on data from healthy subjects, where

we have performed a quantitative review of the different tissue segmentation techniques proposed, with the aim of understanding their advantages and drawbacks. Our experimental results have shown that methods that incorporate morphological prior information and/or spatial constraints are more robust to changes in acquisition sequences and intensity inhomogeneities, when compared with simpler strategy intensity based methods.

In the second stage, we have studied and evaluated the effect of WM lesions on tissue segmentation of MS patient images. In this regard, we have performed several experiments using multi-center 1.5T MS data from different scanners in order to analyze the effects of lesion signal intensities and lesion size on the performance of several tissue segmentation methods not explicitly designed to handle with WM lesions. In all these methods, the results obtained have indicated that the inclusion of WM lesions on tissue segmentation not only biased the total tissue volume measurements by the addition of miss-classified lesion voxels, but also had a direct effect on the differences observed in normal-appearing tissue. This effect has shown to be less relevant in those methods that incorporate prior information and/or spatial context.

In the third stage, we have focused on lesion filling, reviewing and analyzing the accuracy of the different lesion filling techniques proposed in the literature. Motivated by these results, we have proposed a new lesion filling technique with the aim of overcoming the limitations of previously proposed methods. When compared with these methods, our experimental results have shown that the proposed lesion filling method is effective with different databases and is independent of the tissue segmentation method used afterwards.

Finally, we have focused on a comprehensive analysis of the effects of automated lesion segmentation and filling in tissue segmentation. We have evaluated the accuracy of two pipelines that incorporated automated lesion segmentation, lesion filling and tissue segmentation on MS data, with the aim of understanding the extent of the effect of remaining WM lesions on the differences in tissue segmentation. Our findings have shown that up to certain lesion load, pipelines that incorporated automated lesion segmentation and filling are capable of significantly reducing the impact of WM lesions on tissue segmentation, showing a similar performance to pipelines where expert lesion annotations were used.

All these stages have served as the basis in the development of a novel, multi-channel method designed to segment brain tissues in MRI images of MS patients. The proposed tissue segmentation method has been designed and implemented using a combination of intensity along with anatomical and morphological prior maps to guide the tissue segmentation. WM outliers have been estimated and filled before segmentation using a multi-channel post-processing rule-based algorithm with spatial context, and prior anatomical and morphological atlases. The proposed method

has been quantitatively and qualitatively evaluated using different databases of images containing WM lesions, yielding competitive and consistent results in both general and MS specific databases. The percentages of errors obtained in the different experiments carried out show that the proposed algorithm effectively improves automated brain tissue segmentation in images containing lesions.

This PhD thesis is part of several project frameworks carried out by our research group in collaboration with different hospital centers. As part of the goals of these research projects, software implementations of all the proposed methods in this thesis have been released for public use in the research community. The proposed lesion filling method is currently being used by the collaborating hospitals. We believe that the proposed, fully automated tissue segmentation method will also be beneficial in clinical settings.

Resum

L'Esclerosi Múltiple (EM) és la malaltia neurològica crònica incapacitant més comuna del sistema nerviós central, on el recobriment aïllant de les cèl·lules nervioses a la medul·la espinal i el cervell estan danyades. L'EM es caracteritza per la presència de lesions en el cervell, predominantment en el teixit de la substància blanca. Gràcies a la seva sensibilitat per mostrar l'activitat focal de les lesions i el progrés de la malaltia, la ressonància magnètica (RM) s'ha convertit en una eina essencial per al diagnòstic i l'avaluació de l'EM. Igualment, s'ha demostrat que l'atròfia del teixit cerebral mesurada a través de la RM està relacionada amb l'increment de la discapacitat, mostrant que la pèrdua de teixit és un component important de la progressió de la malaltia.

La correlació existent entre l'atròfia del teixit cerebral i l'estat d'incapacitat de la malaltia, ha augmentat la necessitat de desenvolupar eines automàtiques de segmentació amb capacitat per mesurar de forma precisa el volum dels teixits cerebrals. No obstant, la segmentació automàtica del teixit cerebral segueix sent un problema complicat, fonamentalment a causa de factors com la complexitat de les imatges, les diferències en les intensitats de teixit, el soroll de les imatges, les diferències en l'homogeneïtat de les adquisicions o l'absència de models anatòmics capaços de modelar cadascuna de les estructures del cervell. Així mateix, s'ha demostrat també que les lesions de substància blanca redueixen la precisió dels mètodes automàtics de segmentació, subratllant així la necessitat de processar les lesions abans de la segmentació utilitzant un procés conegut com *lesion filling*. Tanmateix, el procés de *lesion filling* requereix que les màscares de lesió siguin conegudes a priori, el que pot ser difícil d'aconseguir, comportant temps i sent propens a variabilitat entre radiòlegs. Aquest fet i la necessitat d'analitzar les lesions d'EM tant en estudis individuals com temporals ha portat al desenvolupament d'un gran nombre de mètodes automàtics de segmentació de les lesions.

L'objectiu principal d'aquesta tesi és el desenvolupament d'un nou mètode de segmentació totalment automàtic capaç de mesurar amb precisió el volum cerebral en imatges de pacients d'EM amb lesions. Per aconseguir-ho, en aquesta tesi ens hem concentrat en cadascun dels processos necessaris per a desenvolupar aquest mètode. Primer, hem fet un resum qualitatiu i quantitatiu de les tècniques de segmentació

ja existents a la literatura utilitzant diferents conjunts d'imatges de subjectes sans, amb l'objectiu d'entendre els avantatges i inconvenients de les diferents tècniques. Els resultats obtinguts demostren que els mètodes que incorporen informació a priori de tipus morfològica o de context local tendeixen a ser menys proclius als canvis en l'adquisició de les seqüències o en les homogeneïtats de les intensitats, en comparació amb mètodes més simples basats només en intensitat.

En segon lloc, hem estudiat i analitzat l'efecte que produeixen les lesions de substància blanca a la segmentació d'imatges de pacients d'EM. A tal fi, hem realitzat diversos experiments utilitzant bases de dades de 1.5T adquirides en diferents escàners per tal d'analitzar l'efecte de la intensitat i el volum de les lesions en les diferències en volum cerebral de diversos mètodes de segmentació de teixit. En tots els mètodes, la inclusió de les lesions en el procés de segmentació no només introdueix errors en els mesuraments del volum total de teixit a causa dels vòxels de les lesions mal classificats, sinó que també té un efecte clar en les diferències de volum en el teixit sa. Aquest efecte és menys rellevant en els mètodes que incorporen informació a priori de tipus morfològica o de context local.

En tercer lloc, ens hem concentrat en el procés de *lesion filling*, on hem resumit i analitzat la precisió de les diferents tècniques proposades en el camp. Aquesta anàlisi ens ha servit de base per proposar una nova tècnica de *lesion filling* que millori les limitacions observades en els mètodes anteriors. Els resultats obtinguts mostren que, en comparació amb la resta de mètodes proposats, el nostre mètode és efectiu amb diferents tipus d'imatges i independentment del mètode de segmentació utilitzat a continuació.

Seguidament, hem realitzat una anàlisi completa dels efectes d'automatitzar la segmentació de les lesions de substància blanca i el *lesion filling* en la posterior segmentació del teixit cerebral. Per això, hem avaluat l'eficàcia de dos sistemes automàtics que incorporen aquests processos per tal d'entendre el paper de les lesions residuals que no van ser detectades i, per tant no processades, en les diferències de volum cerebral. Els nostres resultats mostren que els sistemes on la segmentació de les lesions i el *lesion filling* va ser automàtic redueixen significativament l'impacte de les lesions de substància blanca a la segmentació del teixit, mostrant un eficàcia similar als sistemes amb intervenció manual dels experts.

Cadascuna d'aquestes fases ens ha servit de base per al desenvolupament d'un nou mètode de segmentació multi-canal dissenyat amb l'objectiu de segmentar imatges de RM de pacients d'EM. El mètode que hem proposat s'ha desenvolupat i implementat integrant no només la informació provinent de la intensitat dels vòxels, sinó a través de la incorporació d'atles morfològics i estructurals que guien la segmentació del teixit. Els vòxels candidats de ser lesions són estimats i processats abans de la segmentació del teixit utilitzant un algoritme de post-processat basat en la informació del context local i la informació anatòmica i morfològica prèvia.

Aquest mètode de segmentació ha estat avaluat de forma quantitativa i qualitativa utilitzant diferents conjunts d'imatges que contenen lesions de substància blanca. Els resultats mostren que la precisió del mètode proposat és consistent i molt competitiva en tot tipus d'imatges en comparació amb altres tècniques proposades. En aquest sentit, els percentatges d'error obtinguts en els diferents experiments duts a terme mostren que el mètode proposat millora la segmentació del teixit cerebral de les imatges amb lesions.

Aquesta tesi doctoral forma part de diversos projectes que el nostre grup de recerca està duent a terme en col·laboració amb els diferents centres hospitalaris involucrats. Com a part d'aquests objectius, tots els programes desenvolupats durant aquesta tesi s'han fet públics per al lliure ús de la comunitat científica. En el cas del mètode de *lesion filling*, aquest ja està sent utilitzat en els hospitals col·laboradors. Pensem igualment que el mètode de segmentació proposat serà també útil en futurs entorns d'investigació i assajos clínics.

Resumen

La Esclerosis Múltiple (EM) es la enfermedad neurológica crónica incapacitante más común del sistema nervioso central, en donde el recubrimiento aislante de las células nerviosas en la médula espinal y el cerebro están dañadas. La EM se caracteriza por la presencia de lesiones en el cerebro, predominantemente en el tejido de la sustancia blanca. Gracias a la sensibilidad de la resonancia magnética (RM) para mostrar la actividad focal de las lesiones y el progreso de la enfermedad, la RM se ha convertido en una herramienta esencial para el diagnóstico y la evaluación de la EM. Igualmente, se ha demostrado que la atrofia del tejido cerebral medida a través de la RM está relacionada con el incremento de la discapacidad, mostrando que la pérdida de tejido es un componente importante de la progresión de la enfermedad.

La correlación existente entre la atrofia del tejido cerebral y el estado de incapacidad de la enfermedad, ha aumentado la necesidad de desarrollar herramientas automáticas de segmentación capaces de medir de forma precisa el volumen de los tejidos cerebrales. Sin embargo, la segmentación automática del tejido cerebral sigue siendo un problema complicado, fundamentalmente debido a factores como la complejidad de las imágenes, las diferencias en las intensidades de tejido, el ruido de las imágenes, las diferencias en la homogeneidad de las adquisiciones o la ausencia de modelos anatómicos capaces de modelar cada una de las estructuras del cerebro. Asimismo, se ha demostrado también que las lesiones de sustancia blanca reducen la precisión de los métodos automáticos de segmentación, subrayando así la necesidad de procesar las lesiones antes de la segmentación utilizando un proceso conocido como *lesion filling*. No obstante, el proceso de *lesion filling* requiere que las máscaras de lesión sean conocidas a priori, lo que puede ser difícil de conseguir, conllevando tiempo y siendo propenso a variabilidad entre radiólogos. Este hecho y la necesidad de analizar las lesiones de EM tanto en estudios individuales como temporales ha llevado al desarrollo de un gran número de métodos automáticos de segmentación de las lesiones.

El objetivo principal de esta tesis es el desarrollo de un nuevo método de segmentación totalmente automático capaz de medir con precisión el volumen cerebral en imágenes de pacientes de EM con lesiones. Para conseguirlo, en esta tesis nos hemos concentrado en cada uno de los procesos encadenados necesarios para desar-

rollar tal método. Primero, hemos realizado un resumen cualitativo y cuantitativo de las técnicas de segmentación ya existentes utilizando diferentes conjuntos de imágenes de sujetos sanos, con el objetivo de entender las ventajas e inconvenientes de cada técnica. Los resultados obtenidos demuestran que los métodos que incorporan información a priori de tipo morfológica o de contexto local tienden a ser menos proclives a los cambios en la adquisición de las secuencias o en las homogeneidades de las intensidades, en comparación con métodos más simples basados solamente en intensidad.

En segundo lugar, hemos estudiado y analizado el efecto que producen las lesiones de sustancia blanca en la segmentación de imágenes de pacientes de EM. Para ello, hemos realizado varios experimentos utilizando bases de datos de 1.5T adquiridas en diferentes escáneres con el fin de analizar el efecto de la intensidad y el volumen de las lesiones en las diferencias en volumen cerebral de varios métodos de segmentación de tejido. En todos los métodos, la inclusión de las lesiones en el proceso de segmentación no sólo introduce errores en las mediciones del volumen total de tejido debido a los vóxeles de las lesiones que fueron mal clasificados, sino que también tienen un efecto claro en las diferencias de volumen observadas en el tejido sano. Este efecto es menos relevante en los métodos que incorporan información a priori de tipo morfológica o de contexto local.

En tercer lugar, nos hemos concentrado en el proceso de *lesion filling*, donde hemos resumido y analizado la precisión de las diferentes técnicas propuestas en el campo. Este análisis nos ha servido de base para proponer una nueva técnica de *lesion filling* que mejore las limitaciones observadas en los métodos anteriores. Los resultados obtenidos muestran que en comparación con el resto de métodos propuestos, nuestro método es efectivo con diferentes tipos de imágenes e independientemente del método de segmentación utilizado a continuación.

Seguidamente, hemos realizado un análisis completo de los efectos de automatizar la segmentación de las lesiones de sustancia blanca y el *lesion filling* en la posterior segmentación del tejido cerebral. Para ello, hemos evaluado la eficacia de dos sistemas automáticos que incorporan estos procesos con el fin de entender el papel de las lesiones residuales que no fueron detectadas y, consecuentemente no procesadas, en las diferencias de volumen cerebral observadas. Nuestros resultados muestran que los sistemas donde la segmentación de las lesiones y el *lesion filling* fue automático reducen significativamente el impacto de las lesiones de sustancia blanca en la segmentación del tejido, mostrando una eficacia similar a los sistemas con intervención manual de los expertos.

Cada una de estas fases nos ha servido de base para el desarrollo de un nuevo método de segmentación multicanal diseñado con el objetivo de segmentar imágenes de RM de pacientes de EM. El método que hemos propuesto se ha desarrollado e implementado integrando no sólo la información proveniente de la intensidad de los

vóxeles, sino a través de la incorporación de atlas morfológicos y estructurales que guían la segmentación del tejido. Los vóxeles candidatos de ser lesiones son estimados y procesados antes de la segmentación del tejido utilizando un algoritmo de postproceso basado en la información del contexto local y la información anatómica y morfológica previa. Este método de segmentación ha sido evaluado de forma cuantitativa y cualitativa usando diferentes conjuntos de imágenes que contenían lesiones de sustancia blanca. Los resultados muestran que la precisión del método propuesto es consistente y muy competitiva en todo tipo de imágenes en comparación con otras técnicas propuestas. En este sentido, los porcentajes de error obtenidos en los diferentes experimentos llevados a cabo muestran que el método propuesto mejora la segmentación del tejido cerebral de las imágenes con lesiones.

Esta tesis doctoral forma parte de varios proyectos que nuestro grupo de investigación está llevando a cabo en colaboración con los diferentes centros hospitalarios involucrados. Como parte de estos objetivos, todos los programas desarrollados durante esta tesis se han hecho públicos para el libre uso de la comunidad científica. En el caso del método de *lesion filling*, éste ya está siendo utilizado en los hospitales colaboradores. Pensamos igualmente que el método de segmentación propuesto será también útil en futuros entornos de investigación y ensayos clínicos.

Chapter 1

Introduction

In this first chapter, we introduce the reader to the research context and background of this thesis, situating the work in the research line of our group. Afterwards, we describe the proposed objectives and the respective stages to cover. Finally, we summarize the main structure of this thesis, highlighting the conceptual thread between each of the articles that compose its main core.

1.1 Research context

1.1.1 Multiple Sclerosis

The human nervous system can be divided into the central nervous system (CNS) consisting of the brain and the spinal chord, and the peripheral nervous system, which connects the CNS with the sense organs [7]. CNS is mainly composed of two tissues: gray matter (GM), which consists of neuronal cell bodies; and white matter tissue (WM), which is mainly composed of myelinated axon tracts [67]. The brain itself is composed mostly of GM and WM, both surrounded by the Cerebro-spinal fluid (CSF), which provides basic mechanical and immunological protection to the brain inside the skull [67].

Multiple sclerosis (MS) is the most common chronic immune-mediated disabling neurological disease of the CNS [68], in which the insulating covers of the nerve cells in the spinal chord and brain are damaged [18]. Nowadays, MS is the most frequent non-traumatic neurological disease that causes more disability in young adults. It follows a similar behavior to other putative autoimmune diseases, and affects twice as many women as men [19]. It has a low incidence in childhood, but the probability increases rapidly in young adulthood reaching a peak between 25 and 35 years, and then slowly declines, becoming rare at 50 and older [48]. So far, the world estimate

for the disease is in 2.3 million cases, being relatively common in Europe, the United States, Canada, New Zealand, and parts of Australia, but rare in Asia, and in the tropics and subtropics [48].

MS is characterized by areas of inflammation, demyelination, axonal loss, and gliosis scattered throughout the CNS, often causing motor, sensorial, vision, coordination, deambulation, and cognitive impairment [17]. Demyelination is the process of progressive damage to the protective covering (myelin sheath) around the axon of the neurons. Demyelinated axons conduct impulses at reduced or spontaneous velocity causing impairment in sensation, movement and cognition [18]. The different clinical courses of the disease are generally grouped into four subtype forms [45]. The *Relapsing/Remitting* (RRMS) form of the disease is characterized by exacerbation times where symptoms are present. These periods are followed by periods of remission, where the patient recovers partially or totally from the disease's symptoms. The *Secondary Progressive* (SPMS) form is characterized by a gradual intensification of symptoms between affection relapses. The *Progressive remitting* (PRMS) form is typified by an increase in the relapse times with significant recovery but with worsening symptoms in new relapse intervals. Lastly, the *Primary Progressive* (PPMS) form is characterized by a severe decrease of remission times with special localization in the brain. In general, 50% of RRMS patients develop the SPMS form of the disease after 10 years. After 25 years, 90% of RRMS patients will develop the SPMS form [45].

1.1.2 Magnetic Resonance Imaging in MS

Magnetic Resonance Imaging (MRI) is a noninvasive medical imaging technique used in radiology to generate image representations of different internal anatomical organs and physiological processes of the body. Over the last 40 years, MRI has evolved as a clinical modality [34], and, in particular, as an essential tool for the diagnosis and evaluation of central nervous system disorders such as MS [24]. In MRI, MS plaques are well-delimited regions with hypointense signal intensity with respect to GM on T1-weighted (T1-w), while hyperintense with respect to GM on T2-weighted (T2-w), Proton Density-weighted (PD-w) and Fluid Attenuated Inversion Recovery (FLAIR) modalities (see Figure 1.1).

In this aspect, new criteria for MS diagnosis and monitoring has been revised over the last years [51], due to the sensitivity of structural MRI disseminating WM lesions in time and space [27]. Additionally, various studies have analyzed the correlation between MRI brain tissue atrophy measurements and MS disability status, showing that tissue loss is an important indication of the disease's progression [15, 26, 28, 59]. Tissue loss seems to increase through the course of MS at a similar rate between 0.3% and 0.5% per year, independently of the MS subtype [21, 59]. In general, GM

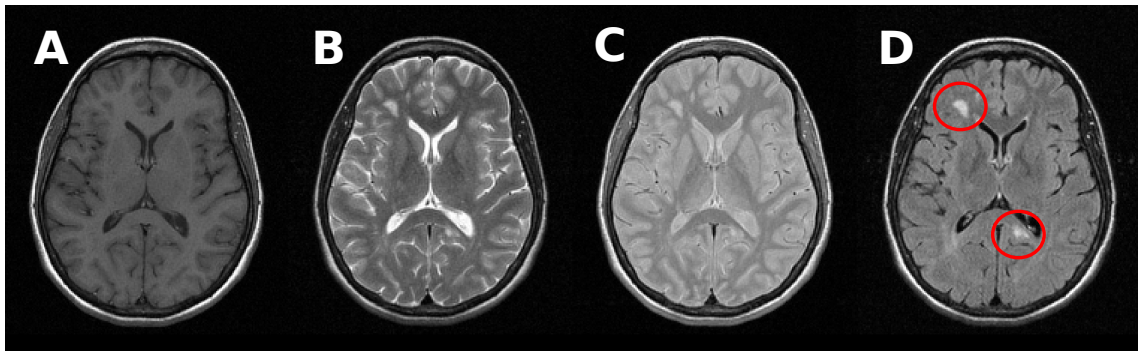


Figure 1.1: MRI image modalities. A) T1-w image sequence. B) T2-w image sequence. C) PD-w image sequence. D) FLAIR sequence. MS plaques are shown inside red circles on the FLAIR modality. MS plaques are hyperintense with respect to GM and WM in T2-w, PD-w and FLAIR sequences, while hypointense with respect to WM on the T1-w modality.

atrophy is associated more with disability changes than with WM atrophy [29], not only in the RRMS and SPMS MS subtypes [28, 59], but also in Clinically Isolated Syndrome (CIS) patients, where several studies have shown significantly greater ventricular cavities and an associated GM loss in MRI scans of CIS patients that will develop MS compared to those who will not [13, 26].

1.1.3 Image analysis in MS

Manual analysis of brain images is impractical in practice, given the large number of two-dimensional slices of each three-dimensional MRI patient image and the possible intra/inter observer variability between experts. This has led to the development since the early nineties of a wide number of lesion and tissue segmentation methods, with the aim of reducing the time needed for manual interaction and the inherent variability of manual annotations [16, 33, 41].

Pre-processing of MRI images

Acquired brain MRI volumes incorporate non-brain tissue parts of the head such as eyes, fat, spinal cord or the skull. Brain tissue extraction from non-brain tissue is commonly referred in the literature as skull-stripping (see Figure 1.2 B and C). Skull-stripping has a direct effect on the performance of automated methods, as the inclusion of skull or eyes as brain tissue may lead to unexpected results in tissue classification [1, 52], while unintended removal of the cortical surface may result

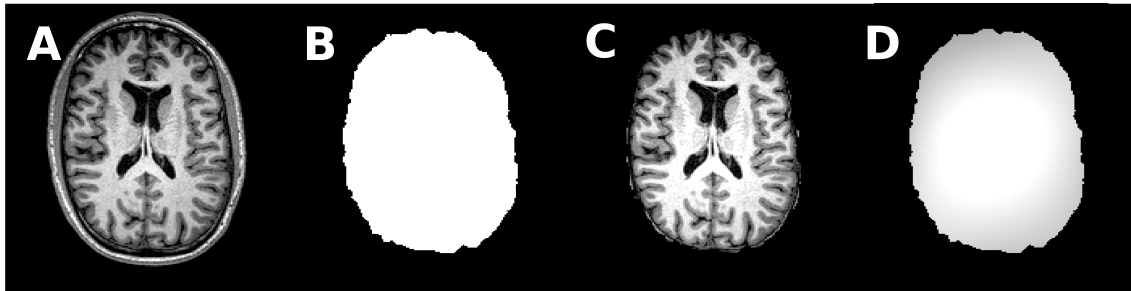


Figure 1.2: MRI pre-processing steps. A) T1-w image sequence. B) Computed brain mask using the BET approach [66] and C) skull stripped T1-w sequence. D) Estimated T1-w bias-field using the N3 method proposed by [65].

in underestimation of the cortical thickness [60]. Among the different methods proposed for skull-stripping [1, 42, 56], methods such as BET [66] and BSE [63] are being replaced by more modern methods such as ROBEX [39] and BEaST [25].

Furthermore, inherent characteristics of the MRI acquisition process such as differences in the magnetic field, bandwidth filtering of the data or eddy currents driven by field gradients usually result in image artifacts that may also have a negative impact on the performance of the methods [64]. In these cases, intensity correction of the MRI images is performed either before lesion/tissue segmentation, or as an integrated part of the tissue segmentation pipeline (see Figure 1.2 D). Among the available strategies [3, 38], the N3 [65] and N4 [72] methods are currently the most widely used tools used for bias field correction.

Automated lesion segmentation

MRI based diagnostic criteria for MS has led to an increasing need to analyze focal MS lesions quantitatively in individual and temporal studies [9, 51]. Different sequences such as, T2-w, PD-w and FLAIR, are often used in lesion detection and segmentation, as MS lesions appear brighter than GM and WM in them. However, WM lesions often present a similar signal intensity profile to CSF in T2-w. In contrast, FLAIR sequences suppress fluids from the image, restraining the CSF tissue effects on the acquired image, although some severe T2-w hyperintense lesions appear similar to CSF in FLAIR [37].

A wide number of automated lesion segmentation techniques have been proposed over the last few years [31, 44]. In these methods, lesion segmentation is based either on supervised or unsupervised strategies. Supervised methods employ a training set of correctly-identified observations that are used as prior information to learn the lesion's characteristics. Newer proposed strategies integrate a spatial decision forest

[32], statistical methods [69], patch-based models [36] or adaptive dictionary learning strategies [22]. In contrast, learning methods using unsupervised intensity models involve grouping data into categories based on some measure of inherent similarity or distance characteristics of the input images. Among these, most recent methods include probabilistic models that separate WM lesions from normal-appearing tissue by considering lesions as an outlier class [37, 40, 71], or techniques that make use of the signal intensity of lesions on FLAIR to apply several thresholding methods with post-processing steps to automatically segment lesions [55, 61].

Automated brain tissue segmentation in MS

The correlation between brain tissue atrophy measurements and MS disability status [26, 28] has increased the necessity of developing robust automated brain tissue segmentation methods capable of measuring brain tissue volume accurately [35]. However, the automated segmentation of brain tissue is still a challenging problem due to the complexity of the images, the existence of lesions, lack of contrast between tissues, noise, intensity inhomogeneities, partial volume effects and the absence of anatomy models that fully capture the deformations possible in each structure [8, 41].

A wide number of brain tissue segmentation methods not designed to deal explicitly with MS lesions have been proposed so far, usually on T1-w sequences, as this modality clearly separates GM from WM. These include unsupervised intensity models based on Bayesian inference [4, 50, 58, 73, 76], Markov Random Fields models [6, 70, 78], or unsupervised clustering methods [11, 49]. In contrast, supervised learning approaches also combine T1-w sequences with other modalities such as T2-w and PD-w using *K-Nearest-Neighbor* classifiers [20, 75], *Support Vector Machines* [2, 74], *Random Forests* [77, 47], or trained *Gaussian mixture models* [54].

However, different studies have shown that tissue abnormalities found in MS patients images such as WM lesions reduce the accuracy of tissue segmentation methods [5, 14]. Effectively, WM lesions on T1-w are hypointense with respect to normal-appearing WM, and therefore, lesion voxels that are classified as GM distort the overall GM volume. However, at a certain lesion volume, lesion voxels may also have an effect on the differences observed in normal-appearing tissue. WM lesions with signal intensity between the GM and WM interface, if are actually classified as WM decrease the mean overall signal intensity of the WM, causing GM voxels with signal intensities similar to WM lesions to be also misclassified as WM. In contrast, if WM lesions are classified as GM, normal-appearing WM voxels with signal intensities similar to lesions may be misclassified as GM.

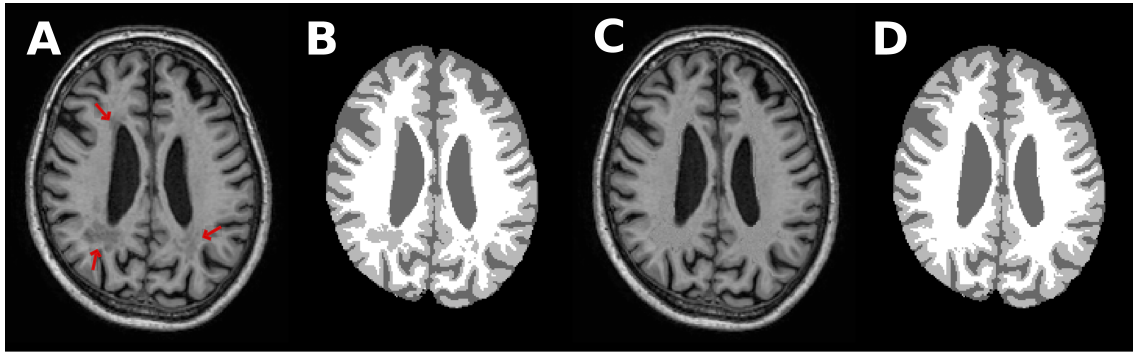


Figure 1.3: Lesion filling example on a slice of a T1-w scan. A) T1-w image sequence containing WM lesions (depicted by red arrows). B) Segmented T1-w sequence containing lesions. GM is depicted in light gray color, WM in white color and CSF in dark gray color. C) T1-w sequence after lesion filling. D) Segmented lesion filled T1-w sequence.

Lesion filling

In MS, when hypointense WM lesions are not included in the segmentation model, they have to be pre-processed before tissue segmentation in order to reduce the effects of WM lesions on the segmentation. Historically, WM lesions have been masked-out of the T1-w before segmentation, and their volume added to the WM afterwards [15]. Although this method effectively reduces the error in tissue volume, it has been shown in several studies that this approach is not optimal [5, 14], because on images with high lesion load, the lack of lesion voxels may be modifying the original WM tissue distribution of the image, introducing significant differences in tissue segmentation.

In this respect, several strategies have proposed in-painting lesions on the T1-w with signal intensities of the normal-appearing WM before tissue segmentation [5, 14, 46, 62], a process known in the literature as lesion filling (see Figure 1.3 for an example). However, most of the available lesion filling methods require manual delineations of lesions, which may be a tedious, challenging and time-consuming task depending on the characteristics of the image [44]. When available, lesion filling has demonstrated a significant reduction not only in the associated errors of WM lesions in tissue volume measurements [53], but also in image registration [12, 23, 62] and cortical thickness measurements [46].

1.2 Research background

This thesis is positioned within the framework of different research projects associated with the Computer Vision and Robotics Institute (VICOROB) of the University of Girona¹. VICOROB has been working on numerous medical image analysis projects since 1996, mainly in segmentation and registration of mammography images. In 2009, this research group started a fruitful collaboration with several medical MS research teams with the aim of developing new automated techniques capable of segmenting MS lesions and calculating atrophy measurements that can be transferred to experts for clinical use. In particular, our research in the MS field has been carried out within the following research projects:

1. [2009 - 2012] PI09/91918 “SALEM: Segmentación Automática de Lesiones de Esclerosis Múltiple en imágenes de resonancia magnética” awarded by the Instituto Carlos III.
2. [2009 - 2012] VALTEC09-1-0025 “SALEM: Eines per a la segmentació automàtica de lesions d’Esclerosi Múltiple en ressonància magnètica” awarded in 2009 by the Generalitat de Catalunya within the “Projectes de valorització VALTEC”.
3. [2015 - 2017] TIN2014-55710-R: NICOLE: “Herramientas de neuroimagen para mejorar el diagnóstico y el seguimiento clínico de los pacientes con Esclerosis Múltiple” awarded in 2014 by the spanish call Retos de investigación 2014.
4. [2015 - 2019] BiomarkEM.cat: “New technologies applied to clinical practice for obtaining biomarkers of atrophy and lesions in magnetic resonance images of patients with multiple sclerosis”. Awarded in 2015 by the Fundació la Marató de TV3.

Since then, the research group has published original contributions in different fields such as image pre-processing [56], MS lesion segmentation [9, 10, 44, 55], temporal analysis [30, 43], image registration [23, 57], and tissue segmentation [8]. All the projects have been carried out in collaboration with different medical MS teams from:

- The Hospital Vall d’Hebron: Dr. Rovira, who is the director of the “Unitat de Ressonància Magnètica-Centre Vall d’Hebron” (URMVH) and has participated in numerous research projects funded by public and private institutions in the last few years, as well as Dr. Pareto and technicians Huerga and Corral. This

¹<http://vicorob.udg.edu>

group is part of the MAGNIMS network, a European network of centers that share an interest in the MS study through MRI.

- The Clínica Girona / Hospital Santa Caterina: Dr. Vilanova and Dr. Barceló are the codirectors of the "Unitat de Ressonància Magnètica" at the Clínica Girona and are members of several national and international radiology societies.
- The Hospital Josep Trueta: Dr. Ramió-Torrentà, who is the current coordinator of the "Unitat de Neuroimmunologia i Esclerosi Múltiple", as well as Drs. Robles and Beltrán, who work in the radiology unit.

1.3 Objectives

As part of the SALEM, NICOLE and BiomarkEM.cat research project frameworks, the main goal of this thesis is:

to develop a novel, fully automated brain tissue segmentation method capable of computing accurate tissue volume measurements in images of MS patients.

Different sub-objectives have to be covered first in order to fulfill the main goal. All these stages can be considered as sub-objectives that allow us to gain a better knowledge of the different parts that compose a fully automated tissue segmentation method for MS images containing lesions. In what follows, we detail these proposed sub-goals:

- **to analyze and evaluate the state of the art of tissue segmentation methods.** This stage aims to quantitatively review and evaluate the different tissue segmentation techniques proposed in order to understand their advantages and drawbacks first on images without MS lesions. In order to fulfill this goal, we plan to perform different experiments using public databases of healthy subjects that incorporate manual tissue annotations, which will allow us to perform a quantitative evaluation of the accuracy of the methods.
- **to study and evaluate the effect of WM lesions on tissue segmentation of MS patient images.** Although it is known that the inclusion of WM lesions in tissue segmentation distorts the measurements of brain volume, this effect has not been studied and compared with different tissue segmentation methods. In this respect, the second stage focuses on the analysis of the effects of WM lesions on the tissue distributions of a set of tissue segmentation

approaches. Our hypothesis here is that a better knowledge of the correlation between lesion attributes, such as signal intensity and lesion size, and the differences observed in tissue volume of the analyzed algorithms may be beneficial to design a tissue segmentation method for MS. Hence, we aim to perform several experiments using multi-center MS data from different scanners in order to analyze the effects of WM lesions on tissue segmentation.

- **to reduce the effect of WM lesions on tissue segmentation of MS patient images designing and implementing a new lesion filling algorithm.** As said in section 1.1.3, WM lesions have to be pre-processed before the tissue segmentation in order to reduce the effects of those lesions on the segmentation. In this regard, the third sub-goal is two-fold: firstly, to compare the accuracy of different lesion filling techniques proposed in the literature, analyzing their accuracy on databases with 1.5T and 3T field strengths, and secondly, after analyzing the benefits and drawbacks of each method proposed, we aim to propose a new lesion filling algorithm in order to overcome the possible limitations of existing methods.
- **to analyze and evaluate the effect of automated algorithms that perform WM lesion segmentation and filling on the tissue segmentation.** Although lesion filling techniques have already been successfully applied to reduce the effect of WM lesions on tissue segmentation, WM lesions are usually annotated manually before tissue segmentation. In contrast, the effect of both automated lesion segmentation and filling on tissue segmentation is still unclear. The fourth stage of this thesis aims to understand the effects of the inherent errors in automated lesion segmentation on the posterior lesion filling and tissue segmentation. Thus, we plan to perform several experiments with different pipelines that incorporate automated lesion segmentation, lesion filling and tissue segmentation. Using these experimental data, we aim to evaluate the accuracy of these pipelines on MS data, analyzing and evaluating the extent of the effect of remaining WM lesions on the differences in tissue segmentation, which may be beneficial in updating the knowledge gained from previous stages.
- **to propose a new, fully automated tissue segmentation method for MS patient images.** Finally, we aim to benefit from these sub-objectives to propose a novel, **fully automated tissue segmentation method** able to deal with images of MS patients with different levels of brain atrophy and lesion loads. In this last stage, we aim to validate the accuracy of the proposed method by comparing it with the state of the art in tissue segmentation in MS.

By developing a novel brain tissue segmentation method intended for MS patients' images, we refer to the tissue segmentation into GM, WM and CSF in transversal

studies. We do not concentrate on the differences in tissue volume at different stages, but on the effect of WM lesions in the final tissue segmentation. All these stages will be carried out using not only public databases but also different 1.5T and 3T databases of MS patients from the collaborating hospital centers. **Furthermore, as part of the goals of the research frameworks in which this thesis is located, implementations of all the proposed methods will be publicly available to the research community.**

1.4 Document structure

A graphic description of the structure of this thesis linking all the chapters presented is shown in Figure 1.4. Connections between the chapters depict the conceptual link between them. The rest of the document is organized as follows:

- **Chapter 2. Comparison of 10 brain tissue segmentation methods using revisited IBSR annotations.** We present here a comprehensive comparison of the accuracy of 10 brain tissue segmentation methods on two public MRI databases. This chapter is based on the paper published in the *Journal of Magnetic Resonance Imaging* in 2015.
- **Chapter 3. Evaluating the effects of white matter multiple sclerosis lesions on the volume estimation of 6 brain tissue segmentation methods.** After reviewing different tissue segmentation techniques using public data, we perform a detailed analysis of the effects of WM lesions on the brain tissue volume measurements of six of these tissue segmentation methods using MS data from different hospital centers collaborating in the research projects. This chapter is based on our paper published in the *American Journal of Neuroradiology* in 2015.
- **Chapter 4. A white matter lesion-filling approach to improve brain tissue volume measurements.** In this chapter, we propose a new technique to fill WM lesions on 1.5T and 3T data, validating its accuracy with respect to other methods in the literature. This chapter is based on the paper published in the *NeuroImage: Clinical* journal in 2014.
- **Chapter 5. Quantifying brain tissue volume in multiple sclerosis with automated lesion segmentation and filling.** In this chapter we present a detailed evaluation of the performance of different automated pipelines that incorporate lesion segmentation, lesion filling and tissue segmentation on MS data. This analysis is novel in the sense that this is the first work to evaluate two automated pipelines on MS data. This chapter is based on the paper published in the *NeuroImage: Clinical* journal in 2015.

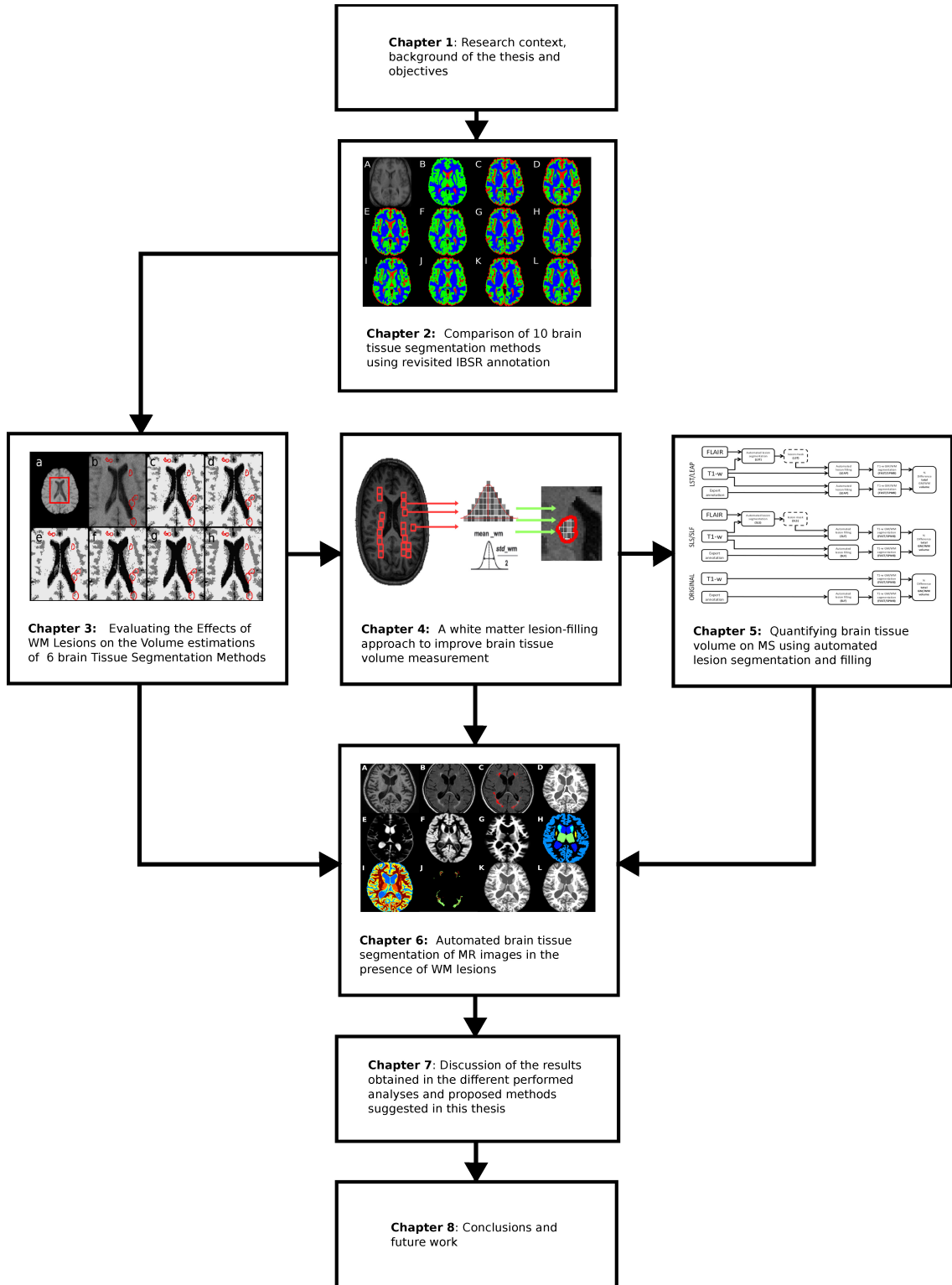


Figure 1.4: Organization of the document. Preliminary Chapter 1 describes the research context and main objectives of this thesis. Chapters 2 to 6 introduce the main contributions of this work based on the different projects submitted or published in research journals. Chapter 7 presents a general discussion of the results obtained from Chapters 2 to 6. Finally, the main conclusions and proposed future work are presented in Chapter 8. Connections between chapters depict a conceptual link between them.

- **Chapter 6. Automated brain tissue segmentation of MR images in the presence of white matter lesions.** Here we propose a new, fully automated tissue segmentation pipeline designed to deal with MS patient images containing lesions. We validate the accuracy of the proposed method comparing the performance with other state-of-the-art techniques. Data from the MRBrainS13 challenge as well as data from our hospital collaborators is used to perform the evaluation. This chapter is based on the paper submitted to the *Medical Image Analysis* journal in 2016.
- **Chapter 7. Results and discussion.** This chapter provides a comprehensive discussion of the results obtained in this thesis.
- **Chapter 8. Conclusions and future work.** Finally, the main conclusions based on the contributions of this thesis are defined. Based on these conclusions, we also point out different future work to improve and extend the work carried out in this thesis.

Chapter 2

Comparison of 10 brain tissue segmentation methods using revisited IBSR annotations

In this chapter, we perform a quantitative evaluation of the accuracy of 10 automated brain tissue segmentation methods. The methods are compared using the Internet Brain Segmentation Repository (IBSR) databases IBSR20 and IBSR18 ¹. The performance of these methods is then evaluated by ranking their accuracy based on their significant differences with respect to the other methods. This proposed evaluation has been published in the following paper:

Paper published in the **Journal of Magnetic Resonance in Medicine** (JMRI)
Volume: 41, Issue: 1, Pages: 93-101, Published: January 2015
DOI: 10.1002/jmri.24517
JCR RNMMI IF: 3.210 Q1(23/125)

¹<https://www.nitrc.org/projects/ibsr/>

Sergi Valverde, Arnau Oliver, Mariano Cabezas, Eloy Roura, Xavier Lladó. "Comparison of 10 brain tissue segmentation methods using revisited IBSR annotations". *Journal of magnetic resonance imaging*. Vol. 41, 1 (Jan. 2015) : p. 93-101

First published: 24 January 2014

DOI: <http://dx.doi.org/10.1002/jmri.24517>

<http://onlinelibrary.wiley.com/doi/10.1002/jmri.24517/full>

ABSTRACT

Purpose

Ground-truth annotations from the well-known *Internet Brain Segmentation Repository*(IBSR) datasets consider Sulcal cerebrospinal fluid (SCSF) voxels as gray matter. This can lead to bias when evaluating the performance of tissue segmentation methods. In this work we compare the accuracy of 10 brain tissue segmentation methods analyzing the effects of SCSF ground-truth voxels on accuracy estimations.

Materials and Methods

The set of methods is composed by FAST, SPM5, SPM8, GAMIXTURE, ANN, FCM, KNN, SVPASEG, FANTASM, and PVC. Methods are evaluated using original IBSR ground-truth and ranked by means of their performance on pairwise comparisons using permutation tests. Afterward, the evaluation is repeated using IBSR ground-truth without considering SCSF.

Results

The Dice coefficient of all methods is affected by changes in SCSF annotations, especially on SPM5, SPM8 and FAST. When not considering SCSF voxels, SVPASEG (0.90 ± 0.01) and SPM8 (0.91 ± 0.01) are the methods from our study that appear more suitable for gray matter tissue segmentation, while FAST (0.89 ± 0.02) is the best tool for segmenting white matter tissue.

Conclusion

The performance and the accuracy of methods on IBSR images vary notably when not considering SCSF voxels. The fact that three of the most common methods (FAST, SPM5, and SPM8) report an important change in their accuracy suggest to consider these differences in labeling for new comparative studies.

Chapter 3

Evaluating the effects of white matter multiple sclerosis lesions on the volume estimation of 6 brain tissue segmentation methods

In this chapter, we present a study of the impact of MS white matter lesions on the brain tissue measurements of six well-known segmentation techniques. These include straightforward techniques such as Artificial Neural Network (ANN) and fuzzy C-means (FCM) as well as more advanced techniques like the Fuzzy And Noise Tolerant Adaptive Segmentation Method (FANTASM), FMRIB's Automated Segmentation Tool (FAST), and Statistical Parametric Mapping (SPM) with versions SPM5 and SPM8. This proposed evaluation has been published in the following paper:

<p>Paper published in the American Journal of Neuroradiology (AJNR) Volume: 36, Pages: 1109-1115, Published: February 2015 DOI: 10.3174/ajnr.A4262 JCR RNMMI IF 3.589, Q1(19/125)</p>
--

Evaluating the Effects of White Matter Multiple Sclerosis Lesions on the Volume Estimation of 6 Brain Tissue Segmentation Methods

S. Valverde,  A. Oliver, Y. Díez, M. Cabezas, J.C. Vilanova, L. Ramió-Torrentà, À. Rovira, and X. Lladó



ABSTRACT

BACKGROUND AND PURPOSE: The accuracy of automatic tissue segmentation methods can be affected by the presence of hypointense white matter lesions during the tissue segmentation process. Our aim was to evaluate the impact of MS white matter lesions on the brain tissue measurements of 6 well-known segmentation techniques. These include straightforward techniques such as Artificial Neural Network and fuzzy C-means as well as more advanced techniques such as the Fuzzy And Noise Tolerant Adaptive Segmentation Method, fMRI of the Brain Automated Segmentation Tool, SPM5, and SPM8.

MATERIALS AND METHODS: Thirty T1-weighted images from patients with MS from 3 different scanners were segmented twice, first including white matter lesions and then masking the lesions before segmentation and relabeling as WM afterward. The differences in total tissue volume and tissue volume outside the lesion regions were computed between the images by using the 2 methodologies.

RESULTS: Total gray matter volume was overestimated by all methods when lesion volume increased. The tissue volume outside the lesion regions was also affected by white matter lesions with differences up to 20 cm³ on images with a high lesion load (≈ 50 cm³). SPM8 and Fuzzy And Noise Tolerant Adaptive Segmentation Method were the methods less influenced by white matter lesions, whereas the effect of white matter lesions was more prominent on fuzzy C-means and the fMRI of the Brain Automated Segmentation Tool.

CONCLUSIONS: Although lesions were removed after segmentation to avoid their impact on tissue segmentation, the methods still overestimated GM tissue in most cases. This finding is especially relevant because on images with high lesion load, this bias will most likely distort actual tissue atrophy measurements.

ABBREVIATIONS: ANN = Artificial Neural Network; FANTASM = Fuzzy And Noise Tolerant Adaptive Segmentation Method; FAST = FMRI Automated Segmentation Tool; FCM = fuzzy C-means; H1 = Hospital Vall d'Hebron, Barcelona, Spain; H2 = Hospital Universitari Dr. Josep Trueta, Girona, Spain; H3 = Clinica Girona, Girona, Spain; WML = white matter lesion


During the past few years, MR imaging brain tissue segmentation techniques have become important tools in the clinical evaluation and progression of MS because they make it possible to measure the changes in brain atrophy and lesion load.^{1–3} However, white matter lesions (WMLs) can significantly affect tissue volume measurements if these lesions are included in the segmentation process.^{4–6} Several studies have analyzed the effects of WMLs on brain tissue measurements of common segmentation

techniques such as SPM5 (<http://www.fil.ion.ucl.ac.uk/spm/>)⁷ and FMRI Automated Segmentation Tool (FAST, <http://fsl.fmrib.ox.ac.uk/fsl/fslwiki/FAST>).⁸ Chard et al⁵ studied the effect of synthetic lesions on SPM5 segmentations for different WML voxel intensities (from 30% to 90% of normal WM intensity) and lesion loads (from 10 to 20 cm³). The authors reported that GM volume was overestimated by $\approx 2.3\%$, whereas WM tissue was underestimated by $\approx 3.6\%$ in scans with 15 cm³ of simulated lesions. More recently, Battaglini et al⁴ also analyzed the effects of different WML intensities and lesion loads on tissue measurements obtained with FAST software. The authors showed again that total GM volume tended to increase with higher lesion loads in segmented images with generated simulated lesions. Gelineau-Morel et al⁶ performed a similar study on the effects of simulated and real WMLs but on tissue volume measurements outside lesion regions. The authors reported that on images with simulated lesions, FAST clearly underestimated GM outside lesion regions as long as lesion volume increased and lesion intensities approximated those of GM tissue. The incidence of

Received August 19, 2014; accepted after revision December 20.

From the Computer Vision and Robotics Group (S.V., A.O., Y.D., X.L.), University of Girona, Campus Montilivi, Girona, Spain; Girona Magnetic Resonance Center (J.C.V.), Girona, Spain; Multiple Sclerosis and Neuroimmunology Unit (L.R.-T.), Dr. Josep Trueta University Hospital, Institut d'Investigació Biomèdica de Girona, Girona, Spain; and Magnetic Resonance Unit (M.C., A.R.), Department of Radiology, Vall d'Hebron University Hospital, Barcelona, Spain.

Please address correspondence to Sergi Valverde, Ed. P-IV, Campus Montilivi, University of Girona, 17071 Girona, Spain; e-mail: svalverde@eia.udg.edu

 Indicates open access to non-subscribers at www.ajnr.org

<http://dx.doi.org/10.3174/ajnr.A4262>

WMLs on real scans was smaller, but FAST still tended to underestimate GM with increasing lesion loads.

On the other hand, various studies have also analyzed the correlation between brain tissue atrophy and MS disability progression.^{9,10} These studies showed a brain atrophy decrease rate between 0.3% and 0.5% of change in brain parenchyma per year in patients with MS,^{9,10} with a decrease in GM and WM volume of up to 0.4% and 0.2% per year, respectively.¹⁰ This statement along with study results such as those found by Battaglini et al⁴ and Gelineau-Morel et al⁶ indicates that a portion of brain atrophy could be hidden by the inclusion of WMLs on tissue segmentation.

In this study, we performed a quantitative evaluation of the effects of WMLs on brain tissue volume measurements to analyze the extent to which tissue estimations are affected by changes in WML volume and intensity. In contrast to other similar studies,^{4–6} our analysis extended the number of segmentation methods involved, offering a comparative evaluation of the effects of WMLs on the volume measurements of 6 segmentation methods. Furthermore, given the reported correlation between brain atrophy rates and disability progression,^{9,10} it can be clinically relevant for the MS community to extend the analysis of the effects of simulated WML to real data of patients with MS; hence, our analysis was focused exclusively on data from the T1-weighted images from patients with clinically confirmed MS.

MATERIALS AND METHODS

Image Acquisition

The dataset consisted of 30 MR images from patients with clinically confirmed MS at 3 different hospitals (Fig 1). Each patient underwent MR imaging by using the same protocol (T1-weighted, T2-weighted, proton-attenuation-weighted, and FLAIR images), though a different scanner was used at each hospital. Ten patient images from Hospital Vall d'Hebron, Barcelona, Spain, (H1) were acquired on a 1.5T Magnetom Symphony Quantum (Siemens, Erlangen, Germany), with 2D conventional spin-echo T1-weighted (TR, 450 ms; TE, 17 ms), dual-echo proton-attenuation T2-weighted sequences (TR, 3750 ms; TE, 14/86 ms), and FLAIR sequences (TR, 9000 ms; TE, 114 ms; and TI, 2500 ms). Ten patient images from Hospital Universitari Dr. Josep Trueta, Girona, Spain, (H2) were acquired on a 1.5T Intera scanner (R12) (Philips Healthcare, Best, the Netherlands) with 2D conventional spin-echo T1-weighted (TR, 653 ms; TE, 14 ms), dual-echo proton-attenuation T2-weighted (TR, 2800 ms; TE, 16/80 ms), and FLAIR sequences (TR, 8153 ms; TE, 105 ms; and TI, 2200 ms). Ten patient images from Clinica Girona, Girona, Spain, (H3) were acquired on a 1.5T Signa HDxt scanner (GE Healthcare, Milwaukee, Wisconsin) with 3D fast-spoiled gradient T1-weighted (TR, 30 ms; TE, 9 ms; flip-angle, 30°), fast spin-echo T2-weighted (TR, 5000–5600 ms; TE, 74–77 ms), proton-attenuation-weighted (TR, 2700 ms; TE, 11.9 ms), and FLAIR sequences (TR, 9002 ms; TE, 80 ms; and TI, 2250 ms). All images were acquired in the axial view with a section thickness of 3 mm.

Images of Patients with MS

WML masks were semiautomatically delineated from proton-attenuation-weighted images by using Jim software (Xinapse Systems,

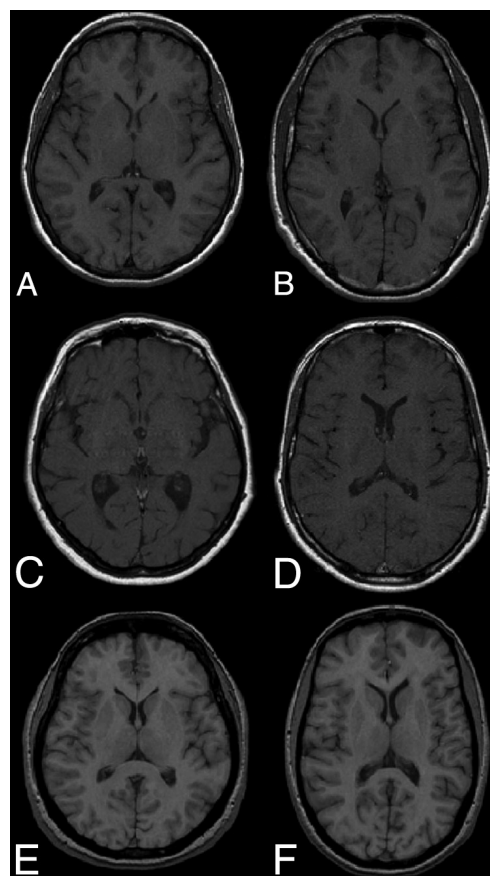


FIG 1. T1-weighted images from the 3 hospitals and scanners involved in the study: 1.5T Magnetom Symphony Quantum (Siemens) from H1 (first row), 1.5T Intera (R12) (Philips) from H2 (middle row), and 1.5T Signa HDxt (GE Healthcare) from H3 (last row).

<http://www.xinapse.com/home.php>) by expert radiologists at each hospital. Then, the proton-attenuation-weighted images and lesion masks were coregistered with T1-weighted images by affine registration.¹¹ The average means and SD lesion volumes for H1, H2, and H3 were $4.15 \pm 4.35 \text{ cm}^3$ (minimum = 0.11, maximum = 11.22 cm^3), $21.79 \pm 17.79 \text{ cm}^3$ (minimum = 0.18, maximum = 52.45 cm^3), and $4.78 \pm 4.60 \text{ cm}^3$ (minimum = 0.43, maximum = 16.34 cm^3).

All T1-weighted patient images were processed following the same pipeline (Fig 2). Internal skull-stripping and intensity-correction options were disabled on SPM5, SPM8 (<http://www.fil.ion.ucl.ac.uk/spm/software/>), and FAST. Instead, to reduce the differences in brain area and signal image intensity produced by different preprocessing tools, we skull-stripped all images by using the Brain Extraction Tool (<http://fsl.fmrib.ox.ac.uk/fsl/fslwiki/BET>)¹² and intensity-corrected them by using N3.¹³

As a second step, 2 sets were produced from preprocessed images: an original set that included WMLs as part of current tissue and a masked set in which the WMLs were masked out before tissue segmentation and relabeled as WM after, following the same procedure used by radiologists of the 3 hospitals.

Segmentation Methods

The set of methods was composed of 6 well-known automatic brain tissue segmentation techniques: Artificial Neural Network (ANN), fuzzy C-means (FCM), Fuzzy And Noise Tolerant Adaptive Segmentation Method (FANTASM), FAST, SPM5, and

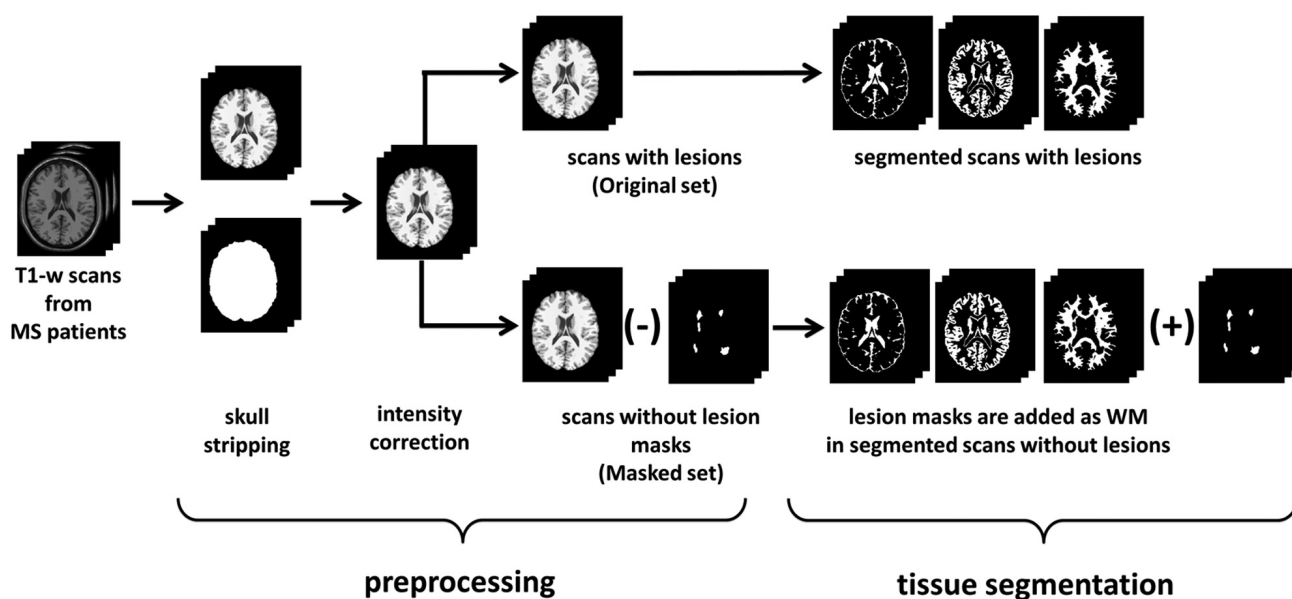


FIG 2. Our pipeline approach. From the 30 T1-weighted scans of patients with MS, nonbrain parts are stripped and brain voxels are corrected for intensity inhomogeneities. From the same corrected set (original), a new set is generated by removing WML masks from scans before segmentation (masked). The scans of both sets are segmented into 1 of the 3 tissue classes (GM, WM, and CSF). Lesion voxels are added as WM after segmentation on masked images.

SPM8. ANN and FCM were implemented for our study, while the rest of the methods were obtained from available repositories. The ANN method is based on self-organizing maps, also known as Kohonen networks.¹⁴ ANN was implemented for our study by using the Matlab 7.12 environment (MathWorks, Natick, Massachusetts) following the technique proposed by Tian et al.¹⁵ FCM¹⁶ and FANTASM¹⁷ are both based on fuzzy-clustering techniques. FCM implements the classic fuzzy-clustering approach, while FANTASM adds neighboring information to increment the robustness of the method to intensity inhomogeneity artifacts and noise. FCM was also implemented by using the Matlab environment and following the technique described in Pham,¹⁶ in which clusters were initialized according to Bezdek et al.¹⁸ FANTASM is included in the MIPAV toolbox (<http://mipav.cit.nih.gov>). FAST⁸ guides the segmentation with spatial information through the optimization of Hidden Markov Random Fields, and the method is included in the fMRI of the Brain Software Library toolbox (<http://fsl.fmrib.ox.ac.uk/fsl/fslwiki/>). SPM5 and SPM8⁷ are based on an iterative Gaussian Mixture Model optimization, weighting the probability of belonging to a certain tissue class with a priori spatial information from tissue-probability atlases. However, SPM8 comes with a set of different characteristics to improve registration and tissue segmentation. Both methods are included in the SPM8 toolbox (<http://www.fil.ion.ucl.ac.uk/spm/software/spm8>). All methods were run with default parameters.

Evaluation

Images from both the original and masked sets were segmented into GM, WM, and CSF tissue classes by using the 6 presented segmentation methods. Then, we computed the normalized tissue volumes as the number of voxels classified as GM, WM, and CSF, respectively, divided by the total number of voxels. Three different analyses were performed on these data. First, we analyzed how lesion voxels were classified by each segmentation

method to establish to what extent the tissue volumes reported by each algorithm on the original and masked images could be expected to be different. Second, we analyzed the direct effect of lesions in the global volume estimation by computing the differences in total tissue volume as the percentage of change between original and masked images. For example, in the case of GM tissue:

$$\%GM = \frac{NGMV_{\text{Original}} - NGMV_{\text{Masked}}}{NGMV_{\text{Masked}}} \times 100,$$

where $NGMV_{\text{Original}}$ and $NGMV_{\text{Masked}}$ stand for the normalized gray matter volumes of original and masked images, respectively. Third, we also investigated the indirect effects of lesions in the rest of the tissue volume outside lesion regions. These are tissue volume estimations that incorporate lesions in the segmentation process but do not consider them when the volume is evaluated.

Statistical Analysis

The correlation among factors (differences in tissue volume, lesion load, and lesion intensity) was calculated by using Pearson linear correlation coefficient (r). The significance level α was set at .05. This level was used both for confidence interval computation and 95% significance hypothesis 2-tailed t tests. All statistical analyses were calculated by using the Matlab environment.

RESULTS

Lesion Classification

Figure 3 depicts the percentage of WML voxels classified either as WM (Fig 3, top) or GM (Fig 3, bottom). Percentages are detailed for each segmentation method and hospital. The amount of WMLs that were classified as GM varied for each method, mostly due to the differences among algorithms. Figure 4 illustrates the differences among methods by showing the output classification performed by each of the 6 segmentation methods.

Observed differences in the percentage of classified WML vox-

els as GM and WM between hospitals can be attributed to each particular scanner acquisition configuration that defines the tissue signal-intensity distributions. The distance between WML and WM mean signal intensities was highest in H3 as computed by each of the 6 methods (range, from $89.2 \pm 4.45\%$ to $92.22 \pm 4.45\%$ of WML mean signal intensity with respect to WM) and was lowest in H2 (range, from $95.3 \pm 1.76\%$ to $100.34 \pm 6.39\%$). As shown in Fig 1, there is a better contrast between GM and WM tissue on the H3 images compared with the H1 and H2 images.

The correlation between the percentage of lesion classification and lesion size was not significant in all cases ($r < 0.33$, $P > .05$). In contrast, the percentage of WML classified as GM or WM and the distance between the mean WML and WM signal intensities showed a moderate correlation in all hospitals ($r > 0.6$, $P < .01$). On the basis of our data, the contrast between tissues computed as the normalized difference between the mean GM and WM signal intensity distributions was correlated with the distance between the WM and WML mean signal intensities ($r = 0.6$, $P < .001$).

Differences in Total Tissue Volume Estimation

The mean percentage differences in total tissue volume between the original and masked images are presented in Table 1. All methods overestimated GM tissue in original scans, regardless of

the hospital, but the overestimation was increased in H2 compared with H1 and H3 due to greater lesion volumes in H2. The differences among methods for the same hospital and tissue were also significantly greater in H2 than in H1 and H3. Abnormally low mean and high SD values observed in SPM5 for both GM (0.10 ± 2.68) and WM (1.04 ± 3.01) in H2 were caused by 2 patients who exhibited very high opposite differences between their respective original and masked images, decreasing the overall mean difference and increasing the SD.

Correlation between the differences in total mean tissue volume and lesion size was significant in all hospitals: Lesion size had a direct effect on tissue segmentation. Table 2 shows the Pearson correlation values obtained between differences in tissue volume and lesion size across methods. All methods except SPM5 presented a positive correlation in GM and a negative correlation in WM in H1 and H2. SPM5 correlated in H1 but not in H2, where it was influenced by abnormal values in the 2 images with highest lesion load. In H3, only FCM, FANTASM, and FAST were positively correlated in GM and negatively correlated in WM. The correlation coefficients for ANN, SPM5, and SPM8 in H3 were weak and not significant in GM and WM.

Volume Estimation of Tissue Outside Lesion Regions

The mean percentage differences in tissue volume outside lesion regions between original and masked images are presented in Table 3. The differences between the images segmented with lesions and images in which the lesions were masked before tissue segmentation were again higher in H2, and the methods still substantially overestimated the GM outside the lesion regions to the detriment of WM, even though analyzed tissues were free of lesion regions. In contrast, only SPM5 and SPM8 reported a noticeable underestimation of GM in H3, also to the detriment of WM.

Differences in tissue volume outside the lesion regions correlated with lesion size for all tissues and hospitals, indicating an effect of lesion size not only on lesion voxels but also on tissue that is not affected by lesions. Table 4 presents the correlation values obtained across methods. In H1, there was a remarkable correlation for ANN, FCM, FANTASM, and FAST in all tissues. The obtained values for SPM8 were also significant in GM and CSF. In H2, the correlation was significant in ANN, FCM, and FANTASM in all tissues. In H3, only FCM and FAST showed a significant correlation in all tissues, whereas FCM, FAST, SPM5, and SPM8 correlated significantly only in WM. All methods except SPM5 and SPM8 reported a significant correlation for CSF.

DISCUSSION

Previous studies have shown that the range of voxel signal intensities composing each of the tissue distributions can be altered by WMLs if these voxels are included in the segmentation process.^{4,5} Lesion load and the apparent lesion signal intensity lead to observed changes in tissue segmentation in original images.

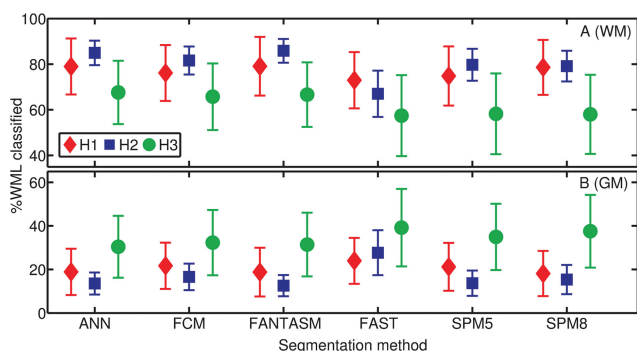


FIG 3. Percentage of voxels in WML regions having been classified as GM (top) and WM (bottom) for each segmentation method and hospital, H1 (◇), H2 (□) or H3 (○). Reported values are means and SDs.

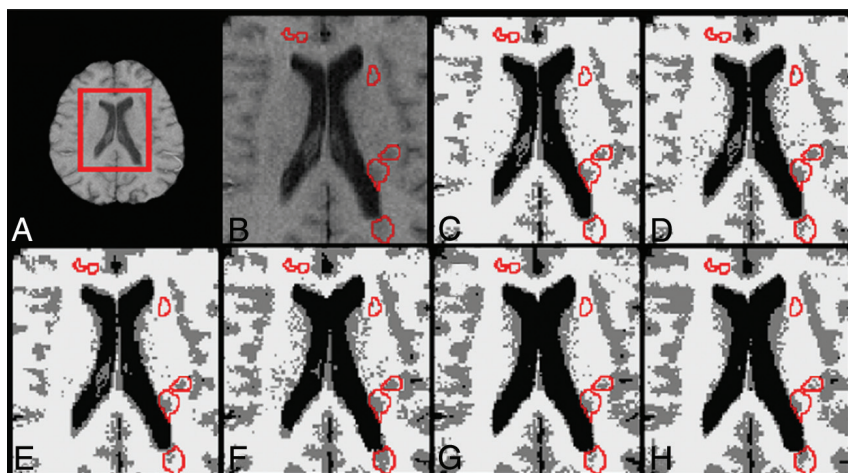


FIG 4. Classification output returned by each segmentation method on the same image. A, T1-weighted scan. B, Zoomed part of the scan with lesions outlined in red. Brain tissue segmentation outputs also with lesions outlined for ANN (C), FCM (D), FANTASM (E), FAST (F), SPM5 (G), and SPM8 (H). C–H, Segmented GM tissue is represented in gray; WM, in white; and CSF, in black.

Table 1: Average percentage of change in total tissue volume estimation between original and masked images^a

Method	H1			H2			H3		
	GM	WM	CSF	GM	WM	CSF	GM	WM	CSF
ANN	0.33 ± 0.42	-0.23 ± 0.28	0.11 ± 0.11	1.59 ± 1.37	-0.56 ± 0.46	0.78 ± 0.76	0.25 ± 0.31	-0.16 ± 0.28	-0.09 ± 0.09
FCM	0.28 ± 0.37	-0.22 ± 0.29	0.09 ± 0.11	2.28 ± 2.26	-0.90 ± 0.83	0.94 ± 0.90	0.28 ± 0.23	-0.25 ± 0.20	0.08 ± 0.09
FANTASM	0.23 ± 0.26	-0.18 ± 0.21	0.08 ± 0.08	1.34 ± 1.13	-0.49 ± 0.37	0.80 ± 0.73	0.26 ± 0.22	-0.24 ± 0.19	0.07 ± 0.08
FAST	0.29 ± 0.36	-0.29 ± 0.36	0.12 ± 0.13	1.92 ± 1.59	-1.28 ± 1.03	0.47 ± 0.39	0.34 ± 0.28	-0.37 ± 0.31	0.12 ± 0.17
SPM5	0.20 ± 0.30	-0.21 ± 0.20	-0.14 ± 0.54	0.10 ± 2.68	-1.04 ± 3.01	0.53 ± 0.51	0.04 ± 0.17	-0.18 ± 0.36	0.15 ± 0.23
SPM8	0.08 ± 0.09	-0.08 ± 0.08	-0.04 ± 0.18	0.55 ± 0.34	-0.93 ± 0.55	0.54 ± 0.42	0.09 ± 0.15	-0.23 ± 0.25	0.17 ± 0.23

^a The results are divided by tissue and hospital. Reported values are the means ± SD. Positive values indicate a tissue overestimation on original images compared with masked.

Table 2: Pearson correlation coefficients between method differences in total volume estimation and WML size^a

Method	GM	WM	CSF
H1			
ANN	0.94	-0.90	0.89
FCM	0.93	-0.89	0.83
FANTASM	0.87	-0.80	0.78
FAST	0.97	-0.97	0.96
SPM5	0.58 ^b	-0.89	-0.21 ^b
SPM8	0.92	-0.63	-0.69
H2			
ANN	0.91	-0.88	0.93
FCM	0.92	-0.94	0.92
FANTASM	0.89	-0.87	0.84
FAST	0.95	-0.96	0.82
SPM5	-0.35 ^b	-0.06 ^b	0.72
SPM8	0.76	-0.79	0.57 ^b
H3			
ANN	0.56 ^b	-0.55 ^b	0.88
FCM	0.77	-0.84	0.88
FANTASM	0.74	-0.82	0.85
FAST	0.88	-0.94	0.92
SPM5	-0.06 ^b	-0.03 ^b	0.21 ^b
SPM8	0.56 ^b	-0.48 ^b	0.09 ^b

^a Correlation was computed for each method and hospital separately. All values were found to be significant (*P* value < .05) unless otherwise noted.

^b Not significant.

For instance, if a portion of the lesion voxels is classified as WM, the mean overall WM intensity decreases, shifts WM boundaries into darker intensities, and narrows GM tissue distribution.^{4,6} Voxels that should have been classified as GM are assigned to WM, increasing the WM volume estimation and decreasing GM volume. If some of the WML voxels are classified as GM, the apparent GM mean intensity increases and the WM tissue distribution narrows. This change occurs because voxels that are theoretically classified as WM are assigned to GM, increasing GM estimation against a lower WM volume estimation.

We compare our results with those in previous studies regarding the effects of WMLs on brain tissue volume measurements. However, given the differences in image data, criterion standards, simulated lesions, and lesion voxel intensities among studies, a direct comparison further than an analysis of trends with similar WML intensities and lesion loads should be carefully performed. Our experiments follow the same trend presented by Battaglini et al,⁴ and both studies show that FAST overestimates total GM volume on images segmented with lesions. Similarly, our results also coincide with those found by Chard et al⁵ in simulated data, and in both studies, SPM5 overestimated GM tissue on images with lesions. In contrast, our results appear to be inconsistent with those reported by Gelineau-Morel et al.⁶ These studies showed a significant correlation between WML intensity and an underesti-

mation of GM volume outside the lesions, especially when the lesions had intensities similar to those of the mean GM. The observed differences are caused by distinct signal-intensity profiles of WMLs in each study. In the case of Gelineau-Morel et al,⁶ the WML signal intensities were noticeably more hypointense compared with our data. The probability of voxels to be classified as GM dropped as a result of the influence of hypointense WML intensities in tissue distributions. Part of WML voxels with a signal intensity similar to that of GM were still classified as WM, reducing the signal intensity threshold between GM and WM. As a result, most of the partial volume voxels with signal intensity in the boundary between GM and WM were classified as WM, artificially reducing the overall number of GM voxels.

Our results show that the classification of WML regions is highly dependent on lesion voxel signal intensities and the variation of their signal intensity in terms of the WM signal distribution. Lesion segmentation is clearly determined by this variation because the probability of WML voxels being classified as WM will be higher as long as WML intensities resemble those of WM. However, the signal-intensity contrast among tissues also plays an important role because it can influence the amount of WML voxels that are classified as GM or WM. As long as the contrast among distributions increases, more lesion voxels will be added into the GM distribution. Although the main factor in the observed differences in tissue volume across methods is caused by lesion volume, the percentage of lesion voxels that are classified as GM and WM might also be a remarkable factor in the observed tissue-volume differences, especially in images with high lesion loads. Therefore, the relationship between image quality and lesion load also might have to be considered to explain the differences in tissue volume.

SPM8 was the method with the lowest difference in total tissue volume between original and masked images. In contrast, FAST was the method that was more affected by lesions. In general, all methods overestimated GM in original scans, though values were more significant in H2 than H1 and H3 due to higher lesion loads in H2. In H1 and H3, most of the underestimated WM was shifted into GM. The small percentage of lesions that were segmented as CSF, especially the low lesion volume, limited the impact of WML voxels on the overall CSF tissue distribution of original images.

SPM8 and FANTASM were the methods with the lowest incidence of WML in tissue volume measurements outside lesion regions, while FCM and FAST showed the largest differences among all methods. Lesion volume also explains the limited effect of WML on tissue segmentation outside lesion regions in H1 and H3, compared with images with higher lesion loads such as the H2 images. In H1 and H3, although the behavior differs slightly for

Table 3: Average percentage change in the volume estimation of tissue outside the lesion regions between original and masked scans^a

Method	H1			H2			H3		
	GM	WM	CSF	GM	WM	CSF	GM	WM	CSF
ANN	0.15 ± 0.26	−0.10 ± 0.18	0.07 ± 0.08	0.70 ± 0.61	−0.31 ± 0.24	0.67 ± 0.69	−0.01 ± 0.28	0.04 ± 0.24	−0.12 ± 0.08
FCM	0.09 ± 0.16	−0.07 ± 0.13	0.05 ± 0.08	1.27 ± 1.69	−0.56 ± 0.62	0.82 ± 0.81	0.01 ± 0.03	−0.03 ± 0.05	0.05 ± 0.07
FANTASM	0.06 ± 0.05	−0.05 ± 0.05	0.03 ± 0.05	0.48 ± 0.48	−0.25 ± 0.18	0.68 ± 0.63	0.00 ± 0.04	−0.02 ± 0.05	0.04 ± 0.07
FAST	0.08 ± 0.14	−0.09 ± 0.14	0.07 ± 0.08	0.56 ± 0.87	−0.45 ± 0.64	0.22 ± 0.33	0.02 ± 0.07	−0.06 ± 0.13	0.08 ± 0.16
SPM5	0.06 ± 0.25	0.02 ± 0.13	−0.19 ± 0.54	−0.29 ± 2.61	−0.47 ± 2.91	0.21 ± 0.32	−0.20 ± 0.24	0.23 ± 0.34	0.06 ± 0.15
SPM8	−0.03 ± 0.06	0.09 ± 0.15	−0.10 ± 0.23	0.13 ± 0.30	−0.29 ± 0.33	0.25 ± 0.26	−0.15 ± 0.12	0.14 ± 0.15	0.10 ± 0.20

^a The results are divided by hospital and tissue. Reported values are the means ± SD. Positive values indicate a tissue overestimation on original images compared with masked.

Table 4: Pearson correlation coefficients among method differences in volume estimation of tissue outside the lesion regions and WML size^a

Method	GM	WM	CSF
H1			
ANN	0.77	−0.74	0.83
FCM	0.82	−0.80	0.71
FANTASM	0.80	−0.73	0.66
FAST	0.86	−0.93	0.97
SPM5	0.11	0.51 ^b	−0.30 ^b
SPM8	−0.57 ^b	0.95	−0.77
H2			
ANN	0.85	−0.92	0.93
FCM	0.71	−0.84	0.94
FANTASM	0.66	−0.82	0.87
FAST	0.33 ^b	−0.46 ^b	0.62 ^b
SPM5	−0.43 ^b	0.18 ^b	0.65 ^b
SPM8	0.16 ^b	−0.37 ^b	0.30 ^b
H3			
ANN	0.07	−0.16 ^b	0.79
FCM	0.50	−0.77	0.89
FANTASM	0.17	−0.57 ^b	0.87
FAST	0.45	−0.73	0.89
SPM5	−0.78 ^b	0.72	0.14 ^b
SPM8	−0.64 ^b	0.72	−0.01 ^b

^a Correlation was computed for each method and hospital separately. All values were found to be significant (*P* value < .05) unless otherwise noted.

^b Not significant.

each method, the differences in tissues outside the lesion regions are very small.

The differences outside the lesion regions are especially important because they highlight the bias introduced by WMLs on the estimation of tissue volume that is not pathologically affected. If one compares the results between total tissue volume and tissue volume outside lesion regions, it can be observed that an important part of the overestimated total GM is essentially derived from the same hypointense WML voxels that are classified as GM. Moreover, it is important to highlight the differences in the algorithms. Methods such as FCM and ANN, which only rely on signal intensity, introduce more errors in tissue segmentation compared with methods such as SPM8 and SPM5, which incorporate spatial information. This reinforces the necessity for selecting a segmentation algorithm that does not depend on signal intensity only. However, even though WML voxels have not been considered for computing tissue volume outside the lesion regions, there is still a clear tendency toward overestimating GM. On images with a high lesion load, the observed differences in GM volume outside lesion regions reach values that are equivalent to the yearly expected GM atrophy.^{9,10} Following these assumptions, SPM8, FANTASM, and SPM5 are the methods with the lowest reported incidence of

WML on brain tissue volume measurements, especially on images with a high lesion load.

The present study is not free of limitations. The principal limitation is the lack of tissue expert annotations, given that the study incorporated a relatively large number of images from 3 different hospitals and this task was time-consuming. A second limitation of the study is the sensitivity of the tissue segmentation methods to changes in the skull-stripping mask. Errors in the brain mask may lead to the inclusion of blood vessels such as the internal carotid arteries with hyperintense signal intensity, which might bias the tissue distributions. A final limitation of the study is the inherent difficulty of comparing previous studies, given the differences in the scanner protocols used to acquire the images of patients with MS. The differences in the acquisition protocol may cause the observed differences in the lesion intensity profile compared with previous works.^{8,10} Our study shows that such an intensity profile introduces variations in GM and WM tissue distributions.

CONCLUSIONS

The results of this study indicate a direct relationship between the differences in brain tissue volume and changes in lesion load and WML intensity. Of the analyzed methods, SPM8 exhibited the lowest incidence of WMLs in volume estimation, whereas FCM yielded the highest GM overestimation. Furthermore, all methods were affected by WMLs in tissue volume outside the lesion regions. SPM8 and FANTASM exhibited the lowest differences in tissue volume outside the lesion regions, whereas the influence of WMLs outside the lesion regions is more important in methods such as FCM and FAST. The latter results are especially important because even when masking lesions after segmentation to avoid the inclusion of lesion voxels segmented as GM into the volume estimation, the methods tend to overestimate GM tissue on images segmented with lesions. On images with high lesion load, this bias might conceal or falsify part of the GM and WM tissue atrophy.

Disclosures: Sergi Valverde—RELATED: Grant: FI-DGR2013 research grant from the Generalitat de Catalunya. Mariano Cabezas—RELATED: holds a 2014 European Committee for Treatment and Research in Multiple Sclerosis—Magnetic Resonance Imaging in MS research fellowship.

REFERENCES

1. Lladó X, Oliver A, Cabezas M, et al. Segmentation of multiple sclerosis lesions in brain MRI: a review of automated approaches. *Information Sciences* 2012;186:164–85
2. Lladó X, Ganiler O, Oliver A, et al. Automated detection of multiple sclerosis lesions in serial brain MRI. *Neuroradiology* 2012;54:787–807

3. Zivadinov R, Bergsland N, Dolezai O, et al. **Evolution of cortical and thalamus atrophy and disability progression in early relapsing-remitting MS during 5 years.** *AJNR Am J Neuroradiol* 2013;34:1931–39
4. Battaglini M, Jenkinson M, De Stefano N. **Evaluating and reducing the impact of white matter lesions on brain volume measurements.** *Hum Brain Mapp* 2012;33:2062–71
5. Chard DT, Jackson JS, Miller DH, et al. **Reducing the impact of white matter lesions on automated measures of brain gray and white matter volumes.** *J Magn Reson Imaging* 2010;32:223–28
6. Gelineau-Morel R, Tomassini V, Jenkinson M, et al. **The effect of hypointense white matter lesions on automated gray matter segmentation in multiple sclerosis.** *Hum Brain Mapp* 2012;33:2802–14
7. Ashburner J, Friston K. **Unified segmentation.** *Neuroimage* 2005;26:839–51
8. Zhang Y, Brady M, Smith S. **Segmentation of brain MR images through a hidden Markov random field model and the expectation-maximization algorithm.** *IEEE Trans Med Imaging* 2001;20:45–57
9. Horsfield MA, Rovaris M, Rocca MA, et al. **Whole-brain atrophy in multiple sclerosis measured by two segmentation processes from various MRI sequences.** *J Neurol Sci* 2003;216:169–77
10. Rudick RA, Lee JC, Nakamura K, et al. **Gray matter atrophy correlates with MS disability progression measured with MSFC but not EDSS.** *J Neurol Sci* 2009;282:106–11
11. Rueckert D, Sonoda LI, Hayes C, et al. **Nonrigid registration using free-form deformations: application to breast MR images.** *IEEE Trans Med Imaging* 1999;18:712–21
12. Smith SM. **Fast robust automated brain extraction.** *Hum Brain Mapp* 2002;17:143–55
13. Sled JG, Zijdenbos AP, Evans CP. **A nonparametric method for automatic correction of intensity nonuniformity in MRI data.** *IEEE Trans Med Imaging* 1997;17:87–97
14. Kohonen T. **The self-organizing map.** *Proceedings of the IEEE* 1990;78:1464–80
15. Tian D, Fan L. **A brain MR images segmentation method based on SOM neural network.** In: *Proceedings of the 1st International Conference on Bioinformatics and Biomedical Engineering ICBBE*, Wuhan, People's Republic of China. July 6–8, 2007:686–89
16. Pham DL. **Spatial models for fuzzy clustering.** *Computer Vision and Image Understanding* 2001;84:285–97
17. Pham DL. **Robust fuzzy segmentation of magnetic resonance images.** In: *Proceedings of the Fourteenth IEEE Symposium on Computer-Based Medical Systems*, Bethesda, Maryland. July 26–27, 2001:127–31
18. Bezdek, JC, Keller J, Krishnapuram R, et al. *Fuzzy Models and Algorithms for Pattern Recognition and Image Processing.* Norwell: Kluwer Academic Publishers; 1999:1650.F89

Chapter 4

A white matter lesion-filling approach to improve brain tissue volume measurements

In this chapter, we propose a new technique to fill WM lesions before the tissue segmentation. The proposed approach is evaluated in both 1.5T and 3T data. We validate our method comparing its accuracy with other proposed automated lesion filling methods on the same data. Furthermore, the proposed technique has been released for public use both as a standalone program or as an SPM8/SPM12 library. This work has been published in the following paper:

<p>Paper published in the NeuroImage: Clinical journal (NICL) Volume: 6, Pages: 86-92, Published: August 2014 DOI: 10.1016/j.nicl.2014.08.016 JCR N IF 2.526, Q2(6/14)</p>



A white matter lesion-filling approach to improve brain tissue volume measurements



Sergi Valverde^{a,*}, Arnau Oliver^a, Xavier Lladó^a

^aComputer Vision and Robotics Group, University of Girona, Campus Montilivi, Ed. P-IV, Girona 17071, Spain

ARTICLE INFO

Article history:

Received 3 April 2014

Received in revised form 16 August 2014

Accepted 21 August 2014

Available online 23 August 2014

Keywords:

Brain

MRI

Multiple sclerosis

Tissue segmentation

White matter lesions

Lesion-filling

ABSTRACT

Multiple sclerosis white matter (WM) lesions can affect brain tissue volume measurements of voxel-wise segmentation methods if these lesions are included in the segmentation process. Several authors have presented different techniques to improve brain tissue volume estimations by filling WM lesions before segmentation with intensities similar to those of WM. Here, we propose a new method to refill WM lesions, where contrary to similar approaches, lesion voxel intensities are replaced by random values of a normal distribution generated from the mean WM signal intensity of each two-dimensional slice. We test the performance of our method by estimating the deviation in tissue volume between a set of 30 T1-w 1.5 T and 30 T1-w 3 T images of healthy subjects and the same images where: WM lesions have been previously registered and afterwards replaced their voxel intensities to those between gray matter (GM) and WM tissue. Tissue volume is computed independently using FAST and SPM8. When compared with the state-of-the-art methods, on 1.5 T data our method yields the lowest deviation in WM between original and filled images, independently of the segmentation method used. It also performs the lowest differences in GM when FAST is used and equals to the best method when SPM8 is employed. On 3 T data, our method also outperforms the state-of-the-art methods when FAST is used while performs similar to the best method when SPM8 is used. The proposed technique is currently available to researchers as a stand-alone program and as an SPM extension.

© 2014 The Authors. Published by Elsevier Inc. This is an open access article under the CC BY-NC-ND license (<http://creativecommons.org/licenses/by-nc-nd/3.0/>).

1. Introduction

Magnetic resonance imaging (MRI) permits to assess tissue abnormalities in vivo and approximate histopathological changes of the multiple sclerosis (MS) disease (Ganiler et al., 2014; Kearney et al., 2014). Several studies have shown that the percentage of change in brain atrophy tends to correlate with the progression of the disease (Pérez-Miralles et al., 2013; Sormani et al., 2014). Moreover, changes in gray matter (GM) atrophy are observed independently from white matter (WM), and hence atrophy measures based on segmentation-based methods are nowadays employed as they allow classifying brain tissues separately (Pérez-Miralles et al., 2013). The performance of different segmentation methods used to quantify brain atrophy or volume estimation has been evaluated deeply in the last 5 years (Klauschen et al., 2009; Derakhshan et al., 2010). However, it is well known that the presence of WM lesions can induce errors on brain tissue volume measurements (Chard et al., 2010; Battaglini et al., 2012; Gelineau-Morel et al., 2012) and non-rigid registration (Sdika and Pelletier, 2009; Diez et al., 2014), if lesions are processed within the images. For instance, if WM lesion voxels are classified as WM, lesion voxels with hypointense signal

intensities are added into the WM tissue distribution, increasing the probability of GM voxels with similar intensity to be misclassified also as WM (Chard et al., 2010).

In the last years, some authors have proposed different techniques to overcome these issues in MS patients by filling WM lesions with intensities similar to those of WM before performing tissue segmentation and image registration. These methods can be divided into two groups: methods which use *local* intensities from the surrounding neighboring voxels of lesions (Sdika and Pelletier, 2009; Battaglini et al., 2012; Magon et al., 2013) and methods which use *global* WM intensities from the whole brain (Chard et al., 2010). In all cases, the performance of these methods is directly related with their ability to minimize the impact of refilled voxels on original tissue distribution, not only due to the addition of these voxels into the tissue distribution, but also due to the effect on the global tissue distributions of filled images.

Within *local* methods, Sdika and Pelletier (2009) have proposed to refill each WM lesion voxel with the mean of its three-dimensional neighboring normal appearance white matter (NAWM) voxels. Battaglini et al. (2012) have suggested refilling each WM lesion voxel with intensities derived from a histogram of NAWM voxels surrounding the two-dimensional lesions. In a recent study, Magon et al. (2013) have proposed to refill each two-dimensional lesion with the intensity from the mean of the surrounding area of the lesion. Regarding *global*

* Corresponding author.

E-mail address: svalverde@eia.udg.edu (S. Valverde).

methods, Chard et al. (2010) have proposed a different approach by using intensities re-sampled from a global WM distribution to refill WM lesion voxels, based on the mean and standard deviation of the total NAWM of the whole image. Both Chard et al. (2010) and Battaglini et al. (2012) methods are available for the community. FSL-L (Battaglini et al., 2012) runs from a computer command-line and does not provide any graphical interface that aids the process. This technique has been integrated into the latest FSL package, and therefore it depends on the whole FSL installation. In the case of LEAP (Chard et al., 2010), the method runs as a stand-alone script also from the command-line and requires the installation and configuration of several external dependencies, which may be difficult to install for non-computer experts.

In this paper we propose a new technique to refill WM lesions which is a compromise between *global* and *local* methods. Hence, for each slice composing the three-dimensional image, we compute the mean and standard deviation of the signal intensity of NAWM tissue. On the one hand, compared to local methods (Battaglini et al., 2012; Magon et al., 2013) which only make use of a limited range of voxel intensities, the fact of using global information from the whole image slice reduces the bias caused by refilled voxels on GM and WM tissue distributions, especially on images with high lesion load. On the other hand, compared to other global methods (Chard et al., 2010), which are based on the mean signal intensity of the NAWM of the three-dimensional image, our method re-computes the mean signal intensity of the NAWM at each two-dimensional slice with the aim of reproducing more precisely the signal variability between MRI slices, especially in low resolution images. In order to easily integrate it into current platforms, the proposed method called SLF is currently available as a stand-alone program and as SPM¹ extension at the SALEM group site (<http://atc.udg.edu/salem/slfToolbox>).

To evaluate the performance of our method, we estimate the deviation in GM and WM tissue volume between a set of healthy images and the same images where artificial WM lesions have been refilled with the proposed technique. To do so, we register WM lesion masks from diagnosed MS patients into two sets of 30 1.5 and 3 T T1-weighted (T1-w) images of healthy subjects, respectively. Afterwards, we simulate realistic lesions on healthy images by replacing the signal intensities of registered lesion voxels with values similar to those of the mean GM/WM interface. Brain tissue volume is computed using both FAST (Zhang et al., 2001) and SPM8 (Ashburner and Friston, 2005) segmentation methods, in order to avoid possible correlations between the filling and segmentation processes. Furthermore, we compare our results with the same images where artificial WM lesions have been segmented as normal tissue, masked-out before tissue segmentation, and refilled using also the methods proposed by Chard et al. (2010); Battaglini et al. (2012), and Magon et al. (2013).

2. Materials and methods

2.1. Image data

The first set of images is composed of 30 images of healthy subjects (matrix size: $176 \times 208 \times 176$, voxel size: $1 \times 1 \times 1.25$ mm), acquired on a 1.5 T Vision scanner (Siemens, Erlangen, Germany) and obtained from the Open Access Series of Imaging Studies (OASIS) repository² (Marcus et al., 2007). Only images from young and middle-aged subjects are selected (age < 50) as they have not been diagnosed with any related pathology. Image references included in the study are as follows: 2, 4, 5, 6, 7, 9, 11, 12, 14, 17, 18, 20, 25, 26, 27, 29, 34, 37, 38, 40, 43, 44, 45, 47, 49, 50, 51, 54, 55, and 57.

The second set of images is composed of 30 images of healthy subjects (matrix size: $256 \times 150 \times 256$, voxel size: $0.92 \times 0.92 \times 1.20$ mm) acquired on a Philips 3 T scanner (Philips Healthcare, Best, NL) and

obtained from the Information eXtraction from Images (IXI) repository maintained by the Imperial College London in London, UK.³ We selected 30 images acquired from the Hammersmith Hospital. Image references included in the study are as follows: 12, 13, 14, 15, 33, 34, 39, 48, 49, 51, 52, 57, 59, 72, 80, 83, 92, 95, 96, 97, 104, 105, 126, 127, 128, 131, 136, 137, 146, and 159.

2.2. Preprocessing

All images are manually reoriented to match the standard MNI space. Skull-stripping is performed using the Brain Extraction Tool (BET) (Smith, 2002), following the optimization workflow suggested by Popescu et al. (2012), with the exception that cerebrospinal fluid tissue has been refilled on skull-stripped images again. This procedure is preferred over other alternatives as it provides the best performance on some lesion-filling methods such as Chard et al. (2010), being also the choice in other recent studies (Popescu et al., 2014). IXI images are corrected from possible intensity non-uniformities and acquisition artifacts using N4, the ITK (Ibáñez et al., 2003) implementation of the N3 package (Sled et al., 1997). N4 is applied on IXI images with default options. Images from the OASIS repository are provided already with N4 applied.

2.3. Lesion generation

We use a set of 37 patients with clinically confirmed MS, provided with *initial* and *follow-up* studies (Diez et al., 2014). In these patients, lesions have been annotated semi-automatically on Proton Density-weighted (PD-w) images by a trained technician using JIM software⁴ and afterwards co-registered with T1-w images. In order to maintain the independence between the 1.5 and 3 T sets of images, we match randomly 30 patients from the *initial* study into the OASIS images, and we repeat the same procedure with the follow-up study and the IXI image set.

MS lesion masks are registered into healthy images by a non-rigid transformation (Rueckert et al., 1999). To ensure that resulting lesion masks are placed on WM, we remove registered lesion voxels that have not been segmented as WM by both FAST and SPM8 on the healthy image. We computed a Wilcoxon rank sum test to analyze the difference in lesion volumes generated between OASIS and IXI datasets, obtaining that differences were not statistically significant ($p = 0.162$). The obtained mean lesion volume on OASIS images was 21.1 ± 20.8 ml (range from 0.5 to 65 ml), while 15.4 ± 16.2 ml (range from 0.8 to 62 ml) on IXI 3 T images. Note that due to the existing anatomical differences between 1.5 and 3 T image subjects and the enforced WM tissue constraint, the effect of registering the same MS lesion mask into a 1.5 and 3 T image results in two different lesion masks. For instance, the effect of registering lesions from the initial study into the 3 T dataset provided different lesion volumes (10.30 ± 12.10 ml) and reported statistically significant differences ($p = 0.007$) on the Wilcoxon rank sum tests.

Artificial lesions are simulated by replacing registered lesion voxel intensities with ones between the GM and WM interface, following the same strategy shown in Battaglini et al. (2012). For each original image, GM and WM tissue distributions are computed using only voxels in agreement between FAST and SPM8. WM lesion voxels are filled with random intensities coming from a newly generated normal distribution, with mean equal to the average of the GM and WM mean values and standard deviation equal to the difference between mean WM and GM, divided by 4 (Battaglini et al., 2012). Artificial lesions are refilled with the aim of simulating a profile which clearly separates their signal intensity with healthy tissue. This intensity profile chosen does not

¹ <http://www.fil.ion.ucl.ac.uk/spm/software/spm8/>.

² Publicly available at: <http://www.oasis-brain.org>.

³ Publicly available at <http://biomedic.doc.ic.ac.uk/brain-development/index.php?n=Main.Datasets>.

⁴ Xinapse Systems, JIM software webpage, <http://www.xinapse.com/home.php>.

reflect the entire scope of possible real lesions, but allows us to visualize the magnitude of the differences in tissue volume between images with artificial lesions and the same images where lesion have been filled with the proposed method. The intensity profile chosen would not affect any of the methods studied since they do not take into account the artificial lesion intensities.

2.4. Lesion filling

The proposed method aims to combine the *global* approach of Chard et al. (2010) with the similarity between refilled voxel intensities and their surrounding voxels of *local* methods such as Battaglini et al. (2012) and Magon et al. (2013). Basically, for each slice composing the three-dimensional image, lesion voxel intensities are replaced by random intensities of a normal distribution generated from the mean NAWM intensity of the current slice. Fig. 1 summarizes the lesion-filling process graphically.

The proposed algorithm requires two input images: a preprocessed T1-w image (skull-stripped and intensity inhomogeneity corrected) and its corresponding binary WM lesion mask. After testing the performance of the method with different skull-stripping approaches (Smith, 2002; Shattuck et al., 2001), we observed that including this step inside the filling process is not necessary, because the skull-stripping method employed seems to not interfere significantly in the results obtained (Wilcoxon significant rank-sum tests between differences in tissue volume between lesion-filled and original images of both datasets for GM and WM tissue, $p > 0.13$).

WM lesions are masked out from the T1-w image using the provided lesion mask, in order to avoid the influence of artificial lesions on tissue distributions. The resulting image is used to estimate the probability of each voxel to be classified as CSF, GM, and NAWM, by segmenting tissue with a Fuzzy-C-means approach (Pham, 2001). The Fuzzy-C-means implementation used here follows the algorithm described in Pham (2001), with clusters initialized according to Bezdek et al. (1999). Moreover, input signal intensities are constrained to the mean plus three standard deviations of the signal intensity of the image, in order to avoid outlier signal intensities, such as residual parts of the eyes or neck. From the obtained tissue segmentation output, we compute the

three-dimensional NAWM mask from the image voxels with the highest probability to pertain to the WM cluster.

Finally, the lesion-filling process is achieved as follows: for each axial slice composing the three-dimensional image, we compute the mean and standard deviation of the signal intensity of NAWM tissue. Axial sampling is motivated because after testing the sampling procedure on the coronal, axial and sagittal planes, we found that the best results were obtained when we sampled the axial plane. This was due to the fact that using the axial plane reduced the variability of possible existing WM intensities, when compared to coronal and sagittal sampling. The Fuzzy-C-means approach used to estimate the tissue probabilities is a simple method which in fact does not take into account neither spatial nor neighboring information, and hyper-intense signal intensities such as residual parts of the eyes or the neck produced in the skull-stripping process can bias significantly the clusters. The risk of adding these parts into the WM distribution is minimized in the axial plane because we are reducing it to a certain slice where lesion volume is usually lower than that in central slices. The computed mean and standard deviation values are used to generate a normal distribution with mean equal to the computed NAWM mean intensity and standard deviation equal to half of the computed NAWM standard deviation. Standard deviation is always fixed to half of the WM mean independently of the dataset used. This value was chosen empirically with the aim of balancing the accuracy of the method with both 1.5 and 3 T images. Although a specific tuning of this parameter could provide a better performance on certain cases, we decided to fix it avoiding therefore the number of parameters to tune. Lesion voxel intensities from the current image slice are replaced by random values of the generated distribution. The procedure is repeated until all image slices are completed.

2.5. Volume analysis

We compute the absolute percentage % difference in normalized gray matter volume (NGMV) and normalized white matter volume (NWMV) between each original and its correspondent lesion-filled images. Normalized volumes are obtained as the ratio of voxels outside lesion regions segmented as GM or WM and the total number of

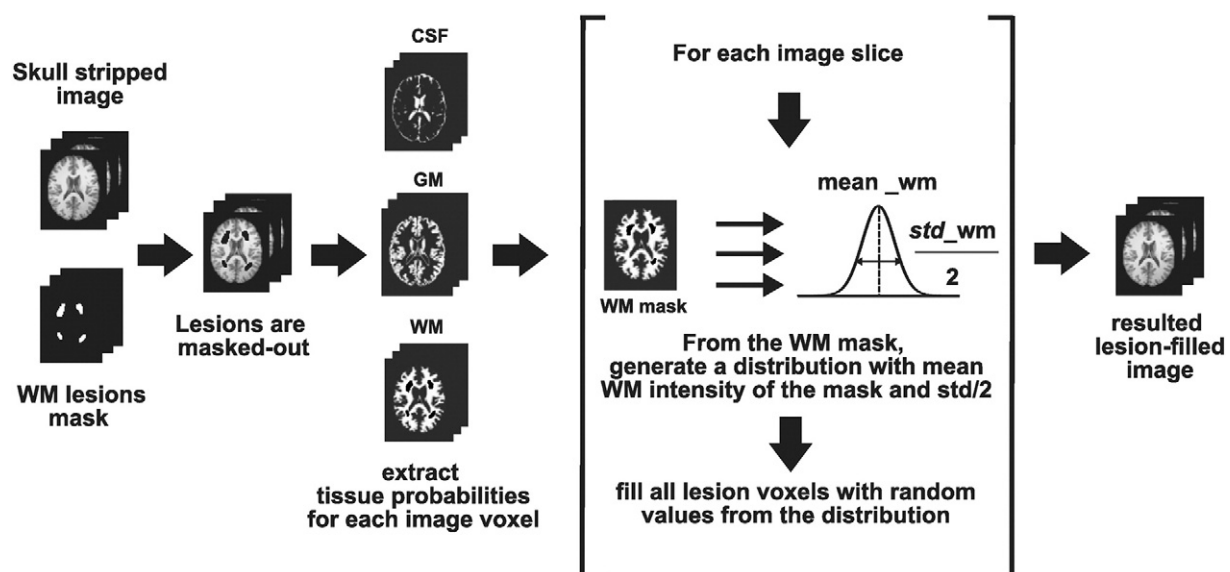


Fig. 1. Proposed algorithm for filling WM lesions. From a preprocessed T1-w image (skull-stripping and intensity inhomogeneity corrected), WM lesions are masked out using the provided WM lesion binary mask. Using a Fuzzy-C-means approach, we estimate the probability of each image voxel to be classified as CSF, GM, and NAWM. For each slice composing the whole image, lesion voxel intensities are replaced by a random intensity derived from a normal distribution with mean and half of the standard deviation of the NAWM tissue intensities of the current slice.

segmented voxels, respectively. For instance, the % difference in NGMV is computed as:

$$\% = \frac{|NGMV_{filled} - NGMV_{orig}|}{NGMV_{orig}} \times 100$$

where $NGMV_{filled}$ and $NGMV_{orig}$ values refer to the computed volumes for the lesion-filled and original images, respectively. The higher the performance of the lesion-filling method, the lower the percentage difference between lesion-filled and original images.

In order to analyze possible correlations between the filling process and the segmentation method employed, brain tissue volume is calculated independently on the same subjects using FAST (Zhang et al., 2001) (v.5.0.5) and SPM8 (Ashburner and Friston, 2005) (v.4667) approaches.

2.6. Statistical analysis

We compare the performance of our method with respect to other existing techniques such as the ones proposed by Chard et al. (2010); Battaglini et al. (2012), and Magon et al. (2013). We also add two more sets of images into the comparison: images segmented with artificial lesions and images where WM lesions have been masked out before tissue segmentation. Given the small differences in NGMV and NWMV between original and lesion-filled images, the use of a standard Analysis of the Variance (ANOVA) or a classic *t*-test is impractical here. Instead, we perform a series of permutation tests to determine significant differences in tissue volume between pairs of methods (Menke and Martínez, 2004; Valverde et al., 2014). The permutation tests return the mean μ and standard deviation σ of the fraction of times that the difference in NGMV and NWMV for a current lesion-filling method is smaller than the rest of methods with p -value ≤ 0.05 . Afterwards, methods are presented in 3 ranks determined by the mean and standard deviation of the best method and the distance with respect to the mean of the rest of the methods (Valverde et al., 2014). In our experiments, we set the number of comparisons between each pair of methods to $N = 1000$.

3. Results

3.1. OASIS dataset (1.5 T data)

Fig. 2 depicts the absolute mean % difference in NGMV and NWMV between the 30 original 1.5 T images and the same images with artificial lesions (NONE), masked-out lesions before segmentation (MASKED), and lesion-filled using Magon et al. (2013) (MAGON), Battaglini et al. (2012) (FSL-L), and Chard et al. (2010) (LEAP), and finally our proposed algorithm SLF.

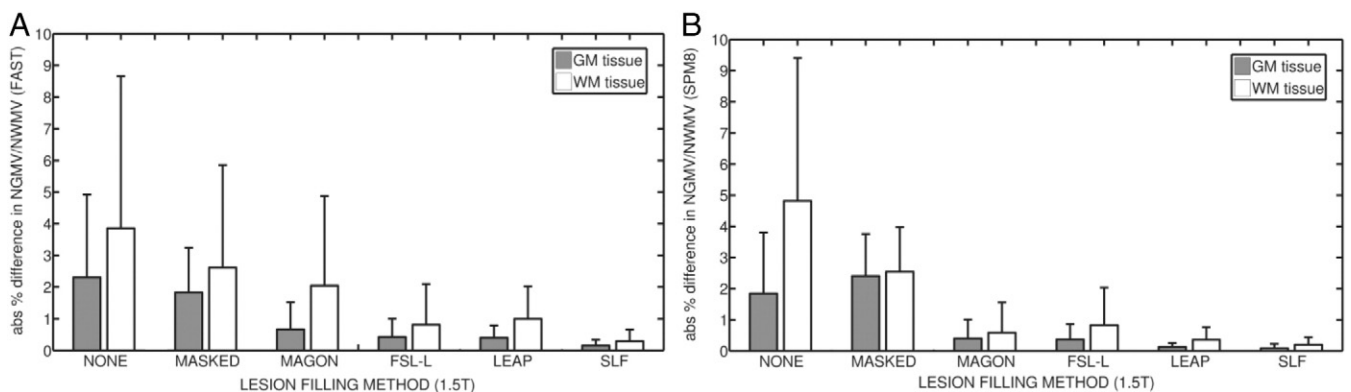


Fig. 2. Absolute % difference in NGMV and NWMV between original and filled images from the OASIS (1.5 T) dataset. (a) Results for images segmented using FAST. (b) Results for images segmented with SPM8. Gray bars represent the absolute mean % difference in NGMV, while white bars represent the absolute mean % difference in NWMV. Lines above each bar represent the standard deviation for each method and tissue.

When FAST is used, SLF reports the lowest absolute mean difference in NGMV (0.16 ± 0.14), followed by LEAP (0.40 ± 0.30) and FSL-L (0.43 ± 0.58) methods. Our proposal also provides the lowest difference in NWMV (0.29 ± 0.36), followed by FSL-L (0.81 ± 1.28). Maximum values in NGMV are found in NONE images, with differences up to 2.30 ± 2.62 in NGMV and 3.85 ± 4.81 in NWMV.

When SPM8 is used, SLF also reports the lowest differences in NGMV (0.09 ± 0.14), followed by LEAP method (0.12 ± 0.13). Our proposed method also performs better than the rest of the methods on NWMV (0.20 ± 0.24), followed by the LEAP method (0.36 ± 0.40). Again, the highest differences in NGMV (1.84 ± 1.97) and NWMV (4.82 ± 4.58) are found in NONE images. Table 1 shows the absolute mean difference in WM volume for all methods where lesion volume has been ranged by size intervals. Results are presented for both SPM8 and FAST segmentation methods.

Table 2 presents the performance of each filling-method after running all possible pair-wise permutation tests. With a significant p -value of ≤ 0.05 , all tests run on images segmented with FAST show the superiority of SLF over the other methods presented. On images segmented with SPM8, all tests show a clear superiority of SLF over the other methods on NWMV, while a similar performance of SLF and LEAP over the other methods on NGMV.

3.2. IXI dataset (3 T data)

We also test the performance of our algorithm using 3 T data. As before, Fig. 3 shows the absolute mean % difference in NGMV and NWMV between the 30 original 3 T images and the same images with added lesions (NONE), masked-out lesions before segmentation (MASKED), and lesion-filled methods MAGON, FSL-L, and LEAP, and our proposed approach SLF.

When FAST is used, SLF reports the lowest absolute mean % difference in NGMV (0.06 ± 0.06), followed by LEAP (0.09 ± 0.10). Our method SLF also performs the lowest difference in NWMV (0.09 ± 0.09), followed again by LEAP (0.12 ± 0.08). Maximum values in NGMV are found in NONE images, with differences up to 1.40 ± 1.56 in NGMV and 1.00 ± 1.32 in NWMV.

When SPM8 is used, both LEAP (0.04 ± 0.06) and SLF (0.05 ± 0.05) yield the lowest absolute % mean difference in NGMV. On NWMV, also LEAP (0.09 ± 0.12) and SLF (0.08 ± 0.09) report the lowest absolute mean % difference in volume between original and lesion-filled images. Again, highest differences in NGMV (1.84 ± 1.97) and NWMV (4.82 ± 4.58) are found in NONE images. Table 3 shows the absolute mean difference in WM volume for all methods on IXI images, where lesion volume has been ranged by size intervals. Results are presented for both SPM8 and FAST segmentation methods.

Table 4 shows the performance of each filling-method after running the permutation tests. Tests run on images segmented with FAST show

Table 1

Absolute mean difference in NWMV between original and filled images from the 1.5 T OASIS images. Results are presented for both SPM8 and FAST segmentation methods. Lesion volume is ranged by size intervals with $n = 6$ by interval. Values indicate the mean and standard deviation of the absolute difference in volume ($\mu \pm \sigma$) of each lesion-filling method at a current lesion interval.

Method/ lesion(ml)	0.5–4 ml ($n = 6$)	4–11 ml ($n = 6$)	11–20 ml ($n = 6$)	25–36 ml ($n = 6$)	>36 ml ($n = 6$)
<i>SPM8 segmentation method</i>					
NONE	0.47 \pm 0.50	1.54 \pm 0.95	2.71 \pm 0.60	7.09 \pm 1.42	10.64 \pm 3.10
MASKED	1.56 \pm 0.94	2.42 \pm 0.70	1.49 \pm 0.43	3.16 \pm 1.35	3.91 \pm 1.76
MAGON	0.03 \pm 0.03	0.08 \pm 0.07	0.24 \pm 0.25	0.32 \pm 0.19	1.95 \pm 1.25
FSL-L	0.03 \pm 0.01	0.10 \pm 0.05	0.31 \pm 0.15	0.55 \pm 0.07	2.38 \pm 1.26
LEAP	0.04 \pm 0.04	0.10 \pm 0.05	0.19 \pm 0.05	0.44 \pm 0.22	0.92 \pm 0.42
SLF	0.03 \pm 0.03	0.04 \pm 0.03	0.09 \pm 0.06	0.23 \pm 0.20	0.55 \pm 0.23
<i>FAST segmentation method</i>					
NONE	0.21 \pm 0.21	0.71 \pm 0.38	1.88 \pm 0.56	4.55 \pm 2.04	8.95 \pm 4.36
MASKED	9.52 \pm 1.20	8.36 \pm 1.30	11.53 \pm 4.91	7.42 \pm 1.08	5.79 \pm 1.92
MAGON	0.08 \pm 0.04	0.25 \pm 0.22	0.91 \pm 0.63	1.28 \pm 0.39	6.24 \pm 2.74
FSL-L	0.03 \pm 0.02	0.05 \pm 0.05	0.30 \pm 0.21	0.58 \pm 0.19	2.13 \pm 1.22
LEAP	0.08 \pm 0.07	0.34 \pm 0.10	0.65 \pm 0.13	1.07 \pm 0.66	2.50 \pm 0.80
SLF	0.07 \pm 0.05	0.13 \pm 0.09	0.22 \pm 0.15	0.36 \pm 0.30	0.42 \pm 0.16

a significant superiority of SLF over the rest of the methods on NWMV, and a slightly better performance of SLF with respect to LEAP on NGMV, although both methods are clearly superior to the rest of methods presented. When SPM8 is used, tests show a similar performance of SLF and LEAP over the rest of the methods on both NWMV and NGMV.

4. Discussion

Several studies have proposed to use different filling techniques in order to reduce the effects of WM lesions on brain tissue measurements of T1-w images. Up to date, only LEAP (Chard et al., 2010)⁵ and FSL-L (Battaglini et al., 2012)⁶ are publicly available methods that permit to refill T1-w images given a WM lesion mask. The Lesion Segmentation Toolbox (LST) proposed by Schmidt et al. (2012) also provides a lesion-filling approach based on the work of Chard et al. (2010), but it is dependent of a FLAIR image and an internal lesion-probability map obtained during the lesion segmentation step.

In general, deviation in tissue volume between original and lesion-filled images tends to be higher on 1.5 T OASIS images than on 3 T IXI images. The observed deviation is caused by differences in intensity, slice thickness and dimensionality between datasets. On IXI images, the distance between GM and WM signal intensity distributions is narrower than that of 1.5 T data. Applying the lesion generation algorithm (Battaglini et al., 2012) with identical parameters of those used with 1.5 T images creates simulated lesions whose intensity are noticeably similar to the mean WM, because the standard deviation of the generated lesion distribution is the mean between the GM and WM tissue divided by 4. However, this fact only explains the difference found on images segmented with artificial lesions. In the rest of the methods, the signal intensity of the generated lesions is not interfering with the obtained results since in all cases lesion voxels are replaced before tissue segmentation. On images where lesions have been masked before segmentation (MASKED), the lower deviation in tissue volume of 3 T images can be explained by the increase in the resolution of the images when compared to 1.5 T data, which reduces the effect of masked voxels in tissue distributions. The same reason can be behind the lower deviation found on all four lesion filling methods. By increasing the number of slices, differences produced by the methods on certain slices can be smoothed by tissue segmentation methods. Moreover, the use of a reduced sampling space or a better tuning of the parameters involved in

the WM tissue distribution generated to refill lesion voxels could increase the performance of the presented method. Nevertheless, in all our experiments we decided to fix the standard deviation to 2 for simplicity.

Analyzing the results by dataset, on 1.5 T images from the OASIS dataset, our results show that compared to the available methods, the proposed algorithm SLF reduces significantly the differences in NWMV between original and filled images, independently of the brain tissue segmentation method used to measure the tissue volume. With the same data, SLF also reduces significantly the differences in NGMV when FAST is used. Although our method reports the lowest mean % difference in NGMV when SPM8 method is used, the permutation test clearly shows that differences between SLF and LEAP are not relevant. On 3 T images from the IXI dataset, SLF also yields the lowest mean % differences in NGMV and NWMV, when FAST is used to measure tissue volume. These results are clearly significant in NWMV, but not in NGMV, although our method reports also the lowest difference among all methods. When SPM8 is used, SLF presents a similar performance of that of LEAP, and both methods tie on the results of the significance tests.

Compared with local methods, our algorithm performs quantitatively better than *local* methods on images with high lesion load (> 36 ml). The MAGON method incorporates all neighbor voxels surrounding a WM lesion region to compute a mean intensity which is used to refill all lesion voxels. On images with high lesion load touching GM tissue, including GM voxels can decrease refilled intensities and modify the tissue distribution of filled images. FSL-L overpasses this limitation by building an intensity distribution based only on WM voxels surrounding lesions. However, on large lesion regions, all lesion voxels will be filled with a narrow range of intensities coming from the neighboring voxels that can have a direct incidence on GM and WM tissue distributions. By contrast, lesion volume appears to affect less *global* methods. In our case, the intensity distribution generated to refill lesion voxels will be independent of both the size and the position of lesion. Furthermore, the effect of filled voxels on the global WM tissue distribution is smoothed by the addition of intensities which try to reassemble the global NAWM of the current slice.

Compared with global methods, there are some interesting differences between our method and LEAP. Contrary to *local* methods, *global* methods have to deal with the skull-stripping process before processing images. LEAP incorporates the skull-stripping process as part of the processing pipeline. In addition, LEAP also allows the user to provide a brain

Table 2

Permutation tests for obtained absolute % differences in NGMV and NWMV on 1.5 T images. Reported values are mean and standard deviation (μ_0 , σ_0) of the fraction of times when each method produces significant p -values ($p \leq 0.05$). (a) Results when using FAST. (b) Results when using SPM8. Positive values indicate that in average, the method outperforms the other methods in pair-wise significant tests. Negative values indicate the contrary. Rank 1: ($\mu_0 - \sigma_0$, μ_0), rank 2: ($\mu_0 - 2\sigma_0$, $\mu_0 - \sigma_0$), rank 3: ($\mu_0 - 3\sigma_0$, $\mu_0 - 2\sigma_0$).

		NGMV			NWMV
		Method	$\mu \pm \sigma$	Method	$\mu \pm \sigma$
<i>(a) FAST segmentation method (1.5 T)</i>					
Rank 1	SLF		0.83 \pm 0.41	SLF	0.83 \pm 0.41
Rank 2	FSL-L		0.33 \pm 0.82	FSL-L	0.33 \pm 0.82
	LEAP		0.33 \pm 0.82	LEAP	0.33 \pm 0.82
Rank 3	MAGON		−0.17 \pm 0.98	MAGON	−0.17 \pm 0.98
	MASKED		−0.23 \pm 0.41	MASKED	−0.23 \pm 0.41
	NONE		−0.50 \pm 0.84	NONE	−0.50 \pm 0.84
<i>(b) SPM8 segmentation method (1.5 T)</i>					
Rank 1	SLF		0.67 \pm 0.52	SLF	0.83 \pm 0.41
	LEAP		0.67 \pm 0.52		
Rank 2	MAGON		0.00 \pm 0.89	LEAP	0.33 \pm 0.82
	FSL-L		0.00 \pm 0.89	MAGON	0.17 \pm 0.75
Rank 3	NONE		−0.67 \pm 0.52	FSL-L	0.00 \pm 0.89
	MASKED		−0.67 \pm 0.52	MASKED	−0.50 \pm 0.84
				NONE	−0.83 \pm 0.41

⁵ <http://www.nmrgroup.ion.ucl.ac.uk/analysis/lesionfill.html>.

⁶ http://fsl.fmrib.ox.ac.uk/fsl/fslwiki/lesion_filling.

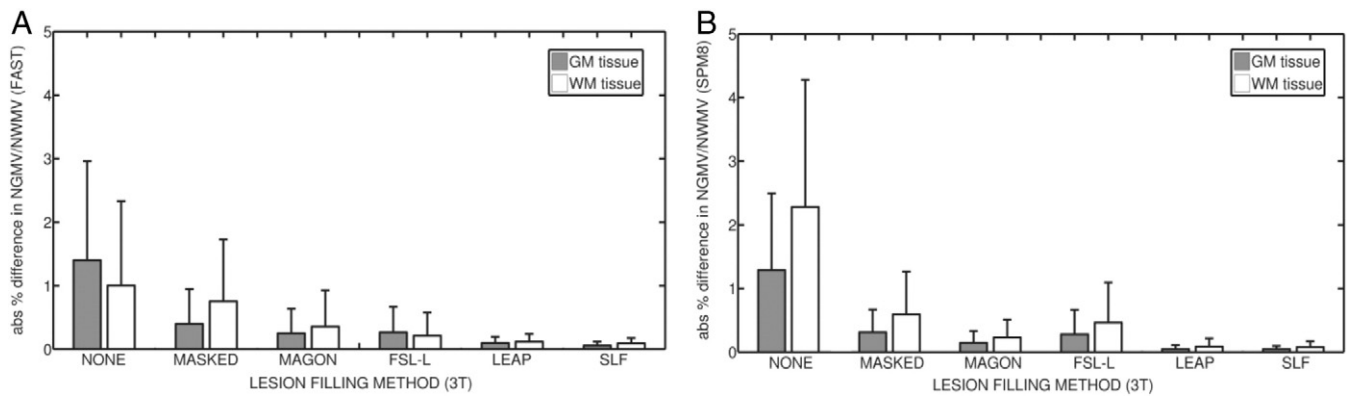


Fig. 3. Absolute mean % difference in NGMV and NWMV between original and filled images from the IXI (3 T) dataset. (a) Results for images segmented using FAST. (b) Results for images segmented with SPM8. Gray bars represent the absolute mean % difference in NGMV, while white bars represent the absolute mean % difference in NWMV. Lines above each bar represent the standard deviation for each method and tissue.

mask. By contrast, our method does not deal with skull-stripping internally, and the method requires an already skull-stripped image or a brain mask. As noted previously, the skull-stripping method employed seems to not interfere significantly in the results obtained by our method. While setting up each of the different processes involved in the proposed pipeline, we found that, at least with our data, the performance of LEAP decreased or failed in 1.5 T scans when the skull-stripping methods BSE (Shattuck et al., 2001) and BET (Smith, 2002) were used with default options. By contrast, LEAP provided the best results when the optimized method proposed by Popescu et al. (2012) was used. This fact motivated the selection of this skull-stripping method for all the experiments of the study.

Furthermore, on both datasets, we have also compared the differences between our method and LEAP estimating the mean NAWM intensity used as a basis to fill lesion voxels. In most of the images, the global mean NAWM intensity does not differ significantly between fityk⁷ on LEAP and our Fuzzy-C-means approach. Hence, we can reject the hypothesis that observed differences in 1.5 T images can be caused by the approach employed to compute the NAWM tissue distribution before filling lesion voxels. However, on both lesion-filling approaches, tissue segmentation methods tended to increase the apparent mean WM tissue distribution on 1.5 T images with high lesion load (>40 ml) due to the increase of voxels refilled with intensities higher than the actual mean WM signal intensity. This effect is clearly more visible on LEAP than in our method, especially when FAST is used. The resolution of the OASIS 1.5 T images ($176 \times 208 \times 176$ slices) is lower than that of IXI 3 T images ($256 \times 150 \times 256$ slices). On images with low number of slices, each slice has a higher weight into the global tissue distribution. After comparing the a priori WM tissue distribution values estimated by both the LEAP and SLF methods with the already computed WM tissue distributions obtained from healthy images, we found that as lesion size increases, global methods such as LEAP and SLF tend to increase the differences in tissue volume with respect to original images. In both methods, we have observed that the a priori estimated mean intensity of the WM distribution tends to be higher than the actual tissue distribution as computed by FAST and SPM8 on healthy images. As lesion volume increases, the addition of more filled voxels with intensity higher than the actual mean tissue intensity is more prominent, causing a displacement of the mean intensity of the WM distribution returned by the segmentation methods on filled images. Consequently, more voxels bordering GM/WM are segmented as GM and WM tissue volume decreases. In this scenario, the strategy followed by SLF, where WM is sampled independently at each slice, is more robust to the increase of lesions size than a global estimation of the WM tissue (LEAP) because

possible errors introduced by a particular slice are not propagated into the rest of the slices. Contrary to SPM8, which estimates the tissue distributions based on a Gaussian Mixture Model approach of the whole image, FAST builds a network of neighboring relations based on a Markov random field approach, more sensible to changes between slices. The same reason can also be behind the better performance of our method on 3 T when FAST is used. Compared with 1.5 T images, the probability of intensity change between slices is less prominent on 3 T images due to a higher resolution between slices.

Analyzing the possible deviations in tissue volume caused by each tissue segmentation process, we obtained results which suggest that the chosen tissue segmentation method does not affect significantly the performance of our filling-method. Results between the same filled images segmented with FAST and SPM8 differ (<0.1%) in the worst case on both datasets and tissues. By contrast, MAGON, FSL-L and LEAP switch their rank on 1.5 T images, depending on the segmentation method used. On 3 T images, only MAGON and FSL-L appear to switch between ranks when FAST or SPM8 is used, respectively.

The present study is not free from limitations. The most important one is the lack of images of MS patients with brain tissue expert annotations. All images from MS patients taken from Diez et al. (2014) have been only provided with lesion annotations delineated by a trained expert, but not brain tissue annotations. To overpass this limitation, we have registered WM lesions from MS patients into healthy images as performed in Battaglini et al. (2012) and double-checked that registered

Table 3

Absolute mean difference in NWMV between original and filled images from the 3 T OASIS images. Results are presented for both SPM8 and FAST segmentation methods. Lesion volume is ranged by size intervals with $n = 6$ by interval. Values indicate the mean and standard deviation of the absolute difference in volume ($\mu \pm \sigma$) of each lesion-filling method at a current lesion interval.

Method/ lesion(ml)	0.8–3 ml (n = 6)	4–6 ml (n = 6)	6–13 ml (n = 6)	16–21 ml (n = 6)	>21 ml (n = 6)
<i>SPM8 segmentation method</i>					
NONE	0.68 \pm 0.56	0.92 \pm 0.31	1.61 \pm 0.85	3.37 \pm 0.81	5.16 \pm 1.83
MASKED	0.07 \pm 0.03	0.21 \pm 0.16	0.34 \pm 0.22	1.07 \pm 0.79	1.42 \pm 0.65
MAGON	0.05 \pm 0.10	0.15 \pm 0.28	0.14 \pm 0.15	0.47 \pm 0.44	0.41 \pm 0.22
FSL-L	0.06 \pm 0.06	0.06 \pm 0.03	0.19 \pm 0.16	0.80 \pm 0.80	1.32 \pm 0.53
LEAP	0.01 \pm 0.01	0.03 \pm 0.02	0.05 \pm 0.05	0.13 \pm 0.15	0.22 \pm 0.18
SLF	0.03 \pm 0.03	0.02 \pm 0.01	0.09 \pm 0.12	0.09 \pm 0.06	0.16 \pm 0.13
<i>FAST segmentation method</i>					
NONE	0.14 \pm 0.10	0.24 \pm 0.06	0.52 \pm 0.34	1.27 \pm 0.35	2.94 \pm 1.67
MASKED	0.07 \pm 0.05	0.17 \pm 0.07	0.41 \pm 0.27	0.95 \pm 0.25	2.23 \pm 1.13
MAGON	0.05 \pm 0.03	0.07 \pm 0.06	0.08 \pm 0.04	0.59 \pm 0.55	1.07 \pm 0.79
FSL-L	0.04 \pm 0.02	0.03 \pm 0.02	0.03 \pm 0.02	0.18 \pm 0.20	0.77 \pm 0.45
LEAP	0.07 \pm 0.05	0.03 \pm 0.03	0.14 \pm 0.13	0.19 \pm 0.16	0.29 \pm 0.13
SLF	0.03 \pm 0.02	0.04 \pm 0.02	0.08 \pm 0.06	0.20 \pm 0.15	0.34 \pm 0.14

⁷ Available at: <http://sourceforge.net/projects/fityk>.

Table 4

Permutation tests for obtained absolute % differences in NGMV and NWMV on 3 T images. Reported values are mean and standard deviation (μ , σ) of the fraction of times when each method produces significant p -values ($p \leq 0.05$). (a) Results when using FAST. (b) Results when using SPM8. Positive values indicate that in average, the method outperforms the other methods in pair-wise significant tests. Negative values indicate the contrary. Rank 1: ($\mu_0 - \sigma_0, \mu_0$), rank 2: ($\mu_0 - 2\sigma_0, \mu_0 - \sigma_0$), rank 3: ($\mu_0 - 3\sigma_0, \mu_0 - 2\sigma_0$).

	NGMV		NWMV	
	Method	$\mu \pm \sigma$	Method	$\mu \pm \sigma$
<i>(a) FAST segmentation method (3 T)</i>				
Rank 1	SLF	0.67 ± 0.52	SLF	0.67 ± 0.52
	LEAP	0.66 ± 0.51	LEAP	0.50 ± 0.55
Rank 2	MAGON	0.00 ± 0.8	MAGON	-0.17 ± 0.98
	FSL-L	0.00 ± 0.3	FSL-L	0.33 ± 0.82
Rank 3	MASKED	-0.50 ± 0.84	MASKED	-0.50 ± 0.84
	NONE	-0.83 ± 0.41	NONE	-0.83 ± 0.41
<i>(b) SPM8 segmentation method (3 T)</i>				
Rank 1	LEAP	0.67 ± 0.52	LEAP	0.67 ± 0.52
	SLF	0.67 ± 0.52	SLF	0.67 ± 0.52
Rank 2	MAGON	0.17 ± 0.98	MAGON	0.17 ± 0.98
	FSL-L	-0.33 ± 0.82	FSL-L	-0.17 ± 0.98
Rank 3	MASKED	-0.33 ± 0.82	MASKED	-0.50 ± 0.84
	NONE	-0.83 ± 0.41	NONE	-0.83 ± 0.41

lesions have replaced voxels segmented as WM by FAST and SPM8. This strategy has a negligible impact on the performance of the filling-methods analyzed in this study, because we assure a priori that generated lesions are on WM, and moreover none of the methods use information from the artificial lesions generated. Furthermore, although we tested the performance of the proposed method with two datasets with different magnetic field strengths, our results are limited to these two different scanners with particular configurations, and hence it is difficult to generalize the results to all 1.5 and 3 T scanners.

In conclusion, the results of this study show that regardless of the lesion size, the SLF method performs consistently well compared to other existing methods such as LEAP, especially on 1.5 T images. Furthermore, the results obtained show that the proposed method can be an effective method for low resolution images. The skull-stripping process does not especially affect the accuracy of the method, which allows integrating it with different preprocessing pipelines. Additionally, volume estimations of lesion filled images processed by our algorithm appear to be not affected by the segmentation method employed. In contrast to other approaches, SLF may be installed by non-computer experts who can easily use it without any parameter tuning. SLF is currently available to researchers as a stand-alone script and as an SPM library extension which facilitates to incorporate the lesion filling process into the expert workflow for tissue volume segmentation.

Acknowledgments

The authors would like to thank Dr. Ferran Prados, PhD, for helpful discussion. Sergi Valverde holds a FI-GDR2013 grant from the Generalitat de Catalunya.

References

- Ashburner, J., Friston, K.J., 2005. Unified segmentation. *Neuroimage* 26, 839–851. <http://dx.doi.org/10.1016/j.neuroimage.2005.02.01815955494>.
- Battaglini, M., Jenkinson, M., De Stefano, N., 2012. Evaluating and reducing the impact of white matter lesions on brain volume measurements. *Human Brain Mapping* 33, 2062–2071. <http://dx.doi.org/10.1002/hbm.2134421882300>.
- Bezdek, J.C., Keller, J., Krishnapuram, R., Pal, N.R., 1999. *Fuzzy Models and Algorithms for Pattern Recognition and Image Processing*. The Handbooks of Fuzzy Sets Series. 4. Springer, New York.
- Chard, D.T., Jackson, J.S., Miller, D.H., Wheeler-Kingshott, C.A., 2010. Reducing the impact of white matter lesions on automated measures of brain gray and white matter volumes. *Journal of Magnetic Resonance Imaging: JMRI* 32, 223–228. <http://dx.doi.org/10.1002/jmri.2221420575080>.

- Derakhshan, M., Caramanos, Z., Giacomini, P.S., Narayanan, S., Maranzano, J., Francis, S.J., Arnold, D.L., Collins, D.L., 2010. Evaluation of automated techniques for the quantification of grey matter atrophy in patients with multiple sclerosis. *Neuroimage* 52, 1261–1267. <http://dx.doi.org/10.1016/j.neuroimage.2010.05.02920483380>.
- Diez, Y., Oliver, A., Cabezas, M., Valverde, S., Martí, R., Vilanova, J.C., Ramió-Torrentà, L., Rovira, A., Lladó, X., 2014. Intensity based methods for brain MRI longitudinal registration. *A study on multiple sclerosis patients. Neuroinformatics* 12, 365–379. <http://dx.doi.org/10.1007/s12021-013-9216-z24338728>.
- Ganiler, O., Oliver, A., Diez, Y., Freixenet, J., Vilanova, J.C., Beltran, B., Ramió-Torrentà, L., Rovira, A., Lladó, X., 2014. A subtraction pipeline for automatic detection of new appearing multiple sclerosis lesions in longitudinal studies. *Neuroradiology* 56 (5), 363–374. <http://dx.doi.org/10.1007/s00234-014-1343-124590302>.
- Gelineau-Morel, R., Tomassini, V., Jenkinson, M., Johansen-Berg, H., Matthews, P.M., Palace, J., 2012. The effect of hypointense white matter lesions on automated gray matter segmentation in multiple sclerosis. *Human Brain Mapping* 33, 2802–2814. <http://dx.doi.org/10.1002/hbm.2140221976406>.
- Ibáñez, L., Schroeder, W., Ng, L., Cates, J., 2003. *The ITK Software Guide: The Insight Segmentation and Registration Toolkit*. Kitware Inc.
- Kearney, H., Rocca, M.A., Valsasina, P., Balk, L., Sastre-Garriga, J., Reinhardt, J., Ruggieri, S., Rovira, A., Stippich, C., Kappos, L., Sprenger, T., Tortorella, P., Rovaris, M., Gasperini, C., Montalban, X., Geurts, J.J.G., Polman, C.H., Barkhof, F., Filippi, M., Altmann, D.R., Ciccarelli, O., Miller, D.H., Chard, D.T., 2014. Magnetic resonance imaging correlates of physical disability in relapse onset multiple sclerosis of long disease duration. *Multiple Sclerosis (Houndmills, Basingstoke, England)* 20 (1), 72–80. <http://dx.doi.org/10.1177/135245851349224523812283>.
- Klauschen, F., Goldman, A., Barra, V., Meyer-Lindenberg, A., Lundervold, A., 2009. Evaluation of automated brain MR image segmentation and volumetry methods. *Human Brain Mapping* 30, 1310–1327. <http://dx.doi.org/10.1002/hbm.2059918537111>.
- Magon S., Chakravarty M., Lerch J., Gaetano L., Naegelin Y., Stippich C., Kappos L., Redue E.W., Sprenger T. (2013). Lesion filling improves the accuracy of cortical thickness measurements in multiple sclerosis patients. *Multiple Sclerosis. Copenhagen, Denmark*, vol. 19, pp 74–558
- Marcus, D.S., Wang, T.H., Parker, J., Csernansky, J.G., Morris, J.C., Buckner, R.L., 2007. Open access series of imaging studies (OASIS): cross-sectional MRI data in young, middle aged, nondemented, and demented older adults. *Journal of Cognitive Neuroscience* 19, 1498–1507. <http://dx.doi.org/10.1162/jocn.2007.19.9.149817714011>.
- Menke, J., Martínez, T.R., 2004. Using permutations instead of Student's t distribution for p -values in paired-difference algorithm comparisons. *Proceedings of the IEEE Joint Conference on Neural Networks*.
- Pham, D.L., 2001. Robust fuzzy segmentation of magnetic resonance images. *Proceedings of the Fourteenth IEEE Symposium on Computer-Based Medical Systems CBMS* 127–134.
- Pérez-Miralles, F., Sastre-Garriga, J., Tintoré, M., Arrambide, G., Nos, C., Perkal, H., Río, J., Edo, M.C., Horga, A., Castilló, J., Auger, C., Huerga, E., Rovira, A., Montalban, X., 2013. Clinical impact of early brain atrophy in clinically isolated syndromes. *Multiple Sclerosis (Houndmills, Basingstoke, England)* 19 (14), 1878–1886. <http://dx.doi.org/10.1177/135245851348823123652215>.
- Popescu, V., Battaglini, M., Hoogstrate, W.S., Verfaillie, S.C., Sluiter, I.C., Van Schijndel, R.A., Van Dijk, B.W., Cover, K.S., Knol, D.L., Jenkinson, M., Barkhof, F., de Stefano, N., Vrenken, H., 2012. Optimizing parameter choice for FSL-Brain Extraction Tool (BET) on 3D T1 images in multiple sclerosis. *Neuroimage* 61, 1484–1494. <http://dx.doi.org/10.1016/j.neuroimage.2012.03.07422484407>.
- Popescu, V., Ran, N.C.G., Barkhof, F., Chard, D., Wheeler-Kingshott, C., Vrenken, H., 2014. Accurate GM atrophy quantification in MS using lesion-filling with co-registered lesion masks. *NeuroImage: Clinical* 4, 366–373. <http://dx.doi.org/10.1016/j.nicl.2014.01.004>.
- Rueckert, D., Sonoda, L.I., Hayes, C., Hill, D.L., Leach, M.O., Hawkes, D.J., 1999. Nonrigid registration using free-form deformations: application to breast MR images. *IEEE Transactions on Medical Imaging* 18, 712–721. <http://dx.doi.org/10.1109/42.79628410534053>.
- Sdika, M., Pelletier, D., 2009. Nonrigid registration of multiple sclerosis brain images using lesion inpainting for morphometry or lesion mapping. *Human Brain Mapping* 30, 1060–1067. <http://dx.doi.org/10.1002/hbm.2056618412131>.
- Schmidt, P., Gaser, C., Arsic, M., Buck, D., Förschler, A., Berthele, A., Hoshi, M., Ilg, R., Schmid, V.J., Zimmer, K., Hemmer, B., Muhlau, B., 2012. An automated tool for detection of FLAIR-hyperintense white-matter lesions in multiple sclerosis. *Neuroimage* 59, 43774–43783.
- Shattuck, D.W., Sandor-Leahy, S.R., Schaper, K.A., Rottenberg, D.A., Leahy, R.M., 2001. Magnetic resonance image tissue classification using a partial volume model. *Neuroimage* 13, 856–876. <http://dx.doi.org/10.1006/nimg.2000.073011304082>.
- Sled, J.G., Zijdenbos, A.P., Evans, C.P., 1997. A nonparametric method for automatic correction of intensity nonuniformity in MRI data. I. *IEEE Transactions on Medical Imaging* 17, 87–97.
- Smith, S.M., 2002. Fast robust automated brain extraction. *Human Brain Mapping* 17, 143–155. <http://dx.doi.org/10.1002/hbm.1006212391568>.
- Sormani, M.P., Arnold, D.L., De Stefano, N., 2014. Treatment effect on brain atrophy correlates with treatment effect on disability in multiple sclerosis. *Annals of Neurology* 75, 43–49. <http://dx.doi.org/10.1002/ana.2401824006277>.
- Valverde, S., Oliver, A., Cabezas, M., Roura, E., Lladó, X., 2014. Comparison of 10 brain tissue segmentation methods using revisited ISX annotations. *Journal of Magnetic Resonance Imaging: JMRI* <http://dx.doi.org/10.1002/jmri.2451724459099>.
- Zhang, Y., Brady, M., Smith, S.A., 2001. Segmentation of brain MR images through a hidden Markov random field model and the expectation-maximization algorithm. *IEEE Transactions on Medical Imaging* 20, 45–57. <http://dx.doi.org/10.1109/42.90642411293691>.

Chapter 5

Quantifying brain tissue volume in multiple sclerosis with automated lesion segmentation and filling

In this chapter, we present a detailed evaluation of the performance of different pipelines that incorporate fully automated processes such as lesion segmentation, lesion filling and tissue segmentation on MS data. For each automated pipeline, we analyze the percentage of error in tissue segmentation between a set of 70 MS images, where WM lesions have been refilled before segmentation and the same images processed at different levels of automation from manually masking lesions to fully automated lesion segmentation and filling. This analysis has been published in the following paper:

Paper published in the NeuroImage: Clinical journal (NICL) Volume: 9, Pages: 640-647, Published: October 2015 DOI: doi:10.1016/j.nicl.2015.10.012 JCR N IF 2.526, Q2(6/14)
--



Quantifying brain tissue volume in multiple sclerosis with automated lesion segmentation and filling



Sergi Valverde^{a,*}, Arnau Oliver^a, Eloy Roura^a, Deborah Pareto^b, Joan C. Vilanova^c, Lluís Ramió-Torrentà^d,
Jaume Sastre-Garriga^e, Xavier Montalban^e, Àlex Rovira^b, Xavier Lladó^a

^aDept. of Computer Architecture and Technology, University of Girona, Spain

^bMagnetic Resonance Unit, Dept. of Radiology, Vall d'Hebron University Hospital, Spain Architecture and Technology, University of Girona, Spain

^cGirona Magnetic Resonance Center, Spain

^dMultiple Sclerosis and Neuro-immunology Unit, Dr. Josep Trueta University Hospital, Spain

^eNeurology Unit, Multiple Sclerosis Centre of Catalonia (Cemcat), Vall d'Hebron University Hospital, Spain

ARTICLE INFO

Article history:

Received 22 July 2015

Received in revised form 21 October 2015

Accepted 23 October 2015

Available online 28 October 2015

Keywords:

Brain

Multiple sclerosis

MRI

Brain atrophy

Automated tissue segmentation

White matter lesions

Lesion filling

ABSTRACT

Lesion filling has been successfully applied to reduce the effect of hypo-intense T1-w Multiple Sclerosis (MS) lesions on automatic brain tissue segmentation. However, a study of fully automated pipelines incorporating lesion segmentation and lesion filling on tissue volume analysis has not yet been performed. Here, we analyzed the % of error introduced by automating the lesion segmentation and filling processes in the tissue segmentation of 70 clinically isolated syndrome patient images. First of all, images were processed using the LST and SLS toolkits with different pipeline combinations that differed in either automated or manual lesion segmentation, and lesion filling or masking out lesions. Then, images processed following each of the pipelines were segmented into gray matter (GM) and white matter (WM) using SPM8, and compared with the same images where expert lesion annotations were filled before segmentation. Our results showed that fully automated lesion segmentation and filling pipelines reduced significantly the % of error in GM and WM volume on images of MS patients, and performed similarly to the images where expert lesion annotations were masked before segmentation. In all the pipelines, the amount of misclassified lesion voxels was the main cause in the observed error in GM and WM volume. However, the % of error was significantly lower when automatically estimated lesions were filled and not masked before segmentation. These results are relevant and suggest that LST and SLS toolboxes allow the performance of accurate brain tissue volume measurements without any kind of manual intervention, which can be convenient not only in terms of time and economic costs, but also to avoid the inherent intra/inter variability between manual annotations.

© 2015 The Authors. Published by Elsevier Inc. This is an open access article under the CC BY-NC-ND license (<http://creativecommons.org/licenses/by-nc-nd/4.0/>).

1. Introduction

Multiple sclerosis (MS) is associated with irreversible brain damage not only in demyelinated plaques, but also in normal-appearing gray matter (GM) and white matter (WM), where recent studies have shown that the rate of tissue loss per year in MS patients ranges from 0.7% to 1.6% in GM, and 0.6% to 0.9% in WM (Filippi et al., 2013; Pérez-Miralles et al., 2013; Sastre-Garriga et al., 2014). Given the correlation between brain atrophy and disease disability, measuring the change in tissue volume is clinically relevant because it allows for optimizing possible treatments and patient management in early stages of the disease (Filippi et al., 2013; Sastre-Garriga et al., 2014; Uher et al., 2014).

Automated tissue segmentation techniques based on magnetic resonance imaging (MRI) such as the Statistical Parametric Mapping (SPM) (Ashburner and Friston, 2005), FAST (Zhang et al., 2001), or SIENA-X (Smith et al., 2002) are currently standard tools to assess brain tissue volume (De Bresser et al., 2011; Valverde et al., 2015a). The reproducibility of these techniques has been analyzed in several studies using scan-rescan measurement tests, reporting mean percentages of error in FAST GM of -0.22% (De Boer et al., 2010), 0.05% (De Boer et al., 2010) and -0.80% (Nakamura et al., 2014) in SPM8 GM, 1.50% (Nakamura et al., 2014) in SIENA-X GM, 0.13% (De Boer et al., 2010) in FAST WM, and 0.25% (De Boer et al., 2010) in SPM WM. However, existing differences for a particular method in different studies may be influenced by the same image data, imaging hardware and acquisition parameters (Clark et al., 2006). Furthermore, several authors have reported that the inclusion of WM lesions in tissue segmentation can affect significantly the accuracy of these techniques (Battaglini et al., 2012; Nakamura and Fisher, 2009; Valverde et al., 2015b), leading to

* Corresponding author at: Ed. P-IV, Campus Montilivi, University of Girona, 17071 Girona, Spain.

E-mail address: svalverde@eia.udg.edu (S. Valverde).

the development of different preprocessing strategies to fill lesion regions with signal intensities similar to WM before tissue segmentation (Battaglini et al., 2012; Chard et al., 2010; Valverde et al., 2014). So far, in all the lesion filling approaches, MS lesions have to be delineated first, usually by their manual annotation, which is a tedious, challenging and time-consuming task (Sanfilipo et al., 2005). This fact and the necessity to analyze quantitatively focal MS lesions in individual (Cabezas et al., 2014) and temporal (Ganiler et al., 2014) studies have been driving in recent years the development of automated new lesion segmentation techniques (García-Lorenzo et al., 2013; Guizard et al., 2015; Lladó et al., 2012).

Although lesion filling techniques have already been applied to assess the progression of GM atrophy of MS patients (Ceccarelli et al., 2012; Nakamura et al., 2014; Popescu et al., 2014), still an extensive analysis of the effect of fully automated pipelines, incorporating both automated MS lesion segmentation and posterior lesion filling on tissue segmentation methods has not yet been performed. In this study, we analyze the effect of two publicly available automated pipelines, Salem Lesion Segmentation (SLS) (Roura et al., 2015) and Lesion Segmentation Toolbox (LST) (Schmidt et al., 2012), on the accuracy of the GM and WM volume estimations of a cohort of 70 clinically isolated syndrome (CIS) patients. For each automated pipeline, we evaluate the deviation in GM and WM volume between images where manual expert annotations have been used to refill lesions before tissue segmentation with SPM8 (Ashburner and Friston, 2005), and the same images where lesions have been automatically segmented and either masked or lesion filled before tissue segmentation.

2. Materials and methods

2.1. Image acquisition

Seventy CIS patients from the same center (Hospital Vall D'Hebron, Barcelona (Spain)) in which the clinical presentation was clearly suggestive of multiple sclerosis underwent MR imaging on the same 3 T Siemens with 12-channel phased-array head coil (Trio Tim, Siemens, Germany). The following pulse sequences were obtained: 1) transverse proton density and T2-weighted fast spin-echo (TR = 2500 ms, TE = 16–91 ms, voxel size = $0.78 \times 0.78 \times 3 \text{ mm}^3$); 2) transverse fast T2-FLAIR (TR = 9000 ms, TE = 93 ms, TI = 2500 ms, flip angle = 120° , voxel size = $0.49 \times 0.49 \times 3 \text{ mm}^3$); and 3) sagittal 3D T1 magnetization prepared rapid gradient-echo (MPRAGE) (TR = 2300 ms, TE = 2 ms; flip angle = 9° ; voxel size = $1 \times 1 \times 1.2 \text{ mm}^3$). White matter lesion masks were semi-automatically delineated from either PD-w (46 patients) or FLAIR (24 patients) images using JIM software (Xinapse Systems, <http://www.xinapse.com/home.php>) by an expert radiologist of the same hospital center with more than 10 years of experience. Mean lesion volume was $4.1 \pm 4.7 \text{ ml}$ (range 0.2–18.3 ml), and $3.65 \pm 3.94 \text{ ml}$ (range 0.1–18.3 ml) on PD-w and FLAIR images, respectively.

2.2. Automated lesion segmentation and filling

Automated lesion segmentation and filling was performed using the T1-w and FLAIR image modalities on two publicly available toolkits implemented for the SPM (<http://www.fil.ion.ucl.ac.uk/spm>) software package:

2.2.1. SLS toolbox

The SLS pipeline (<http://atc.udg.edu/salem/slsToolbox/index.html>) was composed of the following automated steps: T1-w and FLAIR images were first skull-stripped and intensity corrected using the Brain Extraction Tool (BET) (Smith, 2002) with optimized parameter choice as described in Popescu et al. (2012), and the N3 method (Sled et al., 1998), respectively. Corrected T1-w and FLAIR images were then linearly co-registered (12-parameter affine) using internal SPM routines, with normalized mutual information as objective function and trilinear

interpolation with no wrapping. Lesion segmentation was performed by an initial tissue segmentation of the T1-w image to separate lesions from tissue, followed by a thresholding step and a regionwise refinement of the FLAIR image (Roura et al., 2015). The initial parameter used to adjust the detected candidate lesions was set to $\alpha = 2$, while the percentage of lesion candidate regions to belong to WM and GM over cerebro spinal fluid (CSF), percentage of neighbor voxels belonging to WM, and candidate size was set to $\lambda_{ts} = 0.7$, $\lambda_{nb} = 0.6$, and size = 3 mm^3 . Estimated lesion masks were then automatically filled using the method (Valverde et al., 2014), where candidate region voxels were replaced by random values of a normal distribution generated from the mean normal-appearing WM signal intensity of each two-dimensional T1-w slice. The SLF method was run with default parameters.

2.2.2. LST toolbox

The LST pipeline (www.applied-statistics.de/lst) was composed of the following automated steps: T1-w and FLAIR images were skull-stripped and intensity-corrected using the VBM8 toolbox included also as part of the SPM package. Afterwards, corrected T1-w and FLAIR images were linearly (12-parameter affine) and non-linearly co-registered using also internal SPM8 routines. Lesion segmentation was performed by computing an initial tissue segmentation of the T1-w image to compute a lesion belief map based on the FLAIR and T1-w images (Schmidt et al., 2012). This map was refined iteratively weighting the likelihood of belonging to WM or GM against the likelihood of belonging to lesions until no further voxels were assigned to lesions. The required initial threshold kappa was set to $k = 0.15$, while the lesion belief map was set to $l_{bm} = \text{GM}$. Estimated lesion masks were then automatically filled using an internal filling method inspired by a previous technique proposed in Chard et al. (2010), where candidate region voxels were replaced by random intensities from a Gaussian distribution generated from the normal-appearing WM intensities and then filtered to reintroduce the original spatial variation in WM.

2.3. Tissue volume analysis

All images were processed with both toolboxes and compared independently in order to preserve the differences in the internal routines of each toolbox. First, T1-w images processed by the SLS toolbox (see Table 1(a)) were segmented into GM, WM and CSF volumes using SPM8 after following five different pipeline configurations that differed in the level of manual intervention: 1) Original images were segmented including WM lesions (*Original pipeline*); 2) Expert manual lesion annotations were masked before tissue segmentation and relabeled as WM after (*Expert masked pipeline*); 3) Estimated lesion masks provided by the SLS method were masked before tissue segmentation and relabeled as WM after (*SLS masked pipeline*); 4) Estimated lesion masks provided by the SLS method were filled with the SLF method before tissue segmentation (*SLS filled*); and 5) Expert manual lesion annotations were filled before tissue segmentation and used as ground-truth images (*Expert filled pipeline*). In the case of the pipelines where lesions voxels were masked, either with automatic or manual annotations, lesion masks were used to remove lesion voxels in the T1-w image. Therefore, those voxels were not considered during tissue segmentation and were added to the WM class after it to maintain the actual brain volume of each patient. In contrast, in the lesion filling pipelines, automatic or manual lesion annotations were used to refill the correspondent T1-w image voxels with signal intensities similar to the WM, and lesion voxels were considered as normal-appearing WM in tissue segmentation.

All resultant tissue probability maps were binarized into GM, WM and CSF masks by extracting the maximum probability for each particular tissue. GM and WM tissue volume was computed by multiplying the number of voxels in binary masks by the voxel size ($1 \times 1 \times 1.2 \text{ mm}^3$). Volume measures were normalized to correct the differences between subjects by dividing the GM and WM volume by

Table 1

Evaluation pipelines followed in the present study. The set of T1-w images is processed independently for either the SLS (a) and LST (b) toolboxes. First, T1-w images are preprocessed (skull stripped and intensity corrected) using the routines indicated by each toolbox. Then, the preprocessed images are segmented into CSF, GM and WM tissue using SPM8 after following five different pipelines that differ in the level of manual intervention: 1) images are segmented including WM lesions (*Original* pipeline), 2) Expert manual lesion annotations are masked before tissue segmentation (*Expert masked* pipeline), 3) Estimated lesion masks returned by the same toolbox are masked before tissue segmentation (*SLS/LST masked* pipeline), 4) Estimated lesion masks returned by the same toolbox are filled with the lesion-filling method incorporated by each pipeline (*SLS/LST filled* pipeline), and 5) Expert manual lesion annotations are filled before tissue segmentation and used as ground-truth images (*Expert filled* pipeline).

(a)				
Pipeline	Preprocessing	Lesion segmentation	Lesion filling	Tissue segmentation
1. <i>Original</i>	BET + N3	–	–	SPM8
2. <i>Expert masked</i>	BET + N3	Manual	Expert annotations are masked	SPM8
3. <i>SLS masked</i>	BET + N3	SLS	SLS lesion masks are masked	SPM8
4. <i>SLS filled</i>	BET + N3	SLS	SLS lesion masks are filled by SLF	SPM8
5. <i>Expert filled</i> (GT)	BET + N3	Manual	Expert annotations are filled by SLF	SPM8
(b)				
Pipeline	Preprocessing	Lesion segmentation	Lesion filling	Tissue segmentation
1. <i>Original</i>	SPM8	–	–	SPM8
2. <i>Expert masked</i>	SPM8	Manual	Expert annotations are masked	SPM8
3. <i>LST masked</i>	SPM8	LST	LST lesion masks are masked	SPM8
4. <i>LST filled</i>	SPM8	LST	LST lesion masks are filled by LST	SPM8
5. <i>Expert filled</i> (GT)	SPM8	Manual	Expert annotations are filled by LST	SPM8

the whole brain volume. Then, the percent (%) absolute error in total and normal-appearing GM and WM volume was computed between pipelines: *Original* versus *Expert filled* images, *Expert masked* versus *Expert filled*, *SLS masked* versus *Expert filled*, and *SLS filled* versus *Expert filled*. The absolute error in total and normal-appearing GM and WM volume for each automated pipeline were computed using the following equations:

$$GM_{\{1...4\}vs5} = \frac{|NGMV_{\{1...4\}} - NGMV_5|}{NGMV_5} \times 100$$

$$WM_{\{1...4\}vs5} = \frac{|NWMV_{\{1...4\}} - NWMV_5|}{NWMV_5} \times 100$$

where $NGMV_{\{1...4\}}$ and $NWMV_{\{1...4\}}$ refer to the normalized GM and WM tissue volume, and the sub-indexes indicate the pipeline used: (1) *Original*, (2) *Expert masked*, (3) *SLS masked*, (4) *SLS filled* and (5) *Expert filled* pipeline used as ground-truth. Normal-appearing GM and WM volume was computed similarly, but lesion voxels were not considered in normalized GM and WM volume estimations. The procedure was then repeated identically for the LST toolbox (see Table 1(b)).

2.4. Statistical analysis

Statistical analysis was performed using the Matlab software package (<http://es.mathworks.com/products/matlab>). Differences in GM and WM volume of each evaluated pipeline were analyzed using a repeated measures ANOVA model with 3 degrees of freedom for the time variable and 207° for the error, followed by a series of post-hoc pairwise significant t-tests with Bonferroni correction between methods. Moreover, the Pearson's linear correlation coefficient was used to compute the correlation between % differences in GM and WM and lesion volume, and between % differences in GM and WM and the error produced by the automated lesion segmentation methods (Error I type: number of false positive outcomes, and Error II type: false negative outcomes). In all the analysis, we considered data significant at p-values < 0.05.

3. Results

3.1. Differences in tissue volume

First, we analyzed the differences in total tissue volume between the images processed following each of the SLS pipelines and the images

where expert lesion masks had been filled with the SLF method before tissue segmentation. Automated lesion segmentation and filling reduced significantly the % of error in total GM ($p < 0.032$) on the images processed with the fully automated *SLS filled* pipeline when compared with the same images segmented including lesions (*Original* pipeline) (see Fig. 1A). Similarly, the % differences in total WM were also significantly lower on the *Expert masked* ($p < 0.040$) and *SLS filled* ($p < 0.002$) pipelines when compared with the *Original* images (see Fig. 1B). Differences in total GM and WM between the *SLS masked* and *SLS filled* pipelines were not statistically different.

Regarding the LST toolbox, the mean % of error in GM volume was <0.12% in all the evaluated pipelines and similar to the values reported previously by the SLS, but was significantly higher in the *Original* images ($p < 0.003$) (see Fig. 1C). In WM, the effect of hypo-intense lesions was also significantly higher in the *Original* images ($p < 0.001$) when compared with the rest of the pipelines (see Fig. 1D). As in the SLS, the differences in total GM and WM between *LST masked* and *LST filled* were not significant.

The observed % of error in total GM and WM volume was not only distributed in lesion regions but also in normal-appearing tissue (see Fig. 2). In all the evaluated pipelines but the *Expert masked*, normal-appearing WM was overestimated by the effect of hypo-intense lesion voxels that were still present before tissue segmentation, either because they were not processed intentionally (*Original* pipeline), or as the result of misclassified lesion voxels. Lesion voxels that were classified as WM shifted down the signal intensity threshold between GM and WM and caused the actual GM voxels presenting an intensity profile similar to that of the lesions to be reassigned to WM. Identically; normal-appearing GM was underestimated by the opposite effect of lesion voxels in GM tissue volume. More importantly, in the images processed with the *Original*, *SLS masked*, and *SLS filled* pipelines, the actual % of error in total GM and WM volume was partly canceled between the opposite directions of the errors produced in normal-appearing tissue and the number of remaining lesion voxels that were incorrectly classified as GM (see Fig. 2).

As expected, images where expert lesion masks were masked before segmentation (*Expert masked* pipeline) returned the lowest % of error in normal-appearing GM (see Fig. 2A) and WM (see Fig. 2B) when compared not only with *Original* images ($p < 0.001$), but also with images processed with the *SLS masked* pipeline ($p < 0.018$). The % differences in normal-appearing WM of the images where estimated lesions using SLS were filled were significantly lower than in the same images where lesions were masked ($p < 0.024$). In contrast, differences were

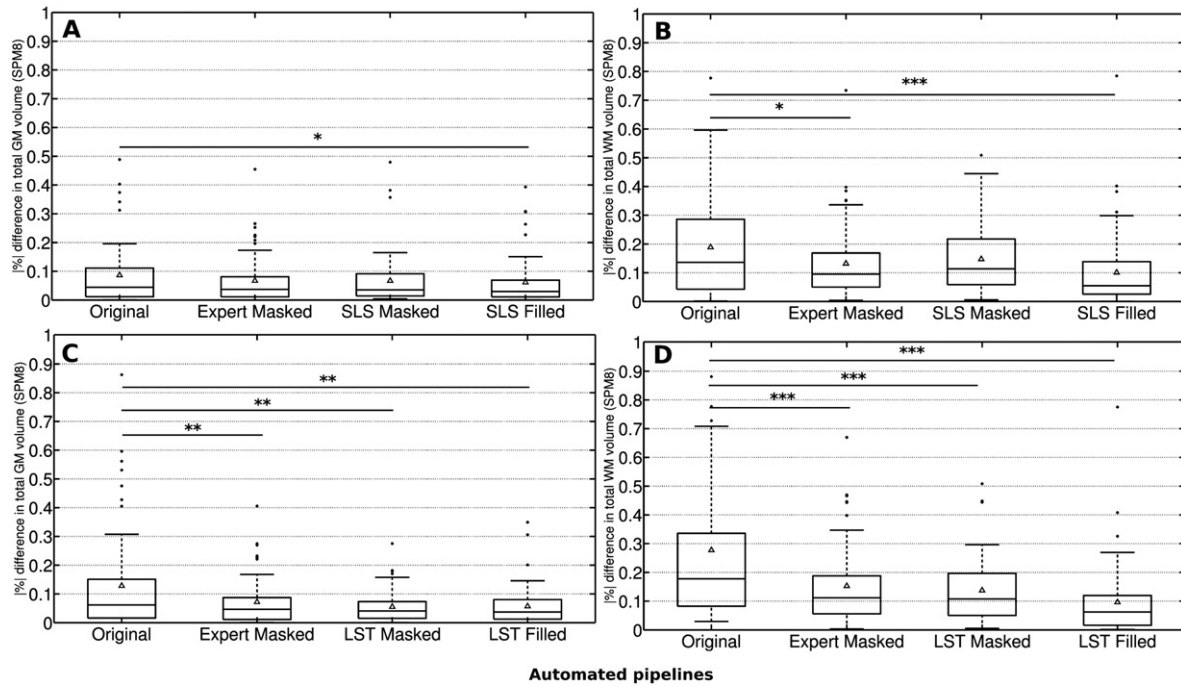


Fig. 1. % of absolute error in total GM and WM volume between segmented images where the annotated lesion masks were refilled before tissue segmentation (*Expert filled*) and the same images processed following the *Original*, *Expert masked*, *SLS/LST masked*, and *SLS/LST filled* pipelines. Results for the SLS toolbox are shown in the top row for GM (A) and WM (B), and for the LST toolbox in the bottom row for GM (C) and WM (D). The Δ symbol depicts the mean % difference in total GM/WM tissue for each pipeline. Horizontal lines show significant differences between evaluated pipelines with * $p < 0.05$, ** $p < 0.01$, *** $p < 0.001$.

similar for both tissues between the fully automated *SLS filled* and the *Expert masked* pipelines, showing that refilled voxels reduced the effect of hypo-intense lesions in normal-appearing tissue.

Similarly, in LST pipelines part of the % differences in total GM and WM was also partly canceled by the opposite direction of the errors in normal-appearing and the remaining lesion voxels that were

incorrectly classified as GM. As expected, the % differences in normal-appearing GM (see Fig. 2C) and WM (see Fig. 2D) were lower in the *Expert masked* pipeline ($p < 0.024$), due to the null effect of hypo-intense lesions in tissue segmentation. As in SLS, the effect of masking expert lesion masks on the errors in tissue segmentation was similar to that in the automated lesion segmentation and filling. The % differences in

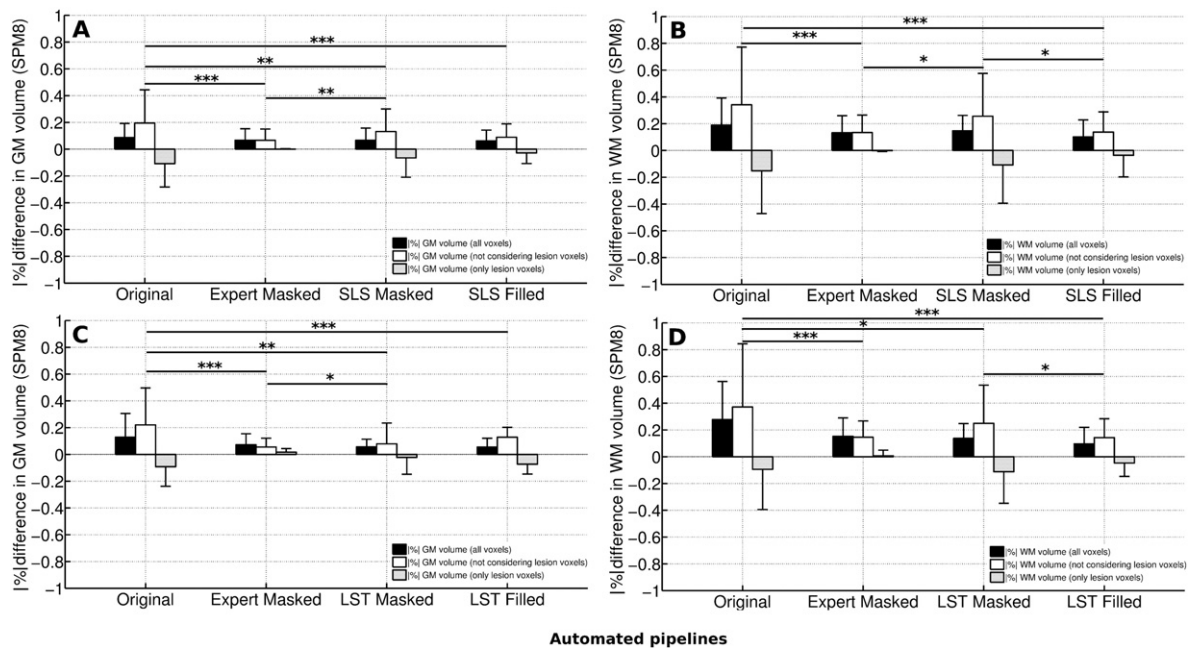


Fig. 2. Mean % of absolute error in tissue volume between segmented images where the annotated lesion masks were refilled before tissue segmentation (*Expert filled*) and the same images processed following each of the evaluated pipelines. Results for the SLS toolbox are shown in the top row for GM (A) and WM (B), and for the LST toolbox in the bottom row for GM (C) and WM (D). Differences in tissue volume are split in three regions: those produced when all voxels are considered (black bars), those produced when not considering lesion voxels (white bars), and those produced only in lesion voxels (gray bars). Lesion regions bars are plotted with negative bars to visualize the opposite direction of the errors in lesion voxels with respect to normal-appearing tissue. Vertical lines at each bar depict the % standard deviation difference in tissue volume for each pipeline. Horizontal lines show significant differences in normal-appearing volume between evaluated pipelines with * $p < 0.05$, ** $p < 0.01$, *** $p < 0.001$.

normal-appearing WM of the images where estimated lesions using LST were filled were also significantly lower than in the same images where lesions were masked ($p < 0.048$).

Fig. 3 depicts for a single patient image, the differences in the overlap of the tissue segmentation classes for each evaluated pipeline and the pertinent *Expert filled* image used as a ground-truth. As expected, the error in normal-appearing tissue (shown in red) was the lowest in the masked pipelines (images F and J), while the number of misclassified lesion voxels (shown in green) was remarkably higher in the *Original* pipelines (images E and I). This fact showed that the inclusion of hypo-intense lesion voxels into the tissue distributions has a clear effect in the misclassification of the normal-appearing tissue between boundaries, and also produces changes in the segmentation of brain structures such as the putamen. In contrast, when compared to these pipelines, the number of misclassified voxels in the automated pipelines incorporating lesion filling (panels H and L) was remarkably lower, although some false negatives were still present in the segmentation due to errors in the automatic lesion segmentation. The number of misclassified voxels was moderately lower in the automated pipelines incorporating lesion filling, when compared with automated pipelines where lesion masks were masked before segmentation (images G and K), although those differences were hardly appreciated in the picture.

When analyzing the % differences in tissue volume between LST and SLS pipelines, we observed that differences in GM between the

evaluated pipelines were not significant. In contrast, the % differences between *masked* and *filled* pipelines were found significant for total WM between *LST filled* and *SLS masked* ($p < 0.191$), normal-appearing WM between *LST masked* and *SLS filled* ($p = 0.007$), and normal-appearing WM between *Lst filled* and *SLS masked* ($p < 0.002$).

Finally, we studied the effect of the image modality used to annotate the expert lesion masks in the overall result. We recomputed the differences in total and normal-appearing GM and WM volume for the two subsets of images where expert masks were annotated using PD-w or FLAIR images. The differences in GM and WM volume between subsets were not statistically different for any of the SLS or LST evaluated pipelines ($p > 0.42$).

3.2. Correlation with lesion volume

We also analyzed the extent to which lesion volume affected the normal-appearing GM and WM volume measurements of each of the evaluated pipelines. Lesion volume strongly correlated with the reported % of error in GM and WM in the *Original*, *Expert masked* and *SLS filled* pipelines ($r > 0.77$, $p < 0.001$), and moderately in the *SLS masked* ($r > 0.41$, $p < 0.001$). However, the effect of lesion volume was different for each evaluated pipeline (Fig. 4A).

As expected, the deviation in normal-appearing GM and WM volume was remarkably higher in the images segmented with lesions,

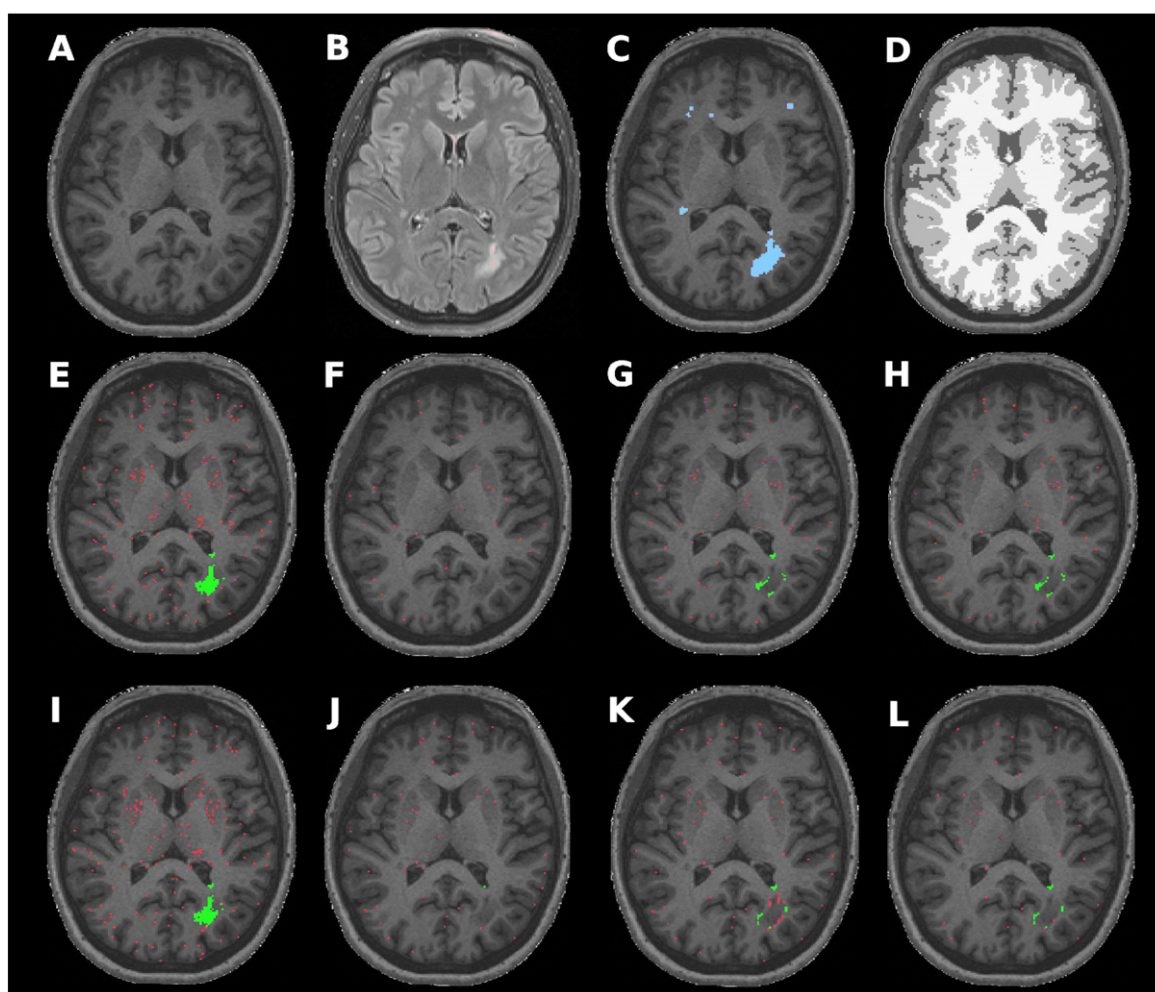


Fig. 3. For a single patient image of the dataset, we show the differences in the overlap of the tissue segmentation classes for each evaluated pipeline and the pertinent *Expert filled* image used as a ground-truth. Differences for any tissue class with respect to *Expert filled* are represented in green for lesion voxels, and in red for normal-appearing voxels. First row: input T1-w (A), input FLAIR (B), T1-w with expert annotations highlighted in blue (C), and T1-w output segmentation for the *Expert filled* image with CSF, GM and WM voxels depicted in black, gray, and white, respectively. Second row: for the images processed with the SLS toolkit, differences in any tissue classes for the *Original* (E), *Masked* (F), *SLS masked* (G), and *SLS filled* (H) pipelines. Third row: for the images processed with the LST toolkit, differences in any tissue class for the *Original* (I), *Masked* (J), *LST masked* (K), and *LST filled* (L) pipelines.

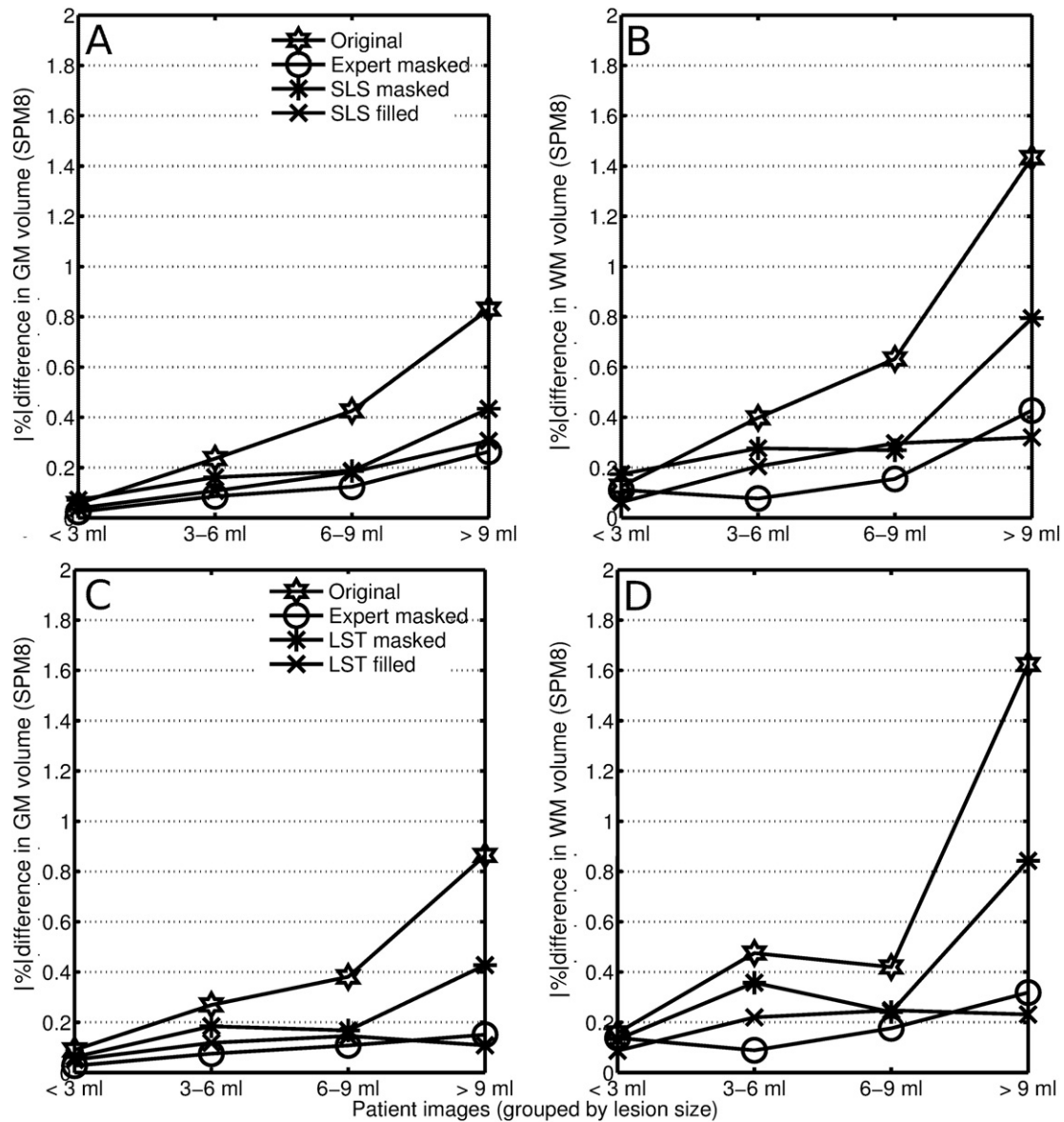


Fig. 4. Mean % of absolute error in normal-appearing GM and WM volume split by image groups with lesion size in the range (<3 ml, 3–6 ml, 6–9 ml, and >9 ml). Values for each group represent the mean % error between the images processed with the *Expert filled* and each of the evaluated pipelines (*Original* (☆), *Expert masked* (○), *SLS/LST masked* (*), and *SLS/LST filled* (✕)). Results for the SLS toolbox are shown in the top row for GM (A) and WM (B), and for the LST toolbox in the bottom row for GM (C) and WM (D).

where the % of error in WM was up to 1.46% on images with >9 ml lesion load (see Fig. 4B). The error in WM increased with lesion volume on images where lesions were automatically segmented, but this was remarkably lower on the *SLS filled* images than those that were masked before segmentation (*SLS masked*). On the subset of images with >9 ml, the performance of the *SLS filled* was similar to that of the *Expert masked* pipeline.

Lesion volume also strongly correlated with the observed differences in normal-appearing GM and WM for the *Original* ($r > 0.78$, $p < 0.001$) and *LST masked* ($r > 0.78$, $p < 0.001$) pipelines, and moderately for the *Expert masked* ($r > 0.36$, $p < 0.001$) and *LST filled* ($r > 0.40$, $p = 0.001$). As in the SLS, the error in GM and WM increased with lesion size on images where lesions were automatically segmented or intentionally left, and also increased remarkably in images where automatic lesion masks were masked instead of filled (see Fig. 4D). The % error in normal-appearing GM and WM of the *LST filled* pipeline was similar to that of the *Expert masked*.

3.3. Effect of lesion segmentation and filling

The lesion detection accuracy rate (true positives) of the SLS method was 0.43 ± 0.21 , while the Dice similarity coefficient (Dice, 1945) between the estimated and manual annotated masks was 0.32 ± 0.17 . The number of false positive lesion voxels (number of voxels misclassified as lesion), and false negative lesion voxels (number of missed lesion voxels) correlated with the % of error in total GM and WM volume of the *SLS filled* ($r > 0.60$, $p < 0.001$), and *LST filled* pipeline images ($r > 0.42$, $p < 0.001$). This suggested that in these pipelines, the observed error in tissue segmentation was mostly caused by the addition of false positive lesion voxels pertaining to GM that were filled with typical WM signal intensity, and also by the effect of missed hypo-intense WM lesion voxels into tissue distributions. In contrast, the % error in normal-appearing GM and WM in the images processed with the *SLS filled* and *LST filled* pipelines only correlated weakly with the number of false positives. Even some actual GM false positive voxels

were reassigned to WM, still WM voxels that were misclassified as lesion voxels were again reassigned to WM reducing the effect of false positives on the observed errors in normal-appearing tissue volume.

Similarly, the detection accuracy rate of the LST method was 0.41 ± 0.20 , with Dice similarity coefficient of 0.35 ± 0.21 , the number of false positives and false negatives correlated with the % of errors in total GM and WM of the *LST masked* pipeline ($r > 0.30$, $p = 0.01$), and only with the error in total GM of the *SLS masked* pipeline ($r > 0.52$, $p < 0.001$). Moreover, the number of false negative lesion voxels correlated weakly with the % of errors in GM and WM ($r > 0.40$, $p = 0.001$) of both pipelines. Contrary to filled images, actual GM voxels that were incorrectly classified as WM were not considered in tissue volume, reducing the linear correlation between the errors in lesion and tissue segmentation.

We also interchanged the lesion filling methods between the SLS and LST toolboxes and segmented again each set of images with the aim of evaluating the effect of each lesion filling process on the observed % differences in tissue volume. Differences were not statistically different with respect to the original pipelines for both GM and WM volume.

4. Discussion

The effect of lesions on total tissue volume was partly limited due to the canceling effect between the errors produced in normal-appearing tissue and the number of lesion voxels that were segmented as GM (Valverde et al., 2015b). This aspect is relevant because it explains why the observed % of error in total tissue volume was small or not significant between the evaluated pipelines of our study, even within the *Original* images intentionally segmented containing lesions. Furthermore, the % of error in total and normal-appearing WM volume in the images automatically segmented with either the SLS or LST was significantly lower when lesions voxels were filled than when they were masked before segmentation. As also reported in previous studies (Battaglini et al., 2012; Chard et al., 2010; Valverde et al., 2014), our results highlight the necessity to refill WM lesions before tissue segmentation for accurate cross-sectional tissue volume measurements.

However, the accuracy of automated lesion segmentation techniques is still low (Roura et al., 2015; Schmidt et al., 2012). Both automated pipelines overestimated normal-appearing WM (and underestimated GM) mostly by the effect of misclassified lesion voxels. Our results showed a significant but moderate correlation between underestimated total WM and the number of false positives of the *SLS filled* and *LST filled* pipelines. In contrast, the number of false positives correlated weakly with the differences in normal-appearing GM and WM, which might indicate that part of the false positive voxels that were actually WM were correctly reclassified after being filled. The % of error in the *SLS filled* and *LST filled* pipelines also correlated with the number of missed lesion voxels, which in addition to the clear correlation between the errors in tissue segmentation and lesion size, suggests that most of the differences observed in normal-appearing tissue volume were produced by the amount of missed lesion voxels that altered the tissue signal intensity distributions. This aspect suggests that the accuracy of new automatic tissue segmentation pipelines may be increased specially by reducing the number of missed lesion voxels, and in particular when those are hypo-intense in T1-w and should be filled before tissue segmentation. However, this study did not evaluate the methods with RRMS or SPSS image data, because the clinical focus of the study was on the initial CIS phenotype of MS, where paraclinical information is more relevant. In this regard, a further analysis of the accuracy of the evaluated pipelines on images with larger lesion load should be performed.

As expected, the *Expert masked* pipeline reported the lowest error in total and normal-appearing volume, although our results confirmed that masking out lesion voxels before tissue segmentation might not be optimal, as the error in tissue segmentation tends to increase with lesion size (Valverde et al., 2014). More interestingly, the performance of

the fully automated *SLS filled* and *LST filled* pipelines was similar to that of the *Expert masked*, which seems to indicate that upon a certain lesion load, the errors produced by misclassified lesion voxels in the fully automated pipelines were comparable to the masking out error produced by not filling the expert annotations before tissue segmentation.

Within our data, the maximum differences in tissue volume produced by the *SLS filled* and *LST filled* might be lower than the own reproducibility of the SPM method, as stated in previous studies (De Boer et al., 2010; Nakamura et al., 2014). However, a direct comparison between studies has to be contemplated with care, because we did not perform a scan-reposition-rescan analysis of the evaluated pipelines, and consequently the differences in tissue volume produced by automated methods should be added to the inner reproducibility of the tissue segmentation method. Additionally, differences in the pre-processing pipelines between studies should be also contemplated, as shown in previous studies (Boyes et al., 2008; Zheng et al., 2009). The maximum differences in tissue volume produced by the fully automated pipelines also raises the question if the observed differences could be considered negligible when compared with the loss in tissue volume observed in follow-up scans. In this aspect, the differences in tissue volume shown by both the *SLS filled* and *LST filled* are remarkably lower than yearly tissue loss reported in recent clinical studies (Filippi et al., 2013; Sastre-Garriga et al., 2014; Uher et al., 2014). Hence, given the small error introduced by these methods, we recommend the use of either the SLS or LST toolkit.

There are a number of limitations in this work that have to be considered. This study was conducted using single-center data, and hence the applicability in a multi-center study was not determined here. The lack of manual tissue annotations does not allow us to analyze the tissue segmentation accuracy of each of the evaluated pipelines. Gold-standard annotations are time-consuming and have to be delineated by trained experts, a task which unfortunately is not always possible, especially when the number of subjects grows. In this aspect, the results of this study have to be understood under the premise that we are not evaluating the accuracy of the tissue segmentation methods, but the differences with respect to the manual expert pipeline that introduces the lowest error in tissue volume in images containing WM lesions (Battaglini et al., 2012; Valverde et al., 2014). The % of error in GM and WM volume introduced by the evaluated pipelines was small, and it was difficult to scale our findings with previous studies, given the differences in preprocessing and internal routines of each pipeline. Furthermore, in spite of the small error observed, our claims about the effectiveness of the fully automated pipelines have to be prudent, given the lesion load of the cohort of CIS patients of our study. As a future work, we will investigate the effect of images with higher lesion load on automated lesion segmentation, the posterior lesion filling process, and the impact of these automated processes in tissue segmentation methods.

In summary, this study shows that the automated lesion segmentation and filling methods included in the LST and SLS toolboxes reduce significantly the impact of T1-w hypo-intense lesions on the SPM8 tissue segmentation method. Our results show that compared with the evaluated pipelines that require manual expert intervention, the accuracy in tissue segmentation is not affected remarkably on images processed with the fully automated pipelines. This is relevant and suggests that LST and SLS toolboxes allow for performing accurate brain tissue volume measurements without any kind of manual intervention. The possibility of filling MS white matter lesions without manual delineation of lesions is pertinent not only in terms of time and economic costs, but also to avoid the inherent *intra/inter* variability between manual annotations.

Acknowledgments

S. Valverde holds a FI-DGR2013 grant from the Generalitat de Catalunya. E. Roura holds a BR-UdG2013 grant. This work has been partially

supported by “La Fundació la Marató de TV3” and by Retos de Investigación TIN2014-55710-R.

References

- Ashburner, J., Friston, K., 2005. Unified segmentation. *NeuroImage* 26, 839–851.
- Battaglini, M., Jenkinson, M., De Stefano, N., 2012. Evaluating and reducing the impact of white matter lesions on brain volume measurements. *Hum. Brain Mapp.* 33 (9), 2062–2071.
- Boyes, R., Gunter, J.L., Frost, C., Janke, A.L., Yeatman, T., Hill, D., Bernstein, M.A., et al., 2008. Intensity non-uniformity correction using N3 on 3-T scanners with multichannel phased array coils. *NeuroImage* 39, 1752–1762.
- Cabezas, M., Oliver, A., Roura, E., Freixenet, J., Vilanova, J.C., Ramió-Torrentà, L., Rovira, A., Lladó, X., 2014. Automatic multiple sclerosis lesion detection in brain MRI by FLAIR thresholding. *Comput. Methods Prog. Biomed.* 115 (3), 147–161.
- Ceccarelli, A., Jackson, J.S., Tauhid, S., Arora, A., Gorky, J., Dell'Oglio, E., Bakshi, A., et al., 2012. The impact of lesion in-painting and registration methods on voxel-based morphometry in detecting regional cerebral gray matter atrophy in multiple sclerosis. *Am. J. Neuroradiol.* 33 (8), 1579–1585.
- Chard, D.T., Jackson, J.S., Miller, D.H., Wheeler-Kingshott, C.A., 2010. Reducing the impact of white matter lesions on automated measures of brain gray and white matter volumes. *J. Magn. Reson. Imaging* 32, 223–228.
- Clark, K.A., Woods, R.P., Rottenberg, D.A., Toga, A.W., Mazziotta, J.C., 2006. Impact of acquisition protocols and processing streams on tissue segmentation of T1-w weighted MR images. *NeuroImage* 29, 185–202.
- De Boer, R., Vrooman, H., Ikram, M., Vernooij, M., Breteler, M., Van der Lugt, A., Niessen, W., 2010. Accuracy and reproducibility study of automatic MRI brain tissue segmentation methods. *NeuroImage* 51 (3), 1047–1056.
- De Bresser, J., Portegies, M.P., Leemans, A., Biessels, G.J., Kappelle, L.J., Viergever, M.A., 2011. A comparison of MR based segmentation methods for measuring brain atrophy progression. *NeuroImage* 54 (2), 760–768.
- Dice, L.R., 1945. Measures of the amount of ecologic association between species. *Ecology* 26 (3), 297–302.
- Filippi, M., Preziosa, P., Copetti, M., Riccitelli, G., Horsfield, M.A., Martinelli, V., Comi, G., Rocca, M.A., 2013. Gray matter damage predicts the accumulation of disability 13 years later in MS. *Neurology* 81 (20), 1759–1967.
- Ganiler, O., Oliver, A., Díez, Y., Freixenet, J., Vilanova, J.C., Beltrán, B., Ramió-Torrentà, L., Rovira, A., Lladó, X., 2014. A subtraction pipeline for automatic detection of new appearing multiple sclerosis lesions in longitudinal studies. *Neuroradiology* 56 (5), 363–374.
- García-Lorenzo, D., Francis, S., Narayanan, S., Arnold, D.L., Collins, D.L., 2013. Review of automatic segmentation methods of multiple sclerosis white matter lesions on conventional magnetic resonance imaging. *Med. Image Anal.* 17 (1), 1–18.
- Guizard, N., Coupé, P., Fonov, V., Manjón, J., Arnold, D.L., Collins, D.L., 2015. Rotation-invariant multi-contrast non-local means for MS lesion segmentation. *NeuroImage Clin.* 8, 376–389.
- Lladó, X., Oliver, A., Cabezas, M., Freixenet, J., Vilanova, J.C., Quiles, A., Valls, L., Ramió-Torrentà, L., Rovira, A., 2012. Segmentation of multiple sclerosis lesions in brain MRI: a review of automated approaches. *Inf. Sci.* 186 (1), 164–185.
- Nakamura, K., Fisher, E., 2009. Segmentation of brain magnetic resonance images for measurement of gray matter atrophy in multiple sclerosis patients. *NeuroImage* 44 (3), 769–776.
- Nakamura, K., Guizard, N., Fonov, V.S., Narayanan, S., Collins, D.L., Arnold, D.L., 2014. Jacobian integration method increases the statistical power to measure gray matter atrophy in multiple sclerosis. *NeuroImage Clin.* 4, 10–17.
- Pérez-Miralles, F., Sastre-Garriga, J., Tintoré, M., Arrambide, G., Nos, C., Perkal, H., Río, J., et al., 2013. Clinical impact of early brain atrophy in clinically isolated syndromes. *Mult. Scler.* 19 (14), 1878–1886.
- Popescu, V., Battaglini, M., Hoogstrate, W.S., et al., 2012. Optimizing parameter choice for FSL-Brain Extraction Tool (BET) on 3D T1 images in multiple sclerosis. *NeuroImage* 61 (4), 1484–1494.
- Popescu, V., Ran, N.C.G., Barkhof, F., Chard, D.T., Wheeler-Kingshott, C.A., Vrenken, H., 2014. Accurate GM atrophy quantification in MS using lesion filling with co-registered 2D lesion masks. *NeuroImage Clin.* 4 (January), 366–373.
- Roura, E., Oliver, A., Cabezas, M., Valverde, S., Pareto, D., Vilanova, J.C., Ramió-Torrentà, L., Rovira, A., Lladó, X., 2015. A toolbox for multiple sclerosis lesion segmentation. *Neuroradiology* <http://dx.doi.org/10.1007/s00234-015-1552-2>.
- Sanfilipo, M.P., Benedict, R.B., Sharma, J., Weinstock-Guttman, B., Bakshi, R., 2005. The relationship between whole brain volume and disability in multiple sclerosis: a comparison of normalized gray vs. white matter with misclassification correction. *NeuroImage* 26 (4), 1068–1077.
- Sastre-Garriga, J., Tur, C., Pareto, D., Vidal-Jordana, A., Auger, C., Río, J., Huerga, E., Tintoré, M., Rovira, A., Montalban, X., 2014. Brain atrophy in natalizumab-treated patients: a 3-year follow-up. *Mult. Scler.* <http://dx.doi.org/10.1177/1352458514556300>.
- Schmidt, P., Gaser, C., Arsic, M., Buck, D., Förschler, A., Berthele, A., Hoshi, M., et al., 2012. An automated tool for detection of FLAIR-hyperintense white-matter lesions in multiple sclerosis. *NeuroImage* 59 (4), 3774–3783.
- Sled, J.G., Zijdenbos, P., Evans, C., 1998. A nonparametric method for automatic correction of intensity nonuniformity in MRI data. *IEEE Trans. Med. Imaging* 17 (1), 87–97.
- Smith, S.M., 2002. Fast robust automated brain extraction. *Hum. Brain Mapp.* 17, 143–155.
- Smith, S.M., Zhang, Y., Jenkinson, M., Chen, J., Matthews, P.M., Federico, A., De Stefano, N., 2002. Accurate, robust, and automated longitudinal and cross-sectional brain change analysis. *NeuroImage* 17 (1), 479–489.
- Uher, T., Horakova, D., Bergsland, N., Tyblova, M., Ramasamy, D.P., Seidl, Z., Vaneckova, M., Krasensky, J., Havrdova, E., Zivadinov, R., 2014. MRI correlates of disability progression in patients with CIS over 48 months. *NeuroImage: Clinical* 6 (January). Elsevier B.V., pp. 312–319.
- Valverde, S., Oliver, A., Lladó, X., 2014. A white matter lesion filling approach to improve brain tissue volume measurements. *NeuroImage Clin.* 6 (January), 86–92.
- Valverde, S., Oliver, A., Cabezas, M., Roura, E., Lladó, X., 2015a. Comparison of 10 brain tissue segmentation methods using revisited IBSR annotations. *J. Magn. Reson. Imaging* 41 (1), 93–101.
- Valverde, S., Oliver, A., Díez, Y., Cabezas, M., Vilanova, J.C., Ramió-Torrentà, L., Rovira, A., Lladó, X., 2015b. Evaluating the effects of white matter multiple sclerosis lesions on the volume estimation of 6 brain tissue segmentation methods. *Am. J. Neuroradiol.* <http://dx.doi.org/10.3174/ajnr.A4262>.
- Zhang, Y., Brady, M., Smith, S., 2001. Segmentation of brain MR images through a hidden Markov random field model and the expectation-maximization algorithm. *IEEE Trans. Med. Imaging* 20, 45–57.
- Zheng, W., Chee, M.W., Zagorodnov, V., 2009. Improvement of brain segmentation accuracy by optimizing non-uniformity correction using N3. *NeuroImage* 48, 73–83.

Chapter 6

Automated tissue segmentation of MR brain images in the presence of white matter lesions

In this chapter, we propose a novel, automated pipeline for tissue segmentation of MS patient images containing lesions. The accuracy of the method is evaluated using both the challenge MRBrainS13 database¹ and a 3T MS database of MS patient images. We validate the accuracy of the proposed method with other state-of-the-art techniques. A public version of this method has been released for public use. The proposed pipeline has been described in detail in the next paper and submitted to the Medical Imaging Journal:

Paper submitted to the Medical Image Analysis (MIA) journal Currently in revision. JCR CSAI IF 3.654, Q1 (10/121)
--

¹<http://mrbrains13.isi.uu.nl/>

Automated tissue segmentation of MR brain images in the presence of white matter lesions

Sergi Valverde^{a,*}, Arnau Oliver^a, Eloy Roura^a, Sandra González^a, Deborah Pareto^b, Joan C. Vilanova^c,
Lluís Ramió-Torrentà^d, Àlex Rovira^b, Xavier Lladó^a

^aResearch institute of Computer Vision and Robotics, University of Girona, Spain

^bMagnetic Resonance Unit, Dept of Radiology, Vall d'Hebron University Hospital, Spain

^cGirona Magnetic Resonance Center, Spain

^dMultiple Sclerosis and Neuroimmunology Unit, Dr. Josep Trueta University Hospital, Spain

Abstract

Over the last few years, the increasing interest in brain tissue volume measurements on clinical settings has led to the development of a wide number of automated tissue segmentation methods. However, white matter lesions are known to reduce the accuracy of automated tissue segmentation methods. This requires manual annotation of the lesions and refilling them before segmentation, which is tedious and time-consuming. Here, we propose a new, fully automated T1-w/FLAIR tissue segmentation approach designed to deal with images in the presence of WM lesions. This approach integrates a robust partial volume tissue segmentation with WM outlier rejection and filling, combining intensity and probabilistic and morphological prior maps. We evaluate the accuracy of this method on the MRBrainS13 tissue segmentation challenge database, and also on a set of Multiple Sclerosis (MS) patient images. On both databases, we validate the performance of our method with other state-of-the-art techniques. On the MRBrainS13 data, the presented approach was the best ranked method relying in unsupervised intensity models of the challenge (7th position) and clearly outperformed the other unsupervised pipelines such as *FAST* and *SPM12*. On MS data, the differences in tissue segmentation between the images segmented with our method and the same images where manual expert annotations were used to refill lesions on T1-w images before segmentation were lower or similar to the best state-of-the-art pipeline incorporating automated lesion segmentation and filling. Our results show that the proposed pipeline quantitatively improved the accuracy of tissue segmentation while it achieved very competitive results on MS images. A public version of this approach is available to download for the neuro-imaging community.

Keywords: Brain, MRI, multiple sclerosis, automatic tissue segmentation, white matter lesions

1. Introduction

Brain tissue volume based on Magnetic Resonance Imaging (MRI) is increasingly being used in clinical settings to assess brain volume in different neurological dis-

eases such as Multiple Sclerosis (MS) (Giorgio and De Stefano, 2013). In MS, several studies have analyzed the histopathological changes in patients with respect to the progress of the disease, showing that the percentage of change in brain volume tends to correlate with worsening conditions (Pérez-Miralles et al., 2013; Sormani et al., 2014). However, manual segmentation of brain tissue is both challenging and time-consuming because of the large number of MRI slices for each patient that make up the three-dimensional information, and the

*Corresponding author. S. Valverde, Ed. P-IV, Campus Montilivi, University of Girona, 17071 Girona (Spain). e-mail: svalverde@eia.udg.edu. Phone: +34 972 418878; Fax: +34 972 418976.

Chapter 7

Main results and discussion

MRI tissue segmentation techniques are being used increasingly as standard tools to assess brain tissue volume. However, automated tissue segmentation is still a challenging task in MS, due to the tissue abnormalities found in MS patient images such as WM lesions that are known to reduce the accuracy of tissue segmentation methods. When expert manual annotations of WM lesions are available, lesion filling has shown to be an effective method to reduce the effects of those lesions on tissue segmentation. However, manual annotations are time-consuming and prone to variability among experts, which in combination with the need to analyze focal MS lesions quantitatively in individual and temporal studies, has led to the development of a wide number of automated lesion segmentation of MS lesions. Therefore, a solid understanding of the effects of MS lesions on automated pipelines that concatenate processes such as lesion segmentation, lesion filling and tissue segmentation is important.

As stated in section 1.3, each of these processes covers a part of the necessary knowledge needed to accomplish the goal of this thesis. This chapter provides a comprehensive discussion of the main results shown in previous chapters, analyzing each of these necessary processes for the development of a fully automated tissue segmentation method for MS images.

7.1 Effect of WM lesions on tissue segmentation

A wide number of automated tissue segmentation methods have been proposed in the literature so far. In Chapter 2, we evaluated the accuracy of ten approaches using the two available public databases of healthy subjects, IBSR18 and IBSR20. With the aim of including a wide set of different segmentation approaches and available tools, the analysis included well-known implementations of image segmentation

algorithms such as ANN, FCM, and KNN, as well as available public toolboxes such as FAST, SPM5, SPM8, PVC, GAMIXTURE, SVPASEG, and FANTASM. Results were presented before and after correcting the CSF masks, as we saw that available annotations ignored sulcal CSF tissue in the original masks. When sulcal CSF was corrected, the SVPASEG, SPM8 and FAST yielded the highest accuracy with both databases. However, the performance of the methods varied when segmenting different manual annotated GM brain structures such as the left and right putamen and ventral diencephalon, due to the lack of contrast and the similar intensity profile of those structures with respect to the WM. These differences in combination with the fact that most of the methods were not robust against changes in acquisition sequences, intensity inhomogeneities and special attributes of the two databases, highlights that brain tissue segmentation was still an open problem, since there was not a single method that achieved a significantly higher accuracy with all tissues.

Afterwards, six of these methods (ANN, FCM, FANTASM, FAST, SPM5 and SPM8) were evaluated on MS data from different hospital centers and scanners in order to analyze the extent to which tissue volume estimations were affected by changes in the WM lesion volume and intensity. Our results showed that the SPM8 had the lowest differences in total volume, while the FANTASM and again, the SPM8 were the methods where the incidence of WM lesions was the lowest on normal-appearing tissue. In general, the differences in tissue volume were lower for methods combining morphological prior information, namely the SPM5 and SPM8, or spatial constraints, like the FANTASM and FAST. In contrast, these differences were higher on simpler intensity based algorithms such as FCM and ANN, that lacked spatial correction. This fact and the higher performance on healthy data of former methods, stressed the necessity of adding morphological prior information and/or spatial constraints to the automated brain tissue segmentation, not only to overcome inherent MRI bias field artifacts but also as an important component to deal with WM lesions.

The main factor in the differences in tissue volume across the methods was caused by lesion volume. Furthermore, WM lesion voxels tended to be classified as GM in images where the variation between the lesion signal intensity and the mean signal intensity of normal-appearing WM was higher, which indicated a direct relationship between the differences in the brain tissue volume and the changes in the lesion load and WM lesion intensity. However, the lesion voxels also had a direct effect on the differences in GM and WM outside the lesion regions. As already mentioned in Chapter 3, these differences are especially important because they highlight the bias introduced by WM lesions on the estimation of tissue volume that is not pathologically affected. Our analysis showed that if lesion voxels were not considered in the computation of the brain volume, methods would still tend to overestimate GM, especially in images with a higher lesion load. The observed differences in normal-appearing tissue volume were important. Although lesion voxels could be reassigned

to WM after segmentation, part of the bias was still present if these lesions were present in image segmentation.

Furthermore, differences in the total tissue volume may be canceled between the errors produced in the same lesion regions as well as the effect of these voxels on normal-appearing tissue. This fact clearly shows the necessity of either processing WM lesions before segmentation or modeling them as part of the tissue segmentation formulation.

7.2 Effect of lesion filling in tissue segmentation

Over the last few years, different techniques have been proposed to reduce the bias introduced by WM lesions on the brain tissue volume measurements in MS images, mostly by in-painting WM lesions on T1-w with signal intensities similar to normal-appearing WM. After reviewing the available related literature in Chapter 4, we classified the existing methods into groups, those that filled WM lesions using the *local* intensities from the surrounding neighboring lesion voxels, and those that used *global* WM intensities from the whole brain to fill WM lesions. Although all these methods had already been validated separately, we performed a general comparison of all the available techniques in order to analyze their accuracy with the same 1.5T and 3T data and also to investigate their performance with different tissue segmentation techniques such as the FAST and SPM8.

This analysis served as a basis for a new technique to refill WM lesions that was a compromise between *global* and *local* methods. Our proposed method filled lesion voxel intensities with random values of a normal distribution generated from the mean WM signal intensity of each two-dimensional slice. Contrary to *local* methods, where lesions were refilled with signal intensities coming from surrounding WM voxels, our approach was capable to reproduce better the original WM tissue distribution on images with high lesion load, because lesion voxels were refilled using random signal intensities from all the WM voxels of the slice. Although on our approach the probability of each tissue was first estimated using a clustering three-dimensional segmentation, we found that filling lesions with signal intensities from the same slice was more appropriate, as this approach reproduced better the intensity distribution of WM tissue at each slice than using the global three-dimensional intensity profile.

Our results showed that when compared to other methods, our approach yielded the lowest deviation in GM and WM volumes with 1.5T and 3T data when the FAST tissue segmentation was used. When the SPM8 tissue segmentation method was used, the performance of our lesion filling method was also very competitive, yielding the lowest differences or similar to those of the best method in GM and

WM. In contrast to the rest of the pipelines, differences in tissue volume between the same images filled with our method and afterwards segmented with either the FAST or SPM8 were very low ($< 0.1\%$), which indicates that the proposed strategy was equally efficient independently of the tissue segmentation chosen.

The proposed algorithm performed significantly better than *local* methods on images with higher lesion loads. In contrast to *global* methods, *local* methods may be limited by the range of similar intensities coming from neighboring voxels, which on images with large lesions may introduce a bias on GM and WM tissue distributions by the addition of a considerable number of voxels with similar intensities. Furthermore, the performance of our approach was also better on images with high lesion loads when compared with *local* methods, specially on images with lower resolution such as 1.5T data, most probably because our method estimated the mean global normal-appearing WM intensity for each slice independently, being sensitive enough to reproduce possible changes in the intensities between slices.

7.3 Effect of automating lesion segmentation and filling on tissue segmentation

As already mentioned earlier, lesion filling has proven to be an effective method to reduce the effects of these lesions on tissue segmentation. However, in all the lesion-filling approaches, including ours, MS lesions have to be known a priori, which requires delineating lesions manually. This is a clear limitation in terms of fully automatizing brain tissue in the presence of MS lesions, which motivated the evaluation of the effect of automated lesion segmentation on tissue segmentation. Although different automated tissue segmentation methods have been proposed, most are based on supervised learning, which requires explicit training, usually with a large amount of labeled data. Labeled data may be not available, which increased the interest of the community in unsupervised methods that can operate without prior data. As shown in Chapter 5, we compared two pipelines that combined automated lesion segmentation and filling as a first step to understand the effect of fully processed images on tissue segmentation.

Given the performance shown in our previous studies and its wide use in clinical studies, the SPM8 was used as a reference tissue segmentation method to measure tissue volume on a set of 70 3T images from CIS patients. On these images, available manual expert annotations were employed to refill WM lesions before segmentation using the pipeline's filling method, and were considered as the ground-truth. Afterwards, we evaluated the differences in the GM and WM volumes between the set of filled images using manual annotations and the same images processed using different variations of the SLS and LST toolkits that differed in the level of manual

intervention. Evaluating different pipelines with distinct levels of automation permitted us to analyze the effect of each of the automated processes involved in the differences in the total and normal-appearing tissue volumes.

As already stated in Chapter 3, this new analysis showed that the effect of lesions on the total tissue volume was limited due to a canceling effect between the errors produced in the same lesion regions, and the effect of these voxels on normal-appearing tissue. In all the pipelines that incorporated automated lesion segmentation, most of the differences observed in normal-appearing tissue were produced by the effect of false positive lesion voxels that were already segmented and had not been refilled. In contrast, there was no relevant correlation between the number of false positive lesion voxels and the differences observed in normal-appearing GM and WM, which suggested that most of these misclassified voxels were actually WM before refilling. The relationship between errors in automated lesion and tissue segmentation also suggest the importance of not only continuously reducing the number of missed lesions, but also stressing the necessity of contextual spatial information of lesion regions in order to confine them in the WM and, hence, reduce the effect of misclassified voxels on the tissue segmentation.

As shown in the results presented in Chapter 4, masking-out lesion voxels before tissue segmentation might not be optimal, as leaving lesion voxels out of the tissue distributions appears to increase the differences in tissue volume with respect to lesion filled images, even if these voxels are re-assigned to WM afterwards. However, although not optimal, masking lesions before segmentation has proven to be a valid alternative to reduce the effects of WM lesions on research and clinical settings, and as a result in recent years, lesion filling techniques have already been applied on research and clinical studies. Regarding this, our results show that at least with the evaluated data, the differences in tissue volume between images where expert lesion masks have been masked-out and the same images where lesions have been automatically segmented and filled, are similar to images with a low lesion load ($< 10ml$). In contrast, from our experiments we observed that differences in tissue volumes tend to increase with the lesion load on masked-out images, while the increase of the error is more moderate in fully-automated images. However, given the data available and the maximum lesion load considered in our analysis ($< 20ml$), these findings should be considered with care.

In any case, our analysis pointed out the fact that automated lesion segmentation and filling methods significantly reduced the impact of WM lesions on tissue segmentation, and had a similar performance to the pipelines that required manual expert intervention. These results were relevant and demonstrated that each of these automated processes could be useful not only in terms of time and economic costs, but also as active processes in fully automated tissue segmentation in the presence of WM lesions.

7.4 Fully automated tissue segmentation of images containing WM lesions

Previous sections of this thesis have stressed the advantages of dealing with MS lesions before the tissue segmentation, showing several general insights that can be useful for automated tissue segmentation of images containing lesions. The results obtained for the different methods evaluated in Chapters 2 and 3 have pointed out the superiority of methods that benefited from morphological prior information or spatial constraints in automated brain tissue segmentation. More importantly, the results obtained in Chapter 3 have evidenced the effect of WM lesion on tissue segmentation and the necessity of dealing with MS lesions in order to reduce not only the bias produced by the same lesions but also the effect of these lesion voxels on normal-appearing tissue. In this scenario, we have proposed a new lesion filling technique that is very competitive with different databases and tissue segmentation methods, as shown in Chapter 4. Finally, we showed in Chapter 5 that the addition of unsupervised lesion segmentation and filling to already existing tissue segmentation pipelines significantly reduced the error in tissue volume when compared with other pipelines where lesions were segmented as normal tissue.

Following these insights, we have developed a new, multi-channel method designed to segment brain tissues in MRI images of MS patients. As explained in Chapter 6, this approach makes use of a combination of intensity, anatomical and morphological prior maps to guide the tissue segmentation. Tissue segmentation has been tackled based on a robust partial volume segmentation where WM outliers have been estimated and refilled before segmentation using a multi-channel post-processing algorithm integrating partial volume segmentation, spatial context, and prior anatomical and morphological atlases. Furthermore, the proposed method takes advantage of new affordable processors, such as GPUs, that reduce up to four times the execution time to register and segment tissue when compared to general purpose CPUs. This property makes this method useful for studies containing a large number of subjects to analyze.

The proposed method has been quantitatively and qualitatively evaluated using different databases of images containing WM lesions. In order to analyze the extent to which the T1-w and FLAIR modalities intervened in the accuracy obtained, the proposed method was run in all the experiments using only the T1-w or using both the T1-w and FLAIR image sequences. As shown by the results, the proposed technique yielded competitive and consistent results in both general and MS specific databases without parameter tweaking. In the MRBrainS tissue segmentation challenge¹, our method, combining both T1-w and FLAIR, was the best non-supervised

¹<http://mrbrains13.isi.uu.nl/>

technique in the challenge, being ranked in 7th position out of 31 participant methods. When only the T1-w modality was used, the accuracy of the proposed method was still clearly superior to methods such as FAST (ranked 21th) and SPM12 (best ranked 17th), even when they used both image modalities. With MS data, the performance of our method, combining the T1-w and FLAIR sequences, was similar to or better than the best evaluated pipeline incorporating lesion segmentation and filling. Differences in tissue volume between images processed with the proposed algorithm and the same images where lesions were filled using expert lesion annotations were lower than 0.15% on all tissues, validating the overall capability of the proposed method reducing the effects of WM lesions on tissue segmentation.

In general, our results showed that the percentages of error in tissue volume of our approach were low or similar with both databases. The percentages of error were lowest when the FLAIR modality was used, which evidences that this image sequence has a direct effect on the efficiency of the algorithm, and, consequently, it should be used when available. However, the accuracy of the method using only the T1-w modality was also superior to other strategies not designed to deal with MS lesions, which also evidences that the improvement in tissue segmentation was not only generated by the addition of the FLAIR modality, but also by the combination of intensity, anatomical and morphological priors, and the use of a specific outlier algorithm with integrated lesion filling.

Chapter 8

Conclusions

This thesis synthesizes our work done over the last three years. Following the same objectives defined in the Introduction, in what follows we summarize the main conclusions and contributions of this thesis:

- We analyzed and evaluated the state of the art in brain tissue segmentation methods. This first sub-objective aimed to quantitatively review and evaluate different proposed tissue segmentation techniques in order to understand their advantages and drawbacks. As part of the resulting analysis published in the *Journal of Magnetic Resonance Imaging* in January of 2015, **our results showed a higher accuracy with several methods that incorporated morphological prior information and/or spatial constraints such as the FAST, SPVASEG or SPM8. These methods were also less prone to changes in acquisition sequences and intensity inhomogeneities.**
- We studied the effect of WM lesions on tissue segmentation of MS patient images. The second sub-objective to cover focused on the analysis of the effects of WM lesions on the tissue distributions. Six of the analyzed methods in Chapter 2 were evaluated with multi-center 1.5T MS data from different scanners. Related to the previous sub-objective, our results stressed **the necessity of adding morphological prior information and/or spatial constraints to the automated brain tissue segmentation, not only to overcome inherent MRI artifacts but also as an important component of dealing with WM lesions.** Furthermore, our analysis of the effects of WM lesions on tissue volume showed that **the inclusion of WM lesions in tissue segmentation not only biased the total tissue volume measurements by the addition of misclassified lesion voxels, but also by the effect of these lesions on differences observed in normal-appearing tissue volume.** The entire analysis was published in the *American Journal of Neuroradiology*

in February 2015.

- We proposed a new technique to reduce the effects of WM lesions on tissue segmentation of MS patient images. The third sub-objective first required comparing the accuracy of different lesion filling techniques proposed in the literature with the aim of then proposing a new technique to reduce the effects of WM lesions on tissue segmentation. **The lesion filling method proposed in this thesis was shown to be effective with different data and independent of the tissue segmentation method used afterwards. Our approach outperformed the rest of methods with both 1.5T and 3T data when the FAST was used, while its performance was similar to or lower than the best available strategy when the SPM8 was used.** The proposed lesion filling method was published in the *NeuroImage: Clinical* journal in August of 2014. **Furthermore, we released a public version of the proposed method that can be downloaded for free from our research team web page¹.** This software is already being used in the collaborating hospitals.
- We analyzed and evaluated the effect of automated WM lesion segmentation and filling on the tissue segmentation. In the fourth sub-objective, we quantitatively evaluated the accuracy of two state-of-the-art automated pipelines that incorporate unsupervised lesion segmentation, lesion filling and tissue segmentation with MS data. As shown in the paper published in the *NeuroImage: Clinical* journal in October of 2015, our analysis showed that **pipelines that incorporated automated lesion segmentation and filling were capable of significantly reducing the impact of WM lesions on tissue segmentation, performing similarly to pipelines that required expert manual intervention.**
- Finally, we proposed a new fully automated tissue segmentation method for MS patient images containing lesions. The main goal of this thesis was to propose a fully automated tissue segmentation method capable of dealing with images from MS patients. As shown in Chapter 6, the proposed method incorporates all the major insights obtained from previous sub-objectives with the aim of providing a robust, fully automated tissue approach for accurate brain volume measurements. Our results showed that **when compared with existing tissue segmentation methods, the presented approach yielded a higher accuracy in tissue segmentation while the influence of MS lesions on tissue segmentation was lower or similar to the best state-of-the-art pipeline incorporating automated lesion segmentation and**

¹The latest version of the proposed lesion filling method can be downloaded from <http://atc.udg.edu/nic/slfToolbox>

filling. This work has been submitted for publication in the *Medical Image Analysis* journal in January 2016. **As part of this work, we also released a public version of the proposed method that can be downloaded for free from our research team web page².**

Throughout this PhD thesis, various collaborations have taken place with other researchers of the VICOROB group. First, we evaluated the effect of MS lesions on longitudinal registration in the published study of Diez et al. [23], where we contributed several processing steps, including lesion filling. More recently, we were also involved in the development of several automated lesion segmentation pipelines that allowed us to gain knowledge on this topic. In this regard, we helped to implement two different lesion segmentation pipelines for MS, which were published in the papers of Cabezas et al. [10] and Roura et al. [55], respectively. Furthermore, we also collaborated on a new pipeline for automated lesion segmentation of lupus lesions proposed by Roura et al., which was submitted for publication recently.

8.1 Future work

Unfortunately, there are several aspects that have not been investigated during this thesis. One of the main limitations in several sub-objectives has been the lack of 3T images with high lesion loads. As pointed out in Chapters 5 and 6, the low mean lesion load of the cohorts analyzed, which indeed has been the major interest for medical experts, has not allowed us to better investigate the performance of the analyzed pipelines in the presence of images with higher lesion loads. In the case of our tissue segmentation method, we believe that an additional analysis of the performance with images with higher lesion loads would be helpful not only to analyze the robustness of the proposed algorithm, but also to investigate the benefits of adding other image sequences such as T2-w or PD-w.

Although the proposed tissue segmentation method has been designed for cross-sectional data, there is an increasing clinical interest in the measuring of longitudinal changes in tissue volume. We believe that the proposed method could be extended to longitudinal changes by re-adapting the pipeline with prior registering of time point images before the tissue segmentation. This is in fact one of the goals that our team has in mind to tackle first within the research framework of the BiomarkEM.cat project, in order to release suitable tools that can be used in clinical settings.

The ultimate goal should be to provide state-of-the-art tools for the collaborating hospitals involved in these research projects that may be useful not only to diagnose and monitor the progression of this disease, but also to evaluate new treatments for

²A public version of the method can be downloaded from <http://atc.udg.edu/nic/msseg>

MS patients. Related to that, the tools developed in this thesis should be integrated with other tools developed in our group in order to implement this complete system capable of providing robust and useful biomarkers in MS such as the number of lesions, lesion volume, brain tissue volume or brain atrophy.

Bibliography

- [1] J. Acosta-Cabronero, GB. Williams, JM. Pereira, G. Pengas, and PJ. Nestor. The impact of skull-stripping and radio-frequency bias correction on grey-matter segmentation for voxel-based morphometry. *NeuroImage*, 39(4):1654–1665, 2008.
- [2] A. Akselrod-Ballin, M. Galun, MJ. Gomori, R. Basri, and A. Brandt. Atlas guided identification of brain structures by combining 3D segmentation and SVM classification. *Medical image computing and computer-assisted intervention : MICCAI 2006 International Conference on Medical Image Computing and Computer-Assisted Intervention*, 9(Pt 2):209–16, 2006.
- [3] JB. Arnold, JS. Liow, KA. Schaper, JJ. Stern, JG. Sled, DW. Shattuck, AJ. Worth, MS. Cohen, RM. Leahy, JC. Mazziotta, and DA. Rottenberg. Qualitative and quantitative evaluation of six algorithms for correcting intensity nonuniformity effects. *NeuroImage*, 13(5):931–943, 2001.
- [4] J. Ashburner and KJ. Friston. Unified segmentation. *NeuroImage*, 26:839–851, 2005.
- [5] M. Battaglini, M. Jenkinson, and N. Stefano. Evaluating and reducing the impact of white matter lesions on brain volume measurements. *Human Brain Mapping*, 33(9):2062–71, 2012.
- [6] S. Bricq, CH. Collet, and JP. Armspach. Unifying framework for multimodal brain MRI segmentation based on hidden markov chains. *Medical Image Analysis*, 12(6):639 – 652, 2008. Special issue on information processing in medical imaging 2007.
- [7] P. Brodal. *The central nervous system*. 2010.
- [8] M. Cabezas, A. Oliver, X. Lladó, J. Freixenet, and M. Bach-Cuadra. A review of atlas-based segmentation for magnetic resonance brain images. *Computer Methods and Programs in Biomedicine*, 104(3):e158–e177, 2011.

- [9] M. Cabezas, A. Oliver, E. Roura, J. Freixenet, JC. Vilanova, L. Ramió-Torrentà, A. Rovira, and X. Lladó. Automatic multiple sclerosis lesion detection in brain MRI by FLAIR thresholding. *Computer Methods and Programs in Biomedicine*, 115(3):147–161, 2014.
- [10] M. Cabezas, A. Oliver, S. Valverde, B. Beltran, J. Freixenet, JC. Vilanova, L. Ramió-Torrentà, A. Rovira, and X. Lladó. BOOST: A supervised approach for multiple sclerosis lesion segmentation. *Journal of Neuroscience Methods*, 237:108–117, 2014.
- [11] B. Caldairou, N. Passat, PA. Habas, C. Studholme, and F. Rousseau. A non-local fuzzy segmentation method: application to brain MRI. *Pattern Recognition*, 44(9):1916–1927, 2011.
- [12] A. Ceccarelli, JS. Jackson, S. Tauhid, A. Arora, J. Gorky, E. Dell’Oglio, A. Bakshi, T. Chitnis, SJ. Khoury, HL. Weiner, CR. Guttmann, R. Bakshi, and M. Neema. The impact of lesion in-painting and registration methods on voxel-based morphometry in detecting regional cerebral gray matter atrophy in multiple sclerosis. *American Journal of Neuroradiology*, 33(8):1579–85, September 2012.
- [13] A. Ceccarelli, MA. Rocca, M. Neema, V. Martinelli, A. Arora, S. Tauhid, A. Ghezzi, G. Comi, R. Bakshi, and M. Filippi. Deep gray matter T2 hypointensity is present in patients with clinically isolated syndromes suggestive of multiple sclerosis. *Multiple sclerosis*, 16(1):39–44, 2010.
- [14] DT. Chard, JS. Jackson, DH. Miller, and CA. Wheeler-Kingshott. Reducing the impact of white matter lesions on automated measures of brain gray and white matter volumes. *Journal of Magnetic Resonance Imaging*, 32:223–228, 2010.
- [15] DT. Chard, GJ. Parker, R. Kapoor, AJ. Thompson, and DH. Miller. Brain atrophy in clinically early relapsing-remitting multiple sclerosis. *Brain*, 125:327–337, 2002.
- [16] HE. Cline, WE. Lorensen, R. Kikinis, and F. Jolesz. Three-Dimensional Segmentation of MR Images of the Head Using Probability and Connectivity. *Journal of Computer Assisted Tomography*, 14(6):1037–1045, 1990.
- [17] A. Compston and A. Coles. Multiple sclerosis. *Lancet*, 359(9313):1221–31, 2002.
- [18] A. Compston and A. Coles. Multiple sclerosis. *Lancet*, 372(9648):1502–17, 2008.
- [19] C. Confavreux, G. Aimard, and M. Devic. Course and prognosis of multiple sclerosis assessed by the computerized data processing of 349 patients. *Brain*, 103(2):281–300, 1980.

- [20] R. De Boer, HA. Vrooman, F. Van Der Lijn, MW. Vernooij, MA. Ikram, A. Van Der Lugt, MB. Breteler, and W. Niessen. White matter lesion extension to automatic brain tissue segmentation on MRI. *NeuroImage*, 45(4):1151–1161, 2009.
- [21] N. De Stefano, A. Giorgio, M. Battaglini, M. Rovaris, MP. Sormani, F. Barkhof, T. Korteweg, C. Enzinger, F. Fazekas, M. Calabrese, D. Dinacci, G. Tedeschi, A. Gass, X. Montalban, A. Rovira, A. Thompson, G. Comi, DH. Miller, and M. Filippi. Assessing brain atrophy rates in a large population of untreated multiple sclerosis subtypes. *Neurology*, 74(23):1868–1876, 2010.
- [22] H. Deshpande, P. Maurel, and C. Barillot. Classification of Multiple Sclerosis Lesions using Adaptive Dictionary Learning. *Computerized Medical Imaging and Graphics*, pages 2–10, 2015.
- [23] Y. Diez, A. Oliver, M. Cabezas, S. Valverde, R. Martí, JC. Vilanova, L. Ramió-Torrentà, A. Rovira, and X. Lladó. Intensity based methods for brain MRI longitudinal registration. A study on multiple sclerosis patients. *Neuroinformatics*, 12(3):365–379, 2014.
- [24] RR. Edelman and S. Warach. Magnetic Resonance Imaging. *New England Journal of Medicine*, 328(10):708–716, 1993.
- [25] SF. Eskildsen, P. Coupé, V. Fonov, JV. Manjón, K. Leung, N. Guizard, SN. Wassef, LR Østergaard, and DL Collins. BEaST: Brain extraction based on nonlocal segmentation technique. *NeuroImage*, 59(3):2362–2373, 2012.
- [26] M. Filippi, P. Preziosa, M. Copetti, G. Riccitelli, MA. Horsfield, V. Martinelli, G. Comi, and MA. Rocca. Gray matter damage predicts the accumulation of disability 13 years later in MS. *Neurology*, 81(20):1759–67, 2013.
- [27] M. Filippi and MA. Rocca. MR imaging of multiple sclerosis. *Radiology*, 259(3):659–81, 2011.
- [28] E. Fisher, JC. Lee, K. Nakamura, and RA. Rudick. Gray matter atrophy in multiple sclerosis: A longitudinal study. *Annals of Neurology*, 64(3):255–265, sep 2008.
- [29] LK. Fisniku, DT. Chard, JS. Jackson, VM. Anderson, DR. Altmann, KA. Miszkiel, AJ. Thompson, and DH. Miller. Gray Matter Atrophy Is Related to Long- Term Disability in Multiple Sclerosis. *Ann Neurol*, 64:247–254, 2008.
- [30] O. Ganiler, A. Oliver, Y. Diez, J. Freixenet, JC. Vilanova, B. Beltran, L. Ramió-Torrentà, A. Rovira, and X. Lladó. A subtraction pipeline for automatic detection of new appearing multiple sclerosis lesions in longitudinal studies. *Neuroradiology*, 56(5):363–374, 2014.

- [31] D. García-Lorenzo, S. Francis, S. Narayanan, DL. Arnold, and DL. Collins. Review of automatic segmentation methods of multiple sclerosis white matter lesions on conventional magnetic resonance imaging. *Medical Image Analysis*, 17(1):1–18, January 2013.
- [32] E. Geremia, O. Clatz, BH. Menze, E Konukoglu, A. Criminisi, and N. Ayache. Spatial decision forests for MS lesion segmentation in multi-channel magnetic resonance images. *NeuroImage*, 57(2):378–390, 2011.
- [33] G. Gerig, J. Martin, R. Kikinis, O. Kubler, M. Shenton, and F. Jolesz. Unsupervised tissue type segmentation of 3D dual-echo MR head data. *Image and Vision Computing*, 10(6):349–360, 1992.
- [34] T. Geva. Magnetic resonance imaging: historical perspective. *Journal of Cardiovascular Magnetic Resonance*, 8(4):573–580, 2006.
- [35] A. Giorgio and N. De Stefano. Clinical use of brain volumetry. *Journal of Magnetic Resonance Imaging*, 37(1):1–14, 2013.
- [36] N. Guizard, P. Coupé, VS. Fonov, JV. Manjón, DL. Arnold, and DL. Collins. Rotation-invariant multi-contrast non-local means for MS lesion segmentation. *NeuroImage: Clinical*, 8:376–389, 2015.
- [37] R. Harmouche, NK. Subbanna, DL. Collins, DL. Arnold, and T. Arbel. Probabilistic multiple sclerosis lesion classification based on modeling regional intensity variability and local neighborhood information. *IEEE transactions on bio-medical engineering*, 62(5):1281–1292, 2015.
- [38] Z. Hou. A review on MR image intensity inhomogeneity correction. *International Journal of Biomedical Imaging*, 2006-49515, 2006.
- [39] JE. Iglesias, CY. Liu, PM. Thompson, and Z. Tu. Robust brain extraction across datasets and comparison with publicly available methods. *IEEE Transactions on Medical Imaging*, 30(9):1617–1634, 2011.
- [40] S. Jain, DM. Sima, A. Ribbens, M. Cambron, A. Maertens, W. Van Hecke, J. De Mey, F. Barkhof, MD. Steenwijk, M. Daams, F. Maes, S. Van Huffel, H. Vrenken, and D Smeets. Automatic segmentation and volumetry of multiple sclerosis brain lesions from MR images. *NeuroImage: Clinical*, 8:367–375, 2015.
- [41] T. Kapur, WE. Grimson, WM. Wells, and R. Kikinis. Segmentation of brain tissue from magnetic resonance images. *Medical image analysis*, 1(2):109–27, 1996.

- [42] JM. Lee, U. Yoon, SH. Nam, JH. Kim, IY. Kim, and SI. Kim. Evaluation of automated and semi-automated skull-stripping algorithms using similarity index and segmentation error. *Computers in Biology and Medicine*, 33(6):495–507, 2003.
- [43] X. Lladó, O. Ganiler, A. Oliver, R. Martí, J. Freixenet, L. Valls, JC. Vilanova, L. Ramió-Torrentà, and A. Rovira. Automated detection of multiple sclerosis lesions in serial brain MRI. *Neuroradiology*, 54:787–807, 2012.
- [44] X. Lladó, A. Oliver, M. Cabezas, J. Freixenet, JC. Vilanova, A. Quiles, L. Valls, L. Ramió-Torrentà, and A. Rovira. Segmentation of multiple sclerosis lesions in brain MRI: A review of automated approaches. *Information Sciences*, 186(1):164–185, March 2012.
- [45] FD. Lublin and SC. Reingold. Defining the clinical course of multiple sclerosis: results of an international survey. National Multiple Sclerosis Society (USA) Advisory Committee on Clinical Trials of New Agents in Multiple Sclerosis. *Neurology*, 46(4):907–911, April 1996.
- [46] S. Magon, L. Gaetano, MM. Chakravarty, JP. Lerch, Y. Naegelin, C. Stippich, L. Kappos, EW. Radue, and T. Sprenger. White matter lesion filling improves the accuracy of cortical thickness measurements in multiple sclerosis patients: a longitudinal study. *BMC Neuroscience.*, 15(1):106, January 2014.
- [47] D. Mahapatra. Analyzing Training Information From Random Forests for Improved Image Segmentation. *Image Processing, IEEE Transactions on*, 23(4):1504–1512, 2014.
- [48] MSIF. Atlas of MS 2013: Mapping Multiple Sclerosis Around the World. *Multiple Sclerosis International Federation*, pages 1–28, 2013.
- [49] DL. Pham. Spatial Models for Fuzzy Clustering. *Computer Vision and Image Understanding*, 297:285–297, 2001.
- [50] KM. Pohl, J. Fisher, W. Grimson, R. Kikinis, and WM. Wells. A Bayesian model for joint segmentation and registration. *NeuroImage*, 31(1):228–239, 2006.
- [51] CH. Polman, SC. Reingold, B. Banwell, M. Clanet, J. a Cohen, M. Filippi, K. Fujihara, E. Havrdova, M. Hutchinson, L. Kappos, FD. Lublin, X. Montalban, P. O’Connor, M. Sandberg-Wollheim, AJ. Thompson, E. Waubant, B. Weinshenker, and JS. Wolinsky. Diagnostic criteria for multiple sclerosis: 2010 revisions to the McDonald criteria. *Annals of neurology*, 69(2):292–302, 2011.

- [52] V. Popescu, M. Battaglini, WS. Hoogstrate, SC Verfaillie, IC. Sluimer, RA. van Schijndel, BW. van Dijk, KS. Cover, DL. Knol, M. Jenkinson, F. Barkhof, N. de Stefano, H. Vrenken, X. Montalban, F. Fazekas, M. Filippi, J. Frederiksen, L. Kappos, D. Miller, J. Palace, C. Polman, M. Rocca, A. Rovira, and T. Yousry. Optimizing parameter choice for FSL-Brain Extraction Tool (BET) on 3D T1 images in multiple sclerosis. *NeuroImage*, 61(4):1484–1494, 2012.
- [53] V. Popescu, NC. Ran, F. Barkhof, DT. Chard, CA. Wheeler-Kingshott, and H. Vrenken. Accurate GM atrophy quantification in MS using lesion-filling with co-registered 2D lesion masks. *NeuroImage: Clinical*, 4:366–373, 2014.
- [54] M. Rajchl, JS. Baxter, AJ. McLeod, J. Yuan, W. Qiu, TM. Peters, and AR. Khan. Hierarchical max-flow segmentation framework for multi-atlas segmentation with Kohonen self-organizing map based Gaussian mixture modeling. *Medical Image Analysis*, 000:1–12, 2015.
- [55] E. Roura, A. Oliver, M. Cabezas, S. Valverde, D. Pareto, JC. Vilanova, L. Ramió-Torrentà, A. Rovira, and X. Lladó. A toolbox for multiple sclerosis lesion segmentation. *Neuroradiology*, 57(10):1031–1043, 2015.
- [56] E. Roura, A. Oliver, M. Cabezas, JC. Vilanova, A. Rovira, L. Ramió-Torrentà, and X. Lladó. MARGA: Multispectral Adaptive Region Growing Algorithm for brain extraction on axial MRI. *Computer Methods and Programs in Biomedicine*, 113(2):655–673, 2014.
- [57] E. Roura, T. Schneider, M. Modat, P. Daga, N. Muhlert, D. Chard, S. Ourselin, X. Lladó, and CA. Wheeler-Kingshott. Multi-channel registration of FA and T1-w images in the presence of atrophy: application to multiple sclerosis. *Functional Neurology*, 30(4), 2015.
- [58] S. Roy, A. Carass, PL. Bazin, S. Resnick, and JL. Prince. Consistent segmentation using a rician classifier. *Medical Image Analysis*, 16(2):524 – 535, 2012.
- [59] RA. Rudick, JC. Lee, K. Nakamura, and E. Fisher. Gray matter atrophy correlates with MS disability progression measured with MSFC but not EDSS. *Journal of the neurological sciences*, 282(1-2):106–11, jul 2009.
- [60] SA. Sadananthan, W. Zheng, MWL. Chee, and V. Zagorodnov. Skull stripping using graph cuts. *NeuroImage*, 49(1):225–239, 2010.
- [61] P. Schmidt, C. Gaser, M. Arsic, D. Buck, A. Förchler, A. Berthele, M. Hoshi, R. Ilg, VJ. Schmid, C. Zimmer, B. Hemmer, and M. Mühlau. An automated tool for detection of FLAIR-hyperintense white-matter lesions in Multiple Sclerosis. *NeuroImage*, 59(4):3774–3783, February 2012.

- [62] M. Sdika and D. Pelletier. Nonrigid registration of multiple sclerosis brain images using lesion inpainting for morphometry or lesion mapping. *Human Brain Mapping*, 30(4):1060–1067, 2009.
- [63] DW. Shattuck, SR. Sandor-Leahy, KA. Schaper, DA. Rottenberg, and RM. Leahy. Magnetic resonance image tissue classification using a partial volume model. *NeuroImage*, 13(5):856–876, 2001.
- [64] A. Simmons, PS. Tofts, GJ. Barker, and SR. Arridge. Sources of intensity nonuniformity in spin echo images at 1.5 T. *Magnetic Resonance in Medicine*, 32(1):121–128, 1994.
- [65] JG. Sled, AP. Zijdenbos, and AC. Evans. A nonparametric method for automatic correction of intensity nonuniformity in MRI data. *IEEE transactions on medical imaging*, 17(1):87–97, 1998.
- [66] SM. Smith. Fast robust automated brain extraction. *Human Brain Mapping*, 17(3):143–155, 2002.
- [67] GH. Sperber. Clinically Oriented Anatomy. *Journal of anatomy*, 208(3):393, 2006.
- [68] L. Steinman. Multiple Sclerosis: A Coordinated Immunological Attack against Myelin in the Central Nervous System. *Cell*, 85(3):299–302, may 1996.
- [69] EM. Sweeney, RT. Shinohara, N. Shiee, FJ. Mateen, AA. Chudgar, JL. Cuzocreo, PA. Calabresi, DL. Pham, DS. Reich, and CM. Crainiceanu. OASIS is Automated Statistical Inference for Segmentation, with applications to multiple sclerosis lesion segmentation in MRI. *NeuroImage: Clinical*, 2:402–13, jan 2013.
- [70] J. Tohka, I. Dinov, DW. Shattuck, and AW. Toga. Brain MRI tissue classification based on local markov random fields. *Magnetic Resonance Imaging*, 28(4):557 – 573, 2010.
- [71] X. Tomas-Fernandez and SK. Warfield. A Model of Population and Subject (MOPS) Intensities with Application to Multiple Sclerosis Lesion Segmentation. *IEEE transactions on medical imaging*, 0062(c):1–15, jan 2015.
- [72] NJ. Tustison, BB. Avants, PA. Cook, Y Zheng, A Egan, PA. Yushkevich, and JC. Gee. N4ITK: Improved N3 bias correction. *IEEE Transactions on Medical Imaging*, 29(6):1310–1320, 2010.
- [73] K Van Leemput, F. Maes, D. Vandermeulen, and P. Suetens. A unifying framework for partial volume segmentation of brain MR images. *IEEE Transactions on Medical Imaging*, 22(1):105–119, 2003.

- [74] A. van Opbroek, F. van der Lijn, and M. de Bruijne. Automated brain-tissue segmentation by multi-feature svm classification. In *Proceedings of the MICCAI Workshops—The MICCAI Grand Challenge on MR Brain Image Segmentation (MRBrainS'13)*, 2013.
- [75] H. Vrooman, F. van der Lijn, and W. Niessen. Auto-knn: brain tissue segmentation using automatically trained knearest-neighbor classification. In *Proceedings of the MICCAI Workshops—The MICCAI Grand Challenge on MR Brain Image Segmentation (MRBrainS'13)*, 2013.
- [76] WM. Wells, WL Crimson, R. Kikinis, and FA. Jolesz. Adaptive segmentation of mri data. *IEEE Transactions on Medical Imaging*, 15(4):429–442, 1996.
- [77] Z. Yi, A. Criminisi, J. Shotton, and A. Blake. Discriminative, semantic segmentation of brain tissue in mr images. In Guang-Zhong Yang, David Hawkes, Daniel Rueckert, Alison Noble, and Chris Taylor, editors, *Medical Image Computing and Computer-Assisted Intervention – MICCAI 2009*, volume 5762 of *Lecture Notes in Computer Science*, pages 558–565. Springer Berlin / Heidelberg, 2009.
- [78] Y. Zhang, M. Brady, and S. Smith. Segmentation of brain MR images through a hidden Markov random field model and the expectation-maximization algorithm. *IEEE Transactions on Medical Imaging*, 20:45–57, 2001.